Università Politecnica delle Marche
Scuola di Dottorato di Ricerca in Scienze dell'Ingegneria
Curriculum in Dipartimento di Scienze Agrarie, Alimentari ed Ambientali

---

Sustainable management of local olive production by using precision farming systems and development of territory

Ph.D. Dissertation of:

Arash Khosravi

Advisor:

Prof. Davide Neri

Co-Advisor:

Prof. Andrea Galli

Curriculum supervisor:

Prof. Bruno Mezzetti

May 2023

Università Politecnica delle Marche
Scuola di Dottorato di Ricerca in Scienze dell'Ingegneria
Curriculum in Dipartimento di Scienze Agrarie, Alimentari ed Ambientali

---

Sustainable management of local olive production by using precision farming systems and development of territory

Ph.D. Dissertation of:

Arash Khosravi

Advisor:

Prof. Davide Neri

Co-Advisor:

Prof. Andrea Galli

Curriculum supervisor:

Prof. Bruno Mezzetti

May 2023

Università Politecnica delle Marche
Dipartimento di Scienze Agrarie, Alimentari ed Ambientali
Via Brecce Bianche — 60131 - Ancona, Italy

Acknowledgements

Special thanks to Regione Marche and Marche Polytechnic University for providing research opportunity through the POR Marche FSE 2014/2020 Progetto “Dottorato Innovativo”-Borse di studio per dottorato di ricerca per l’innovazione del sistema regionale, Edizione Anno 2020.

I would like to express my sincere gratitude to my supervisor prof. Davide Neri for the continuous supports in all the time of research and writing of this PhD thesis, for his patience, motivation, and immense knowledge. His mentoring attitude was a source of enhancement for my personal and academical career.

My appreciation also extends to my co-supervisor Prof. Andrea Galli for his mentoring and encouragement. In addition, I would like to thank Prof. Cornelia Weltzien and Prof. Manuela Zude-Sasse who provided me an opportunity to join their group as visiting PhD student.

I want to thanks all professors, friends and colleagues that kindly support and collaboration during this PhD, especially Veronica, Matteo, Monica, Samuele, Marco, Jebu.

Last but not the least, I would like to appreciate and dedicate this thesis to my wife and daughter whose love, support, encouragement and patience have enriched my soul and inspired me to pursue and complete this research.

Abstract

Fruit growth monitoring is a beneficial tool in precision orchard management which can provide various physiological indicators such as ripening and water status. To obtain accurate indicators, using constant high-resolution data collection (ranging from seasonal period up to minute intervals) has been suggested. There are different proximal and remote sensing techniques, which are able to collect a wide range of data about fruit growth. Concurrently, development of innovative methods to adjust sensor output to physiologically meaningful parameters is advantageous.
In the first study, at the intensive olive grove in Gallignano of Ancona (central Italy), combination of extensimeter and RGB camera has been used for continuous monitoring of olive fruit growth (*Olea europaea* L. cv. 'Frantoio'), in the attempt to determine whether fruit growth dynamically responds to environmental variables such as diurnal vapor pressure deficit (VPD) change in different stages of fruit development. In order to data analysis, different types of hysteresis curves for daily response of fruit diameter (FD) to VPD have been employed. In the II and III phases of fruit growth 85% (100 out of 118) of cases formed complete clockwise hysteresis loops, however, it reduced to 2% (1 out of 42) in the IV phase of fruit growth (fruit maturation). We conclude that disappearance of complete clockwise hysteresis loops could be a good indicator of fruit maturation phase (IV). Additionally, Images of the RGB camera have been analyzed by the Labelbox platform (Labelbox Inc., San Francisco, CA, USA) for fruit maturation detection and results were in line with what we obtained from hysteretic patterns.

In the second study, at the high-intensive olive orchard in Agugliano of Ancona (central Italy), FD of four olive cultivars ('Ascolana dura', 'Piantone di Falerone', 'Arbequina', and 'Lea') was monitored continuously by extensimeters in order to monitor fruit growth dynamics under deficit irrigation treatments. The assessment of fruit growth parameters of the daily diameter fluctuation (ΔD, mm), the daily growth (ΔG, mm), the cumulative fruit growth (CFG, mm), and the fruit relative growth rate (RGR, mm mm^{-1} h^{-1}) showed cultivar-specific response to water stress. However, evaluation of magnitude change in the hysteretic pattern of FD versus VPD , showed a non-cultivar-specific pattern. A quantitative index (height of hysteresis curves) used for explanation of hysteresis magnitude change according to the deficit irrigation treatments. The results showed a significant reduction of height of hysteresis curves by irrigation treatments in the four olive cultivars and can efficiently estimate the plant water response to irrigation treatment in olive orchards.

Development of extra virgin olive oil (EVOO) as a typical product (consisting of DOP and IGP certification), becomes a territorial development strategy. Ripening and water status detection are beneficial for production of high quality EVOO, meanwhile nutritional and organoleptic quality EVOO are affected by them. Accurate ripening detection by employment of various types of hysteresis curve and water status detection by employment of magnitude of hysteresis curve has been derived from results of our first and second study.

In the third study, at an apple orchard (Malus x domestica, cv. 'Gala') in the experimental field of ATB (Potsdam, Germany), 3D fruit temperature (Instead of canopy temperature) was measured by integration of LiDAR and thermal camera in order to develop an innovative methodology for crop water stress index (CWSI) calculation. The CWSI has been computed via 3 different approaches (by manually measured temperature (T_{Ref}) and 3D temperature (T_{Est}). Among them, 2 methods showed a strong relation between CWSI obtained by T_{Ref} and T_{Est} ($R^2 = 0.99$).

(Italian)
Il monitoraggio della crescita dei frutti è uno strumento efficace nella frutticoltura di precisione che può fornire vari indicatori fisiologici come la maturazione e il contenuto idrico. Per ottenere indicatori accurati, è stato suggerito di utilizzare una raccolta dati ad alta risoluzione continuativa nel tempo (ad intervalli che possono arrivare fino al minuto). Esistono diverse tecniche di rilevamento prossimale e remoto, che sono in grado di raccogliere un'ampia gamma di dati sulla crescita dei frutti, tuttavia il punto chiave è mettere a punto metodi innovativi per correlare i dati raccolti dai sensori a parametri fisiologicamente significativi.
Nel primo studio, presso l'oliveto intensivo di Gallignano di Ancona (Italia centrale), è stata utilizzata una combinazione di estensimetro e telecamera RGB per il monitoraggio continuo della crescita del frutto dell'olivo (Olea europaea L. cv. 'Frantoio'), nel tentativo per determinare se la crescita dei frutti risponde dinamicamente a variabili ambientali come la variazione del deficit di pressione di vapore diurna (VPD) nelle diverse fasi di sviluppo dei frutti. Per l'analisi dei dati, sono stati impiegati diversi tipi di curve di isteresi per la risposta giornaliera, dal diametro del frutto (FD) alla VPD. Nelle fasi II e III della crescita del frutto l'85% (100 su 118) dei casi ha formato cicli di isteresi completi in senso orario, tuttavia, si è ridotto al 2% (1 su 42) nella fase IV della crescita del frutto (maturazione del frutto). Concludiamo che la scomparsa dei cicli di isteresi in senso orario completi potrebbe essere un buon indicatore della fase di maturazione del frutto (IV). Inoltre, le immagini della telecamera RGB sono state analizzate dalla piattaforma Labelbox (Labelbox Inc., San Francisco, CA, USA) per il rilevamento della maturazione dei frutti e i risultati erano in linea con quanto ottenuto dai modelli isteretici.
Nel secondo studio, presso l'oliveto ad alta intensità di Agugliano di Ancona (Italia centrale), è stata monitorata in continuo la DF di quattro cultivar di olivo ('Ascolana dura', 'Piantone di Falerone', 'Arbequina' e 'Lea') mediante estensimetri al fine di monitorare la dinamica di accrescimento dei frutti nei trattamenti di irrigazione in deficit. La valutazione dei parametri di crescita dei frutti, la fluttuazione giornaliera del diametro (ΔD, mm), la crescita giornaliera (ΔG, mm), la crescita cumulativa dei frutti (CFG, mm) e il tasso di crescita relativo dei frutti (RGR, mm mm− 1 h−1) hanno mostrato una risposta specifica della cultivar allo stress idrico. Tuttavia, la valutazione del cambiamento di grandezza, nel confronto tra il modello isteretico di FD rispetto a VPD, ha mostrato un modello non specifico della cultivar. Un indice quantitativo (altezza delle curve di isteresi), utilizzato per spiegare la variazione dell'entità dell'isteresi, cambia in base ai trattamenti di irrigazione deficitaria. I risultati hanno mostrato una significativa riduzione dell'altezza delle curve di isteresi mediante trattamenti di irrigazione nelle quattro cultivar di olivo e possono stimare in modo efficiente la risposta dell'acqua della pianta al trattamento di irrigazione negli oliveti.
La valorizzazione dell'olio extravergine di oliva (EVO) come prodotto tipico (costituito da certificazione DOP e IGP), diventa strategia di sviluppo territoriale. Il rilevamento della maturazione e dello stato dell'acqua sono vantaggiosi per la produzione di EVO di alta qualità, mentre la qualità nutrizionale e organolettica di EVO ne risentono. Il rilevamento accurato della maturazione mediante l'impiego di vari tipi di curva di isteresi e il rilevamento dello stato dell'acqua mediante l'impiego dell'ampiezza della curva di isteresi è stato derivato dai risultati del nostro primo e secondo studio.

Nel terzo studio, in un meleto (Malus x domestica, cv. 'Gala') nel campo sperimentale di ATB (Potsdam, Germania), è stata misurata la temperatura 3D della frutta (invece della temperatura della chioma) mediante l'utilizzo di LiDAR e termocamera, al fine di sviluppare una metodologia innovativa per il calcolo dell'indice di stress idrico delle colture (CWSI). Il CWSI è stato calcolato tramite 3 diversi approcci - mediante temperatura misurata manualmente (TRef) e temperatura 3D (TEst). Tra questi, 2 metodi hanno mostrato una forte relazione tra CWSI ottenuto da TRef e TEst (R2 = 0,99).

Contents

List of Figures

List of Tables

Chapter 1

Introduction

Olive (*Olea europaea* L.) is an evergreen tree which was originally come from Mediterranean basin, from where it spread later on, to many parts of the world with Mediterranean climate (Khosravi et al., 2021a). In the recent decades, olive fruit and olive oil consumption has been increased with a noticeable breakthrough in the global scale, both in traditionally producing regions and in new regions and countries (Amanpour et al., 2019). It imposed a greater need for agricultural inputs as we address resource scarcity and climate change (Seifi et al., 2015; Rodrigues et al., 2018; Fraga et al., 2020). In addition to this, the growth of the fruit is the result of genetic, metabolic, hormonal and environmental interactions that determine the size, shape and oil composition (Gucci et al., 2009). Such degree of complexity in olive fruit growth demands a more accurate crop management to maintaining production constant and high (in both aspect of quality and quantity) (Khosravi et al., 2021a). One of the most recent concepts in this regard is precision farming (synonym of precision agriculture). Precision farming (PF) emphasize on utilization of technology to record and manage the variation of crops and soils within a field, thus reducing surplus inputs (e.g. fertilizer), increasing yields and aiding environmental sustainability (Morgado et al., 2020). For PF promotes an advance stage of collecting and using high-resolution data (ranging from seasonal period up to minute intervals) for on-time agricultural practices with respect to soil, plant and climate (Shafi et al., 2019). Therefore, constant data collection (continuous monitoring) is beneficial in PF.

Monitoring is a continuous function that uses the systematic collection of data on specified indicators, to provide information via analyzing of data (Scheerens et al., 2003; Kusek, 2010). The aim of continuous monitoring in the olive orchard is to obtain orchard properties for real-time optimization of orchard performance. In the olive orchards several types of data can be collected during the growing season either from micro-climate, soil and plant (Fernández 2014, Zude-Sasse et al., 2016). Among these data types, plant-based data are the most mainstream of continuous measurement methods. In soil plant atmosphere continuum (SPAC), plants play an interface role between soil and environment, and its physiological response is a combination of results of both soil and environment (Measham et al., 2014; Fernández, 2017; Scalisi et al., 2020). The plant-based monitoring could be performed on root, trunk/stem, flower, leaf/canopy and fruit. Each of them has own pros and cons, however olive fruit represents the actual goal of production, and optimal fruit growth is caused by efficient physiological conditions on trees (Boini et al., 2019). Consequently, olive fruit growth monitoring could be a prominent aspects of olive orchard management. Fruit monitoring has numerous applications like growth assessment, ripening stage detection, accurate fruit load determination, fruit quality control, water stress assessment, orchard yield mapping, mechanized/robotic fruit harvesting, fruit tree disease treatments, and precise agronomic and agrochemical applications (Pourreza et al., 2015; Sa et al., 2016; Amatya et al., 2016; Gené-Mola et al., 2019; Wu et al., 2019; Saedi et al., 2020; Khosravi et al., 2021b) (Table 1.1). For instance, Fazari et al. (2021) applied spectral imaging (visible and near-infrared hyperspectral images) for detection of anthracnose in

olive fruit, where it achieved 100% of accuracy, sensitivity, and specificity, when the damages on the skin of the olives were still minor and had a visual aspect of a small stain.

Table 1.1: Applications of olive fruit monitoring

Purpose	References
Ripening assessment	Khosravi et al., 2021a; Khosravi et al., 2021b
Water status detection	Fernandes et al., 2018; Scalisi et al., 2020; Marino et al., 2021; Khosravi et al., 2022
Phenological phase detection	Khosravi et al., 2021a
Fruit growth mechanism	Hernandez-Santana et al., 2018 and 2021
Lepra fruit rot, Parlatoria oleae, Aspidiotus nerii	Alruwaili et al., 2019
Fruit size and load determination	Ponce et al., 2019
Fruit quality	Fazari et al., 2021; Sepulcre-Cantó et al., 2007
Orchard yield mapping	Sepulcre-Cantó et al., 2007
Precise agronomic and agrochemical applications	Fernandes et al., 2018

According to our goals for monitoring and in order to obtain accurate results, the resolution of collected data and collecting time's intervals should be considered. For instance, several research (Scalisi et al., 2020; Marino et al., 2021; Khosravi et al., 2021a) suggested that precise fruit management obtained through fruit's growth monitoring in short time intervals (up to minute), whereas sensor installed in proximity of fruit. In this case, sensor's outputs can be employed for various aspects including growth assessment, ripening detection and water stress assessment. With consideration of data collection during all phases of olive fruit growth in continuous manner and with short time intervals, the most adopted sensor's platform is stationary loggers. According to research of Zude-Sasse et al. (2016) applicable sensor in stationary platform range from soil sensors, climate data, balance, acoustic system, cameras, water sensors, dendrometer, extensimeter (fruit gauge) and optical fruit sensor. Among these, extensimeter is the most common sensor which has been used for continuous olive fruit growth monitoring (Scalisi et al., 2020; Marino et al., 2021; Khosravi et al., 2021a). Extensimeter is plant-based sensor which measures fruit's diameter (FD). Production of highly precise instruments for accurate measurement of fruit growth has been developed and there are various experimental as well as commercial instruments (Morandi et al., 2007). Nevertheless, Morandi et al. (2007) described that, in most cases, the instrument consists of a sensor, supported by a frame, placed in contact with the epidermis of the growing fruit. FD monitoring has been investigated in several studies by researchers to measure daily fluctuation in the volume of olive fruit (Fernandes et al., 2018; Scalisi et al., 2020; Marino et al., 2021; Khosravi et al., 2021a). A common challenge with tree-based sensors is to adjust their output to physiologically meaningful parameters in a consistent manner (Fernández, 2017; Khosravi et al., 2021a; Zucchini et al., 2021). Therefore, innovative approach of data analysis is highly recommended.

In this paradigm, the project (innovative PhD program with industrial characterization and financed by Marche Region) was planned with the title of "Sustainable management of local olive productions by using precision farming systems and development of territory" .

It designed to develop precision farming techniques, with more emphasize on regional (Marche region , central Italy) olive orchards. In relation to this particular subject, olive fruit's monitoring at intensive and high-intensive olive orchard was set to enhance monitoring systems, optimizing olive grove's performance in both terms of quality and quantity and reach territorial development through the production of high quality olive oil (extra virgin olive oil). Two different types of experiment were designed. The first study was conducted in 2019 in the intensive olive grove (*Olea europaea* L., cv. 'Frantoio') of the experimental research station and botanical garden of Polytechnic University of Marche at Gallignano of Ancona (AN), Italy. Trees were planted 6 × 6 m and trained as free open vase. These were about 40 years old at the time of experiment. it was designed to hourly monitor FD from approximately initial pit hardening (II Phase), extension (III Phase) until harvest time (IV Phase) in the attempt to determine whether fruit growth dynamically responds to environmental variables such as diurnal VPD change in different stages of fruit development. The second experiment was carried out in 2021 at the experimental farm of the Polytechnic University of Marche, located in Agugliano (Marche, Italy), in a high-density olive orchard in four self-rooted olive (*Olea europaea* L.) cultivars of 'Ascolana dura', 'Piantone di Falerone', 'Arbequina' and 'Lea'. The trees were planted 4 × 2 m (1250 tree ha^{-1}) in May 2012, about 9 years old at the time of experiment. It was designed to hourly measure FD in order to monitor fruit growth dynamics under deficit irrigation treatments.
Finally, in 2022 at the experimental field of ATB (Field Lab for digital agriculture, Potsdam, Germany), an innovative method of crop water stress index calculation was tested. This innovative method could be used in precision irrigation management of orchards.
Accordingly, this PhD project was conducted in the mentioned areas based on the following objectives and hypotheses.

Objectives and Hypotheses
1) Enhancement of proximal and remote monitoring systems at intensive and high-intensive olive orchard.
Hi. Continuous fruit's growth monitoring by application of extensimeter and RGB camera will be an efficient monitoring systems.
2) Optimization of the olive grove's performance (both quality and quantity).
Hii. Continuous fruit's growth monitoring will enhance orchard performance by fruit maturation detection.
3) Development of the irrigation management of orchards
Hiii. Continuous fruit's growth monitoring will enhance orchard performance by water status detection.
Hiv. Crop water stress index detection by integration of LiDAR and thermal camera and employment of fruit temperature for computation of index, could be innovative method of water status detection.
4) Development of local olive products and territory through the resilient production of extra virgin olive oil.
Hv. Continuous fruit's growth monitoring will provide beneficial data for appropriate management of orchard to achieve high quality olive products (olive oil and table olive).

The dissertation is written in seven chapters to address the above-mentioned goals. Chapter 1 provides a general introduction to precision farming including different data collection approaches, followed by description of importance of continuous plant-based monitoring via continuous monitoring of fruit as a final goal of the production. Chapters 2, 3, 4, and 5 have been written in multiple paper formats. Chapter 2 is under submission in Acta Horticulturae (Leuven). This methodological review addressed current applications and challenges of continuous plant-based monitoring of olive tree and fruit via ground-based platforms. Chapter 3 has been published in Horticulturae (Basel). This paper focused on objectives 1 and 2, which assessed the olive fruit growth in 2019 and focused on circadian monitoring as an important orchard management tool through the ripening detection by proximal and remote sensing (integration of Extensimeter and RGB camera). Chapter 4 has been published in Horticulturae (Basel), where we evaluated objective 1, 2 and 3. In 2021 the transversal fruit diameter (FD) was monitored continuously in order to monitor fruit growth dynamics under deficit irrigation treatments and a quantitative index for water status detection has been introduced. Chapter 5 covered objective 3, and it is under submission to Journal of plant science (Amsterdam), where we discussed the new methodology of crop water stress index computing by integration of LiDAR and thermal camera, in 2022. In addition for the first time fruit temperature has been employed for water stress index calculation. Chapter 6 described development of territory by implementation of finding of chapter 3 and 4. It focused on objective 4. Chapter 7 will provide a synthesis of the findings of the whole PhD project and describe the implications of adapting findings in orchard management and propose directions for future research.

References

Alruwaili, M., Alanazi, S., El-Ghany, S. A., & Shehab, A. (2019). An efficient deep learning model for olive diseases detection. International Journal of Advanced Computer Science and Applications, 10(8), 486-492.

Amanpour, A., Kelebek, H., & Selli, S. (2019). LC-DAD-ESI-MS/MS–based phenolic profiling and antioxidant activity in Turkish cv. Nizip Yaglik olive oils from different maturity olives. Journal of mass spectrometry, 54(3), 227-238.

Amatya, S., Karkee, M., Gongal, A., Zhang, Q., & Whiting, M. D. (2016). Detection of cherry tree branches with full foliage in planar architecture for automated sweet-cherry harvesting. Biosystems engineering, 146, 3-15.

Boini, A., Manfrini, L., Bortolotti, G., Corelli-Grappadelli, L., & Morandi, B. (2019). Monitoring fruit daily growth indicates the onset of mild drought stress in apple. Scientia Horticulturae, 256, 108520.

Fazari, A., Pellicer-Valero, O. J., Gómez-Sanchıs, J., Bernardi, B., Cubero, S., Benalia, S., ... & Blasco, J. (2021). Application of deep convolutional neural networks for the detection of anthracnose in olives using VIS/NIR hyperspectral images. Computers and Electronics in Agriculture, 187, 106252.

Fernandes, R. D. M., Cuevas, M. V., Diaz-Espejo, A., & Hernandez-Santana, V. (2018). Effects of water stress on fruit growth and water relations between fruits and leaves in a hedgerow olive orchard. Agricultural water management, 210, 32-40

Fernández, J. E. (2014). Plant-based sensing to monitor water stress: Applicability to commercial orchards. Agric. Water Manag. 142, 99–109. doi: 10.1016/j.agwat. 2014.04.017

Fernández, J. E. (2017). Plant-based methods for irrigation scheduling of woody crops. Horticulturae 3:35. doi: 10.3390/horticulturae3020035

Fernández, J. E., Diaz-Espejo, A., Romero, R., Hernandez-Santana, V., García, J. M., Padilla-Díaz, C. M., & Cuevas, M. V. (2018). Precision irrigation in olive (Olea europaea L.) tree orchards. In Water scarcity and sustainable agriculture in semiarid environment (pp. 179-217). Academic Press

Gené-Mola, J., Vilaplana, V., Rosell-Polo, J. R., Morros, J.-R., Ruiz-Hidalgo, J., & Gregorio, E. (2019). Multi-modal deep learning for Fuji apple detection using RGB-D cameras and their radiometric capabilities. Computers and Electronics in Agriculture, 162, 689–698. https://doi.org/10.1016/j.compag.2019.05.016

Gucci, R., Lodolini, E. M., & Rapoport, H. F. (2009). Water deficit-induced changes in mesocarp cellular processes and the relationship between mesocarp and endocarp during olive fruit development. Tree physiology, 29(12), 1575-1585.

Hernandez-Santana, V., Fernandes, R. D., Perez-Arcoiza, A., Fernández, J. E., Garcia, J. M., & Diaz-Espejo, A. (2018). Relationships between fruit growth and oil accumulation with simulated seasonal dynamics of leaf gas exchange in the olive tree. Agricultural and Forest Meteorology, 256, 458-469.

Hernandez-Santana, V., Perez-Arcoiza, A., Gomez-Jimenez, M. C., & Diaz-Espejo, A. (2021). Disentangling the link between leaf photosynthesis and turgor in fruit growth. The Plant Journal, 107(6), 1788-1801.

Khosravi, A., Zucchini, M., Giorgi, V., Mancini, A., & Neri, D. (2021a). Continuous monitoring of olive fruit growth by automatic extensimeter in response to vapor pressure deficit from pit hardening to harvest. Horticulturae, 7(10), 349.

Khosravi, H., Saedi, S. I., & Rezaei, M. (2021b). Real-time recognition of on-branch olive ripening stages by a deep convolutional neural network. Scientia Horticulturae, 287, 110252.

Khosravi, A., Zucchini, M., Mancini, A., & Neri, D. (2022). Continuous Third Phase Fruit Monitoring in Olive with Regulated Deficit Irrigation to Set a Quantitative Index of Water Stress. Horticulturae, 8(12), 1221

Kusek, J. Z. (2010). Making monitoring and evaluation systems work: A capacity development toolkit. World Bank Publications.

Marino, G., Scalisi, A., Guzmán-Delgado, P., Caruso, T., Marra, F. P., & Lo Bianco, R. (2021). Detecting mild water stress in olive with multiple plant-based continuous sensors. Plants, 10(1), 131

Measham, P. F., Wilson, S. J., Gracie, A. J., & Bound, S. A. (2014). Tree water relations: flow and fruit. Agricultural Water Management, 137, 59-67.

Morandi, B., Manfrini, L., Zibordi, M., Noferini, M., Fiori, G., & Grappadelli, L. C. (2007). A low-cost device for accurate and continuous measurements of fruit diameter. HortScience, 42(6), 1380-1382.

Morgado, R., Santana, J., Porto, M., Sánchez-Oliver, J. S., Reino, L., Herrera, J. M., ... & Moreira, F. (2020). A Mediterranean silent spring? The effects of olive farming intensification on breeding bird communities. Agriculture, Ecosystems & Environment, 288, 106694.

Ponce, Juan Manuel, Arturo Aquino, Borja Millan, and Jose M. Andujar. "Automatic counting and individual size and mass estimation of olive-fruits through computer vision techniques." IEEE Access 7 (2019): 59451-59465

Pourreza, A., Lee, W. S., Ehsani, R., Schueller, J. K., & Raveh, E. (2015). An optimum method for real-time in-field detection of Huanglongbing disease using a vision sensor. Computers and Electronics in Agriculture, 110, 221–232. https://doi.org/10.1016/j.compag.2014.11.021.

Rodrigues, N., Casal, S., Peres, A. M., Baptista, P., Bento, A., Martín, H., ... & Pereira, J. A. (2018). Effect of olive trees density on the quality and composition of olive oil from cv. Arbequina. Scientia Horticulturae, 238, 222-233.

Saedi, S. I., & Khosravi, H. (2020). A deep neural network approach towards real-time on-branch fruit recognition for precision horticulture. Expert Systems with Applications, 159, 113594.

Scalisi, A., Marino, G., Marra, F. P., Caruso, T., & Lo Bianco, R. (2020). A Cultivar-Sensitive Approach for the Continuous Monitoring of Olive (Olea europaea L.) Tree Water Status by Fruit and Leaf Sensing. Frontiers in plant science, 11, 340.

Scheerens, J., Glas, C. A., Thomas, S. M., & Thomas, S. (2003). Educational evaluation, assessment, and monitoring: A systemic approach (Vol. 13). Taylor & Francis.

Seifi, E., Guerin, J., Kaiser, B., & Sedgley, M. (2015). Flowering and fruit set in olive: a review. Iran. J. Plant Physiol, 5(2), 1263-1272.

Sepulcre-Cantó, G., Zarco-Tejada, P. J., Jiménez-Muñoz, J. C., Sobrino, J. A., Soriano, M. A., Fereres, E., ... & Pastor, M. (2007). Monitoring yield and fruit quality

parameters in open-canopy tree crops under water stress. Implications for ASTER. Remote Sensing of Environment, 107(3), 455-470

Shafi, U., Mumtaz, R., García-Nieto, J., Hassan, S. A., Zaidi, S. A. R., & Iqbal, N. (2019). Precision agriculture techniques and practices: From considerations to applications. Sensors, 19(17), 3796.

Wu, J., Zhang, B., Zhou, J., Xiong, Y., Gu, B., & Yang, X. (2019). Automatic recognition of ripening tomatoes by combining multi-feature fusion with a bi-layer classification strategy for harvesting robots. Sensors (Basel, Switzerland), 19(3), 612. https://doi.org/10.3390/s19030612

Zucchini, M., Khosravi, A., Giorgi, V., Mancini, A., & Neri, D. (2021). Is There Daily Growth Hysteresis versus Vapor Pressure Deficit in Cherry Fruit?. Horticulturae, 7(6), 131.

Zude-Sasse, M., Fountas, S., Gemtos, T. A., & Abu-Khalaf, N. (2016). Applications of precision agriculture in horticultural crops.

Chapter 2.

Ground-Based Sensor Platforms for Continuous Monitoring of Olive Tree and Fruit: A review

Arash Khosravi[1], Zahra Mohammadi[1] and Davide Neri[1],*

[1]Department of Agricultural, Food and Environmental Science, Marche Polytechnic University, 60131 Ancona, Italy; a.khosravi@pm.univpm.it (A.K.); maryam4885@gmail.com (Z.M.)

* Correspondence: d.neri@staff.univpm.it

Abstract has been accepted in International olive symposium 2023, Davis, CA (USA).
(Acta Horticulturae)

2.1 Abstract

Precision agriculture (PA) is a farming management concept that emphasizes the application of information technology to collecting and using high-resolution data (ranging from seasonal period up to minute intervals) for on-time agricultural practices with respect to soil, plant and climate. Therefore, constant data collection (continuous monitoring) is beneficial in PA. Continuous monitoring could be performed on soil, plant and environment, however, plants act as a connector between soil and environment and its physiological response reflects integrated effect. Accordingly, continuous plant-based monitoring can be employed for olive tree and fruit management widely. Several sensor platforms have been used for monitoring of olive orchards and among them, ground-based is the most suitable platform for continuous plant-based monitoring (up to minute intervals). Several fundamental information for precision olive orchards management including water stress, disease and pest status, fruit growth, fruit maturation, fruit size and yield could be provided by continuous plant-based monitoring via ground-based sensor platforms. This methodological review addressed current applications and challenges of continuous plant-based monitoring of olive tree and fruit via ground-based platforms. Finally, we hypothesize possible future development of it for providing wider services for agricultural practices.

Keywords: olive precision farming, continuous data collection, stem and trunk monitoring, flower and fruit monitoring, leaf and canopy monitoring

2.2 Introduction

The olive (*Olea europaea* L.) is an ancient and evergreen tree which originally comes from the Mediterranean basin and has been cultivated for its fruit and oil. It is significant element of Mediterranean diet nevertheless in the recent decades, olive fruit and olive oil consumption has been increased with a noticeable breakthrough in the global scale, both in traditionally producing regions and in new regions and countries such as Japan, United States, Canada, United Kingdom, and Germany (Amanpour et al., 2019). Consequently, major increases in olive production through agricultural intensification are generally deemed necessary to meet the demands of a fast-increasing global population (Crist et al., 2017; Morgado et al., 2020). However, in the last three decades there has been an accelerating trend towards the intensification of olive production, with the standard intensive systems involving high-yielding irrigated orchards (4.0–10.0 tones ha^{-1}) designed for harvest with trunk-shakers, and with 200–450 trees ha^{-1} (Tous et al., 2014; Silveira et al., 2018; Morgado et al., 2020). More recently, high intensive irrigated hedgerow systems have been developed, using highly productive dwarf varieties and densities of 1,000–2,500 trees ha−1, which facilitate the use of continuous over the row mechanical harvesters and the achievement of very high yields (8.5–10.5 tons ha^{-1}) within only 3–4 years after planting (Tous et al., 2014; Connor et al., 2014; Silveira et al., 2018; Morgado et al., 2020). Besides, changes in orchard structure and mechanization levels, the intensification of olive production is associated with higher inputs of inorganic fertilizers and pesticides (Tous et al., 2014; Sánchez-Martínez and Cabrera, 2015; Infante-Amate et al., 2016; Russo et al., 2016; Morgado et al., 2020). At present, the high intensive olive production systems are fast expanding in the Mediterranean region, either replacing traditional orchards or occupying areas formerly used to produce other crops (Herrera et al., 2015; Sánchez-Martínez and Cabrera, 2015; Infante-Amate et al., 2016; Morgado et al., 2020). Although this production intensification process is contributing to improve farmer's incomes and the global competitiveness of the olive sector, it is raising increasing concerns on the sustainability of olive farming (Moreira et al., 2019). Therefore implementation of innovative agricultural practices, methods and concepts which introduce sustainable orchard management is essential. One of the most recent concepts in this regard is precision farming. Precision farming practices, also known as precision agriculture or site-specific farming, have been used within agriculture for several decades, but within the past few years have become more common (Webber et al., 2019). Precision farming aims to utilize technology to record and manage the variation of crops and soils within a field, thus reducing surplus inputs (e.g. fertilizer), increasing yields and aiding environmental sustainability (Morgado et al., 2020). Precision farming represents a new level of high-resolution data collection on farms with regard to soil mapping, soil nutrient analysis and crop growth data. In the other word, precision farming with monitoring and real time actions enables farmers to know precisely what parameters are needed for a healthy crop, where these parameters are needed and what amount at a particular instance of time (Shafi et al., 2019). In order to improve the efficiency of the data collection procedure, and to improve the precision with which agricultural operations are managed, it is helpful an automated system that collects data, especially to record long-term and up-to-the-minute fluctuations (Jiang et al., 2008). Thus, continuous monitoring and collecting data is a

fundamental component in precision agriculture. Monitoring is a systematic approach of supervision of activity along with regular collection and analyzing of data. The aim of continuous monitoring in the olive orchard is to obtain orchard properties for real time optimization of orchard performance. In the olive orchards several types of data can be collected during the growing season either from micro-climate, soil, plant and fruit (Fernández, 2014; Zude-Sasse et al., 2016). Among these data types, fruit and plant-based data are the most mainstream of continuous measurement methods. In soil plant atmosphere continuum (SPAC), plants play an interface role between soil and environment, and its physiological response is a combination of results of both soil and environment (Measham et al., 2014; Fernández, 2017; Scalisi et al., 2020). Besides, olive fruit represents the actual goal of production, whereas olive fruit growth is the result of diverse genetic, metabolic, hormonal and environmental interactions (Gucci et al., 2009) therefore, optimal fruit growth is caused by efficient physiological conditions on trees (Boini et al., 2019). Consequently, olive fruit and plant monitoring could be prominent aspects of olive orchard management. There are several different ways for categorizing current continuous monitoring systems of olive orchards such as technological point of view, application area, etc. (Zude-Sasse et al., 2016). According to research of Zude-Sasse et al. (2016) applicable sensor platforming orchards range from satellite, autonomous platform, unmanned aerial system to stationary sensor at the tree. The possible platforms for continuous monitoring in orchards are satellite and stationary sensors at the tree. However, continuous or frequent satellite scanning during a season can be problematic due to cloud cover and/or other limitations/uncertainties associated with the sensor platform (e.g., revisit period) (Primicerio et al., 2012; Sishodia et al., 2020). Additionally, recent findings (Fernández, 2014, 2017; Scalisi et al., 2017, 2020) mentioned that for continuous monitoring, In most cases, sensors are installed on aboveground organs such as trunk, stem, leaves and fruit. With consideration of different categorizing methods of continuous monitoring and according to our goals, the stationary sensor at different aboveground organs of the tree was considered a prominent categorizing approach for this paper. Sishodia et al. (2020) suggested that stationary sensors (ground-based) platforms can be classified into three categories of hand-held, free standing in the field as well as mounted on tractor or farm machinery. Recent research (Sishodia et al., 2020) mentioned that ground-based systems are located in close proximity to the object (organ) surface and counted as proximal remote sensing. The only fitted category for continuous ground-based monitoring is free standing in the field. As a result, for tailor approach, the continuous monitoring through the free standing in the field platform has been described for each organ.

Therefore taking into account the significance of continuous plant-based monitoring at precision agriculture and the necessity of application of them in the olive groves, the present paper contributes to having an overview on the continuous olive tree and fruit monitoring via ground-based sensor platforms in intensive olive orchards. The rest of article is presented as follows: section 2 describes continuous trunk/stem-based monitoring in olive; section 3 presents continuous leaf-based monitoring in olive; section 4 presents continuous flower-based monitoring in olive; section 5 presents continuous fruit-based monitoring in olive; section 6 describes continuous canopy-based monitoring in olive; section 7 describes combination of sensors for continuous monitoring in olive; section 8 describes soft computing development; outlook and conclusion is presented on the section 9.

2.3 Trunk/Stem-Based Monitoring in Olive

Sap flow (SF) was considered as one of the most common continuous trunk/stem-Based measurement parameters for olive. SF defined as a movement of fluid through xylem tissues and thermometric methods of tracing fluid movement through xylem tissues have been called sap flow methods (Burgess and Dawson, 2008; Forster, 2017). For the first time SF measurement in olive carried out by Moreno et al. (1996). But, due to the research of Fernández et al. (2018) the continuous measurement of SF has been done later for evaluation of olive water status and monitoring water stress and for scheduling irrigation. Production of highly precise instruments for accurate measurement of sap flow has been developed and there are various experimental as well as commercial instruments (Smith and Allen, 1996; Vandegehuchte and Steppe, 2013; Forster, 2017). Findings by Smith and Allen (1996) and Forster (2017) described that, Sap flow measurements are mostly conducted with sensors based on thermal dissipation (or heat dissipation) (TD), heat balance (HB), or heat pulse velocity (HPV) methods. Nevertheless, some researchers (Steppe et al., 2010; Fernández et al., 2018) added heat field deformation (HFD) sensor as another important SF sensor. Sap flow sensors are helpful as they can potentially estimate transpiration rate without the need for sensor calibration. Consequently, sensors can be employed across disparate species, with different anatomies, saving the time and expense of laborious calibrations (Forster, 2017). The most demanding point related to SF method is related to installation; most of the SF methods suitable for fruit trees are invasive, such that sensors must be located within the trunk of the trees (Fernández, 2014; López-Bernal et al., 2017). In olive, SF sensors measure a wide range of flow rates, including low, zero, and reverse flows (Testi and Villalobos, 2009; Nadezhdina et al., 2012; Green and Romero, 2012; Ferreira et al., 2013). Depending on the method, the sensors usually consist of two to four thin needles which measure the temperature variations at one or several points after or during the application of heat (one of the needles is always a heater), with sap velocity being subsequently estimated from the temperature changes in response to heating (López-Bernal et al., 2017). The thermal dissipation, heat balance and heat field deformation require continuous heat application to the plant and measure mass heat flow whereas heat pulse velocity methods require a periodic pulse of heat and measure its velocity (Steppe et al., 2010; Forster, 2017). Significant amount of research has demonstrated that sap flow sensors are not reliable in direct estimations of transpiration (Forster, 2017). In fact, sap flow rate demonstrates transpiration dynamics that depend on stomatal activity and environmental variables (Scalisi et al., 2019), and for calculation of sap velocity and sap flow from sensor data, conversion factors are required (Forster, 2017). Continuous measurement of SF in olive orchard (Table 2.1) has been applied for detecting water stress (Fernández et al., 2001, 2011; Diaz-Espejo et al., 2012; Cuevas et al., 2013; Hernández-Santana et al., 2016; Marino et al., 2021), monitoring water status (Nadezhdina et al., 2007; López-Bernal et al., 2012; Vandegehuchte et al., 2012) as well as precision irrigation (Nadezhdina et al., 2007; Vandegehuchte et al., 2012; Egea et al., 2017). Application of SF methods also consist of some uncertainties and limitations. The common sources of error in SF measurement are wounding of xylem tissue, probe misalignment, sapwood radial and azimuthal variability as well as wood thermal diffusivity (Green et al., 2003; Fernández et al., 2006 ; Forster, 2017). Recently, noticeable studies have been done

on improving SF methods such as single-probe heat pulse by López-Bernal et al. (2017) nevertheless, further investigations need to be done to promote more accurate SF methods.
Another continuous monitored parameter for olive is xylem sap concentration. The main target is assessment of nutrient availability and to minimize agriculture dependency on mineral fertilization and/or face nutrition stress (Amato et al., 2021). The organic electrochemical transistors (OECT) device examined by Amato et al. (2021) to estimate ion accumulation rate in leaves, and demonstrated that the signal response of an OECT sensor is inversely proportional to the water flux density flowing-through the transpiring tree. OECTs are devices based on a semiconductor, typically an organic polymer, that is permeable to the ions of a solution and can be doped/dedoped by those ions under the action of an external voltage (Gentile et al., 2020). Findings by Amato et al. (2021) suggested that OECT output should be analyzed according to the time of day (i.e., "morning", "afternoon", "night"), beside, possible hysteresis pattern versus Vapor pressure deficit (VPD) should be considered. Application of OECTs is attracting attention for their potential, however, with consideration of xylem tissue as a live material, it is faced with some challenges. Xylem consists of diverse specialized, water-conducting cells with variation of conformation, resistance and conductivity (Gentile et al., 2020; Amato et al., 2021). It may change over the time depending on the sap content of the plant, and in turn may depend on external factors, such as irrigation (Gentile et al., 2020). Consequently, time, space and spice dependency should be taken into account (Coppedè et al., 2017; Gentile et al., 2020; Amato et al., 2021).

Table 2.1: Continuous trunk/stem-based measurement which was applied on olive.

Parameter	Sensor/Method	Purpose	References
SF	TD	Mild water stress detection	Marino et al., 2021
	TD	Water status, precision irrigation	Vandegehuchte et al., 2012
	HFD	Water status, precision irrigation	Nadezhdina et al., 2007
	HB	Perecision irrigation	Agüero Alcaras et al., 2016
	HPV	Water stress assessment	Fernández et al., 2001 and 2011; Diaz-Espejo et al., 2012; Cuevas et al., 2013
	HPV/Has not been mentioned	Financial assessment of Perecision irrigation	Egea et al., 2017
	HPV/Compansated heat-pulse	Water stress assessment	López-Bernal et al., 2010 and 2012; Hernández-Santana et al., 2016
	HPV/Compansated heat-pulse	Development of SPHP method	López-Bernal et al., 2017
SC	OECT	Ion accumulation rate	Amato et al., 2021
TDV	LVDT/MDS	Water stress assessment	Cuevas et al., 2010
	LVDT/Has not been mentioned	Financial assessment of Perecision irrigation	Egea et al., 2017
	LVDT/MDS & TGR	Water status	Moriana et al., 2010
	LVDT/MDS & TGR	Perecision irrigation	Girón et al., 2015a
	LVDT/TGR & MXTD	Perecision irrigation	Agüero Alcaras et al., 2016
	LVDT/MDS & TGR	Water stress assessment	Girón et al., 2015a
	LVDT/MDS & MXTD	Water stress assessment	Fernández et al., 2011; Cuevas et al., 2013
	Strain gauge/TGR	Water stress assessment	Martín-Palomo et al., 2021
Trunk surface	Camera (RGB) / Deep learning	Olive disease (Canker)	Alruwaili et al., 2019

The trunk diameter variations (TDV) are daily cycles of swelling and shrinking which depends on the hydration level of the plant (Girón et al., 2015a; Fernández et al., 2018) and reported for the first time in the second half of the 20th century (Klepper et al., 1971; Martín-Palomo et al., 2021). This cycle is produced for the lag between transpiration and root uptake that is partially compensated with the water of the trunk (Moriana et al., 2010).

Daily TDV varies from a few tens of micrometers to a few hundred micrometers (Fernández et al., 2018), consequently, the significance of a highly precise instrument (dendrometer) for accurate TDV measurement is obvious. The appearance of electronic devices permitted accurate measurements of daily TDV (Kozlowski, 1967; Ortuño et al., 2010). There are several different ways for categorizing dendrometers such as technological point of view, measurement type (contact and noncontact) and other (Clark et al., 2000; Dangare et al., 2018). The most commercially available sensors for Micrometric TDV measurements are Linear Variable Displacement Transducer (LVDT) and strain gauge type (Ortuño et al., 2010). LVDT is the sensor that transduces the movement of the trunk/stem in electrical signals. The trunk moves an electromagnetic rib that is between two electrical circuits, one charged with continuous power and other which is off. The movement of the rib produces an induced electrical power that is linearly related with the displacement (Ortuño et al., 2010). Strain gauge is the sensor that transforms fluctuation of the trunk/stem to electrical resistance (Link et al ., 1998; Ortuño et al., 2010). Strain gauge is a physically simple device, which can easily be applied in a straightforward manner for elementary measurement of surface strains (Hannah and Reed, 1992). It is a caliper style gauge that sensor mounted on the flexible frame then provides an electrical output proportional to applied force (translate trunk/stem deformations) (Hannah and Reed, 1992). The main obtained indicators from TDV are maximum daily shrinkage (MDS), trunk growth rate (TGR) and maximum trunk diameter (MXTD) (Table 2.1). TDV employed in olive orchards to assess water stress and to schedule irrigation (Girón et al., 2015a; Agüero Alcaras et al., 2016; Fernández et al., 2018). Cuevas et al., 2010) mentioned that the first paper published by Michelakis (1997) on the use of TDV to optimize irrigation scheduling in olive by evaluating the response of MDS and TGR. In olive trees, MDS is not reported as a useful indicator, while TGR is considered an early water stress detector (Girón et al., 2015a; Fernández et al., 2018). Nevertheless, the range of daily TGR variations are too wide in olive trees, so patterns and differences are not always clear (Girón et al., 2015a; Agüero-Alcaras et al., 2016; Corell et al., 2019; Martín-Palomo et al., 2021). Such variations were only partially related to changes in the evaporative demand (Girón et al., 2015a; Corell et al., 2019). Besides, relationship between TGR and water potential was not simple and, even in full irrigated trees, values of TGR could be changeable (Corell et al., 2019; Martín-Palomo et al., 2021). Findings by Corell et al. (2017) suggested that TGR was real indicator of water stress only when values of it was lower than − 0.1 mm day− 1. MXTD, as another important index driven from TDV monitoring, was investigated in some researches (Fernández et al., 2011; Agüero Alcaras et al., 2016). Recent researches suggested that the monitoring of MXTD was useful to indicate the onset, and severity, of water stress in deficit irrigated olive trees. Lastly, trunk diameter fluctuations are affected by plant age and size, crop load, environmental variables and growth patterns (Fernández, 2017). In this sense, choosing an exact dendrometer, employing effective TDV indicators as well as precise analyzing of outcomes is necessary.

Application of trunk/stem surface monitoring for disease detection has also been presented. Plant diseases adversely influence both the quality and quantity of crop production. Thus, the early detection of such diseases proves efficient in enhancing the crop quality and reducing the production loss (Alruwaili et al., 2019). Recent research developed a deep learning model that could achieve an overall accuracy of 99.1% to detect Canker. However, it did not perform continuous monitoring, and developed a model by RGB image from a

plant-village dataset but It explained that classification during testing runs quickly in a few seconds even on a CPU. Therefore, the model could be easily implemented on a smartphone. Consequently, a combination of this method with RGB cameras could be applied in real-time continuous monitoring of trunk/stem surface in orchards.

2.4 Leaf-Based Monitoring in Olive

The leaf is one of the most important organs of the plant with key functionalities such as photosynthesis, controlling transpiration rate, several metabolic activities, etc. (Hamed et al., 2021). Besides, the appearance of leaves could address some abnormality in plants including lack of nutrients, disease and pest effect.

In the last few years, many researchers suggested continuous monitoring of olive leaf water status by leaf patch clamp pressure (LPCP) probe (Table 2.2), both to assess plant water stress and to schedule irrigation (Fernández et al., 2018; Scalisi et al.,2020; Marino et al., 2021). LPCP for the first time, as a novel and non-invasive online monitoring leaf-based probe, was introduced in 2008 by Zimmermann (Zimmermann et al., 2008). The technology includes a miniaturized silicone pressure sensor integrated into a spring clamp that is clamped to a patch of an intact plant leaf. The patch clamp pressure probe measures the attenuated pressure response of the leaf patch upon the application of a constant, clamped pressure (Zimmermann et al., 2008). Indeed, the output of LPCP probes is expressed as attenuated pressure of leaf patches (Pp), which is inversely related to cell turgor pressure (Pc) (Zimmermann et al., 2008; Fernández et al., 2011b; Scalisi et al., 2020). The shape of the daily Pp curve has been employed as an indicator for tree water status (Fernández et al., 2018; Scalisi et al.,2020; Marino et al., 2021). However, consideration of the factors that affect the tree response to water stress, such as genotype, management, orchard characteristics, and location is an important aspect of employing published data of daily Pp curve (Fernández et al., 2018). The long term application of LPCP might damage leaf cuticle and alter measurements (Scalisi et al., 2017). In addition, Brunetti et al. (2022), explained that water stress can be detected by LPCP probes only when trees have already activated physiological changes in tissue mechanical properties and osmotic adjustments, consequently, to early detection of olive tree response to water stress, it introduced novel sensor based on photon attenuation of radiation through the leaf. The sensor is a non-invasive tool for measuring leaf water content through the measurement of the absorption of radiation when this propagates through the leaf tissues (Brunetti et al., 2022). It mentioned that an early detection of tree response to water stress could be provided by assessment of the changes in leaf water status under deficit irrigation regime. But, the future development of this technique is needed for commercial use in water status detection and automatic irrigation (Brunetti et al., 2022).

Stomatal conductance (g_c) is another important parameter, however, it cannot be automatically and continuously recorded (Fernández et al., 2018). Nevertheless, some researchers demonstrate that it could be estimated continuously through other plant-based sensors. Hernández-Santana et al. (2016) employed heat pulse velocity (HPV) sensor and showed the possibility of estimation of (g_c) in olive trees automatically and in-continuous under field conditions by using sap flux density data directly without need of up-scaling to tree transpiration. Then after, Rodriguez-Dominguez et al. (2019) combined HPV and

LPCP probes and demonstrated that measurement of leaf turgor pressure can be used to infer the large variability in maximum stomatal conductance under moderate drought conditions in an olive hedgerow orchard.

Olive disease detection by leaf monitoring has been explained by many researchers (Al-Tarawneh, 2013; Cruz et al., 2017; Alruwaili et al., 2019) (Table 2.2). The leaf level monitoring provides a relatively pure signal of symptoms caused by a disease, which helps understand their spectral responses (Zhang et al., 2019). Optical sensing techniques are useful in identifying primary disease foci (Mahlein, 2016). Optical sensors range from RGB, multispectral, hyperspectral, thermal, chlorophyll-fluorescence as well as 3D-sensors (Mahlein, 2016; Zhang et al., 2019). The problem in the implementation of sensors is related to the large amount and complexity of collected data, therefore, to achieve accurate results, advanced data analysis and statistical methods are essential (Mahlein, 2016). However, data mining methods and deep learning techniques have been widely employed for accurate data assessment (Al-Tarawneh, 2013; Mahlein, 2016 ; Cruz et al., 2017; Alruwaili et al., 2019; Zhang et al., 2019). Deep learning technique was applied by Alruwaili et al. (2019) to detect Peacock Spot disease in olive orchards. It analyzed RGB images and demonstrated high overall accuracy (99.1%) in disease detection. Peacock Spot disease in olive orchards also was examined by Uğuz and Uysal (2021). In addition, they worked on Aculus olearius, an important olive mite pest in Turkey. They analyzed a data set consisting of 3400 olive leaves samples and pointed out that Aculus olearius and olive peacock spot diseases can be identified at a high accuracy rating without necessitating an expert in the field.

Olive quick decline syndrome (OQDC) caused by Xylella fastidiosa is another investigated disease. Cruz et al. (2017) developed an algorithm that detected OQDS with a true positive rate of 98.6 ± 1.5% in testing, showing great potential for image analysis for this disease. It demonstrates that it is possible to automatically detect leaf scorch in olive trees from leaf clipping images and that it can be discriminated against by other disorders or pathogens, despite the strong similarity (Cruz et al., 2017). However, recent research mentioned that this disease detection algorithm could not obtain specificity and sensibility of traditional diagnostic methods such as ELISA or qPCR. Finding by Zhang et al. (2019) suggested a general framework which may provide a reference in monitoring not only known but also any unknown diseases or pests. It mentioned that main challenges in monitoring plant disease and pests could be categorized as 1) the detection of plant diseases or pests at an early stage, 2) accurately detect a specific disease/pest under realistic field conditions, 3) continuously track the dynamics of the diseases or pests at a fine resolution as well as 4) data and information sharing. All mentioned researches related to olive disease detection by leaf monitoring (Cruz et al., 2017; Alruwaili et al., 2019; Uğuz and Uysal, 2021) have a great potential to use in field condition and with coupling with RGB camera could be utilized in real-time continuous monitoring in orchards.

Table 2.2: Continuous leaf-based measurement which was applied on olive.

Parameter	Sensor	Purpose	References
Cell turgor	LPCP	Water status	Fernández et al., 2011b; Scalisi et al., 2020
	LPCP	Mild water stress detection	Marino et al., 2021
	LPCP	Fruit growth mechanism	Hernandez-Santana et al., 2021
Relative water contenct and water potential	Leaf water meter	Water status	Brunetti et al., 2022
Leaf surface	Camera (RGB)	Peacock spot	Alruwaili et al., 2019; Uğuz and Uysal., 2021
	Camera (RGB)	Aculus olearius	Uğuz and Uysal.,2021
	Camera (RGB)	Olive quick decline syndrome	Cruz et al., 2017

2.5 Flower-Based Monitoring in Olive

Olive flowering has been investigated in several researches (Mancuso et al., 2002; Milicevic et al., 2020; Garrido et al., 2020) with different aims. For instance, Milicevic et al. (2020), used deep learning to analyze images of RGB cameras to accurately detect olive tree flowering phenophase. It showed the final classification accuracy of 97.2%. This means that the entire process is viable and applicable under real conditions (Milicevic et al., 2020). Olive phenology is a sensitive indicator of climatic warming, besides detection of it represents an important parameter for applying various agricultural procedures (Osborne et al., 2000; Milicevic et al., 2020). For example, a specific protection product may have an optimal application date when 5% of the flowers have opened. For an individual micro location, the application time window can be limited to only 2 to 3 days, which requires the precise and timely detection of crop phenophases (Milicevic et al., 2020).

2.6 Fruit-Based Monitoring in Olive

Fruit monitoring has numerous applications like fruit recognition (detection), growth assessment as well as water stress assessment. Various approaches to fruit recognition have been introduced (Saedi et al., 2020). These are mostly dependent on the visual characteristics of the fruits, and the associated method is responsible for distinguishing fruits from other objects using image processing techniques. This is a challenging task, since the environmental effects like complex background, variable light (Feng et al., 2019), overlaps and occlusions with other plant parts (Wang et al., 2017) make it difficult to recognize fruits accurately. Other challenges are about the generalization property as well as the running time of a method, meaning that a proposed algorithm should be able to recognize different kinds of fruits in real-time for on-the-go applications (Saedi et al., 2020).

Real-time and accurate on-branch fruit recognition could facilitate Precision horticulture practices (Saeidi et al., 2020). The main goals of olive fruit detection are ripening stage assessment, accurate fruit load determination, fruit quality control, orchard yield mapping, mechanized/robotic fruit harvesting, fruit tree disease treatments, and precise agronomic and agrochemical applications (Pourreza et al., 2015; Sa et al., 2016; Amatya et al., 2016; Gené-Mola et al., 2019; Wu et al., 2019; Saeidi et al., 2020; Khosravi et al., 2021a). The most common method for assessing the olives' maturity is based on the visual

determination of the maturity index (MI); it includes evaluating skin and flesh color changes as the fruit matures and classifying them by color (Camposeo et al., 2013; Khosravi et al., 2021a).

Olive maturation could be investigated by application of optical sensors (range from RGB to hyperspectral camera) or extensimeter (synonym of fruit gauge). There are several ways of analyzing collected data including application of deep learning methods or statistical analysis. For instance Khosravi et al. (2021a) used deep learning methods to analyze RGB images for ripening assessment and reached an accuracy of 91.9 %. Another researcher (Khosravi et al., 2021b) combined RGB camera with extensimeter and used the LabelBox platform (Labelbox Inc., San Francisco, CA, USA) to analyze images for both ripening assessment and fruit detection. Besides, it evaluated daily fruit growth pattern versus vapor pressure deficit (VPD) as one the most significant environmental variables. It performed statistical analysis and suggested that visualization of hysteresis curve, in normalized daily diameter versus VPD, can be a tool to translate measured data to precise phenological phases of fruit growth.

The fruit gauge detects fruit growth dynamics continuously and output has various applications. For instance Fernandes et al. (2018) confirmed that olive fruit growth is sensitive to water stress and shows a remarkable capacity to recover following the employed irrigation strategy. Scalisi et al. (2020) and Marino et al. (2021) applied fruit gauge for water status assessment in olive orchards. Tracking fruit growth could serve as a promising approach to schedule regulated deficit irrigation. Moreover, fruit growth is a highly relevant variable to measure because of its relationship to fruit yield (Fernandes et al., 2018). Khosravi et al. (2022) performed different deficit irrigation regimes and tracked third phase of fruit growth by mounting extensimeter on four olive cultivars. It showed a hysteretic pattern of daily fruit diameter variation versus VPD and suggested that hysteresis magnitude changes can be used as a quantitative index of water stress. Indeed, it considered height of hysteresis curves as a quantitative index and showed a significant reduction of height of hysteresis curves by irrigation treatments which were not cultivar-specific (Table 2.3).

Disease detection, as another application of fruit monitoring, has been performed by some researchers. Alruwaili et al. (2019) via deep learning methods analyzed images of RGB cameras. Recent research suggested a deep learning model which detected Lepra fruit rot, Parlatoria oleae as well as Aspidiotus nerii with an overall accuracy of 99.1%.

Table 2.3: Continuous fruit-based measurement which was applied on olive.

Parameter	Sensor	Purpose	References
Fruit skin color	Camera (RGB)	Ripening assessment	Khosravi et al., 2021a; Khosravi et al., 2021b
Fruit growth (diameter)	Fruit gauge	Water status	Fernandes et al., 2018; Scalisi et al., 2020; Marino et al., 2021; Khosravi et al., 2022
		Phenological phase detection	Khosravi et al., 2021b
		Fruit growth mechanism	Hernandez-Santana et al., 2018 and 2021
Fruit surface	Camera (RGB)	Lepra fruit rot, Parlatoria oleae, Aspidiotus nerii	Alruwaili et al., 2019

2.7 Canopy-Based Monitoring in Olive

Canopy is not an individual organ, but, according to the importance of it, many ground-based continuous monitoring has been performed on it. It investigated various aims including, water status assessment, scheduling precision irrigation, pruning and training systems, disease and pest monitoring, integrated pest management as well as nutrition stress monitoring. Moreover, evaluation of the canopy in olive orchards could be well adapted for focused specific intervention (e.g., presence of cold damage) (Assirelliet al., 2021). For instance, Assirelli et al. (2021) investigated on evaluations of canopy in terms of the differential canopy index (delta CI). It showed different distribution of the canopy thickness (reduced and developed) which is helpful for the verification of the possibility of the practical application such as manual pruning intervention which sees the main advantage in indicating the points and intensity of intervention and avoiding the continuous direct field control of the operators (Assirelli et al., 2021). In addition, canopy level monitoring can collect information that can be linked well with observations acquired by other sensor platforms such as airborne or satellite platforms (Zhang et al ., 2019; Assirelli et al., 2021).
Canopy temperature has long been recognized as an indicator of plant water availability (Gates, 1964; Agam et al., 2013). With consideration of technological developments, there is a great potential to acquire information on surface temperature, and thus facilitate mapping of canopy temperature variability over different scales from local (e.g., mounting an infrared thermometer on an elevated device) to regional (satellite images covering large areas, but at the expense of lower spatial resolution) (Agam et al., 2013). Canopy temperature is determined not only by the water status of the plant, but also by environmental conditions. Therefore, In order to use canopy temperature as a water status indicator it must be normalized to account for the varying environmental conditions (Agam et al., 2013). For instance, crop water stress index (CWSI) has been employed by Agam et al. (2013) to characterize water status dynamics of olive trees as they enter into and recover from stress, and on a diurnal scale. The empirical and analytical CWSI were calculated based on canopy temperature extracted from high resolution thermal images. It used an uncooled infrared thermal camera which was mounted on a crane about 3 m above the canopy. Tree canopy temperatures were determined by averaging pixels extracted from the central area of the canopy. The empirical CWSI differentiated between well-watered and stressed trees, and depicted the water status dynamics during the drought and recovery periods as well as on a diurnal scale (Agam et al., 2013) (Table 2.4).
Infrared temperature (IRT) sensors is another type of sensor which applied successfully for monitoring crown temperature as an indicator of water stress (Berni et al., 2009; Zarco-Tejada et al., 2012; Calderón et al., 2013). In addition, it suggested that water stress detection could be a suitable method for early detection of Verticillium wilt (VW) in olive orchards. It applied techniques based on the detection of the effects of VW infection and colonization on water flow that eventually cause water stress effects, assessed with thermal, multispectral and hyperspectral domains (Calderón et al., 2013). It showed that canopy temperature and physiological hyperspectral indices (i.e., Photochemical Reflectance Index (PRI) and chlorophyll fluorescence) are related with physiological stress caused by VW and suggested that crown temperature and CWSI are good indicators to detect VW at early stages of disease development (Calderón et al., 2013) (Table 2.4).

Automatic real-time monitoring of the pest is another aspect of canopy monitoring. It provides accurate information about the abundance of the targeted pest, and when geolocated, to a better understanding of the spatial and temporal distribution of the pest (Jiang et al., 2008; Miranda et al., 2019). Indeed, automatic real-time monitoring improved the efficiency of the data collection procedure and with time-sensitive gathering of information including pest population dynamics and the related ecological factors, the precision pest control or Integrated pest management at the right time in the right place is accessible (Jiang et al., 2008; Ding and Taylor 2016; Miranda et al., 2019; Cardim Ferreira Lima et al., 2020).

Olive fruit fly is one of the important pests of olive which if not controlled, fruit damage due to it can reach up to 90–100% (Tzanakakis, 2003; Miranda et al., 2019). Olive fruit fly management by electronic traps (e-traps) has been investigated in several researches to pest detection and counting (Ding and Taylor, 2016; Miranda et al., 2019). However, coupling e-traps with deep learning techniques was one step further. Whereas, manual counting and identification of the pest captured on digital images which is labor intensive, slow, expensive, and sometimes error-prone, has been substituted by deep learning techniques (Ding and Taylor, 2016). Miranda et al. (2019) developed electronic traps for monitoring the spatial and temporal distribution of the olive fruit fly (Table 2.4), but it still requires human intervention for counting. Ding and Taylor (2016) presented an automatic method for monitoring pests from images taken inside field traps, where a convolutional neural network is applied to image patches to determine the probability of containing a specific pest type. It applied to a commercial codling moth dataset, and showed promising performance both qualitatively and quantitatively. Another researcher Jiang et al. (2008) developed a monitoring system to remote wireless measurements of environmental parameters and population dynamics of the oriental fruit fly in real-time. It showed reliability of about 95%. The major contribution of recent study was that it makes large scale, long distance, and long-term monitoring for agricultural information achievable. High spatial and temporal resolutions for monitoring the data of the oriental fruit flies with respect to environmental changes. Overall, real-time continuous monitoring system is an significant part in integrated pest management (IPM) practices, and the efficiency of monitoring system is resulted by accurate data collection and applying appropriate method of data analysis (Jiang et al., 2008; Cardim Ferreira Lima et al., 2020).

Table 2.4: Continuous Canopy-based measurement which was applied on olive.

Parameter	Sensor	Purpose	References
Canopy temperature	Infrared thermal camera	Water status	Agam et al., 2013
	Infrared temperature (IRT) sensors	Water status	Berni et al., 2009; Zarco-Tejada et al., 2012; Calderón et al., 2013
	Multispectral and hyperspectral domains	Verticillium wilt (VW)	Calderón et al., 2013
Captured pests	Electronic traps (e-traps)/ Deep learning	Olive fruit fly	Ding and Taylor, 2016; Miranda et al., 2019
	Electronic traps (e-traps)	Olive fruit fly	Jiang et al., 2008

2.8 Combination of Plant-based Sensors

One of the main solution to face with challenges is combination of different kind of plant-based sensors for continuous monitoring (Fernández et al., 2011a; Cuevas et al., 2013; Scalisi et al., 2020; Marino et al., 2021)

The Integration of sap flow sensors with trunk dendrometer sensor has been investigated by several researchers (Fernández et al., 2011a; Cuevas et al., 2013) to water status assessment of olive. Integration of SF and TDV sensors lead to better understanding of water flow kinetics within the tree, however, there is some critical point in implementation of them including difficulty to replicate continuous measurements on large numbers of trees (Marino et al., 2021), identification of accurate location and number of the instrumented trees (Fernández et al., 2011a; Cuevas et al., 2013), knowledge of cultivar-specific physiological response to water stress as well as cultivar-specific threshold and indices for water stress detection. Among all mentioned issues, detection of cultivar-specific indices or parameters is more crucial. For instance Fernández (Fernández et al., 2011a) suggested that in water stress detection of old, big “Manzanilla” trees with heavy fruit load, simultaneous use of maximum trunk diameter (DMXTD) and DEp values (daily difference of daily plant water consumption between the each deficit irrigation treatment tree and the full irrigated tree) provides more accurate information. Whereas Cuevas et al. (2013) showed same results on the heavy fruit load Arbequina trees but mentioned that the reliability of the DMXTD index was poorer than that of DEp. Recent research explained peculiarities on the response DEp to changes in water stressing conditions. Consequently, as thresholds of indices are different in various water stress conditions and environmental stress conditions, the user should take action to set and use correct indices. Moreover, soil water-holding condition and cultivar-specific drought resistance mechanisms should be considered. Interestingly, Fernandez et al. (2011a) demonstrated hysteresis pattern on daily behavior of sap flow versus trunk diameter and mentioned that with the most demanding atmospheric conditions, hysteresis pattern is more obvious, however it did not investigate on magnitude of hysteresis curve and did not suggest any quantitative index for water stress assessment by hysteresis phenomenon. Several characteristics and rotational patterns of hysteresis curves in plant-based sensors have been investigated (Khosravi et al., 2021b and 2022), and have been used to tentatively set quantitative index for water status assessment in olive

orchard (Khosravi et al., 2022). Application of hysteresis concept for analyzing the sensor's output could be a useful solution, although further investigation should be done for pattern recognition and accurate model development.

Another common combination of sensors to measure plant water status, is related to detection of midday stem water potential (Ψstem) (Ahumada-Orellana et al., 2017; Marino et al., 2018 and 2021; Scalisi et al., 2020). However, the reported values of Ψstem are not consistent (Marino et al., 2018). The lack of consistency transformed it to cultivar-specific indexes which should be modified according to different genotypes and under different environmental conditions. Research by Marino (Marino et al., 2018) suggested three different levels of stress represented by thresholds in Ψstem values which were above about −2.0 (MPa) for no stress, between about −2 and −3.5 (MPa) for moderate stress and below about −3.5 (MPa) for high stress levels. Another research by Girón et al. (2015b) identified Ψstem threshold of −2.5 (MPa) for moderate stress during the second phase of olive fruit growth (pit hardening) and explained different physiological response of tree during the period of moderate stress. In addition Scalisi et al. (Scalisi et al., 2020) examined 2 olive cultivars during second and third phases of fruit growth and demonstrated diverse threshold of Ψstem during different growth phases. Besides, threshold of Ψstem was not same among the different cultivars. The differences of Ψstem threshold among the different cultivars caused by different drought resistance mechanism of each cultivar which highlighted need for genotype-specific models in olive. Other uncertainty regarding the use of Ψstem thresholds for irrigation is related to set of accurate threshold to suppress yield reduction (Ahumada-Orellana et al., 2017). Finding by Ahumada-Orellana et al. (2017) explained that thresholds around −3.5 (MPa) did not have significant effect on the yield reduction in the olive trees (cv. 'Arbequina'), but Moriana et al. (Moriana et al., 2012) observed 30% yield reduction in olive trees (cv. 'Cornicabra') at Ψstem below −2.0 (MPa). Trentacoste et al. (Trentacoste et al., 2015) explained that fruit yield for olive trees (cv. 'Frantoio') at Ψstem around −2.5 (MPa) was statistically similar to the control. Although Ψstem optimized irrigation scheduling but need further development to become index for precise irrigation scheduling. Besides, it is generally obtained by the Scholander pressure chamber, which does not allow for continuous monitoring and automated irrigation (Scalisi et al., 2020). To set precise threshold of Ψstem, continuous monitoring of water flow's kinetics between stem, leaves and fruits is necessary (Marino et al., 2021). This necessity prompted integration of leaf patch clamp pressure (LPCP) with fruit gauge and sap flow sensors.

Scalisi et al. (2020) measured Ψstem and at the same time used LPCP with fruit gauge. It suggested equation for the daily prediction of Ψstem based on relative rates of fruit diameter change (RR_{fruit}) and relative rates leaf pressure change (RR_{leaf}). This research also emphasized on various strategies of fruit and leaf water exchanges in droughted trees. Interestingly, it showed anti-clockwise hysteretic relationships between (RR_{fruit}) and (RR_{leaf}) and briefly explained daily magnitude change of hysteresis curves, however did not present any quantitative index for water stress assessment through the hysteresis phenomenon. Marino et al. (2021) combined sap flow sensor, LPCP and fruit gauge and suggested that monitoring continuously leaf, fruit, and stem water dynamics can help detect desirable water stress levels in olive earlier than a single commonly used indicator of water stress.

2.9 Soft Computing Development

Ground-based sensor platforms are able to collect large amounts of data which should be analyzed by effective approaches. In the past many analyzing techniques were based on a hard computing approach. The hard computing approach works on exact input data by sequential computing method to produce precise outcomes. However, in the real world which we face with many uncertainties, probabilities and pervasive imprecisions (Zadeh, 1998a) in collected (input) data. Therefore, the necessity of novel approach was beneficial. On the opposite of hard computing the term of soft computing (SC) was introduced. SC is a combination of methodologies such as fuzzy logic, neurocomputing, genetic computing and probabilistic computing which provide for the conception, design and deployment of intelligent systems (Zadeh, 1998a and 1998b). SC methods have been applied for continuous monitoring previously, however, development in mentioned methods could enhance continuous monitoring. Indeed, by advanced dynamic data analysis, accurate pattern recognition and efficient modeling, the SC is able to perform more precise data assessment. Optimize big data assessment helps researchers to create more physiologically meaningful indexes from sensor's outputs. Besides, in the case of combination of sensors, it facilitates integration of outputs.

2.10 Outlook and Conclusion

The significance of the continuous plant-based monitoring of olive orchards through the ground-based platforms and restriction aspects of them has been described. To cope with the challenges there are some points which can be mentioned. Technological advancement is moving forward rapidly which decreases the difficulty of implementation of continuous monitoring. One future development of continuous measurement is referred to parameter that is not possible to measured continuously now including stem water potential (Ψstem) or leaf gas exchange. Technological development and presenting new sensors could solve the issues. One of the novel sensor categories is Nano sensors which introduce revolutionary approaches for agriculture (Das et al., 2022). They can be applied in various agricultural fields ranging from field sensing of crops up to detection of infection long before symptoms in plants (Das et al., 2022). Another possibility is related to enhancement of intelligence systems (i.e. machine learning, deep learning etc.). It promotes more advanced data collection systems. For instance in time-sensitive cases (i.e. disease or pest detection etc.) it facilitates real-time continuous monitoring. A further utilization is the combination of non-continuous data collection systems with continuous monitoring systems. Many advanced sensing methods or platforms are not suitable for continuous monitoring (i.e. light detection and ranging (LiDAR), or unmanned aerial vehicle (UAV)), however, their outputs can increase efficiency of decisions made by continuous monitoring systems. Besides, advances in CS reduce data processing time by reducing the computational time.

In conclusion, continuous plant-based monitoring in olive orchards via ground-based platforms is useful in precision orchard management by demonstrating several tree status including water stress, nutrition, disease, pest, and fruit behavior, starting from flower and

set, growth and maturation up to harvest. Each continuous monitoring technique has its pros and cons, however accurate choosing of sensors and employment of proper data analyzing methods are essential. Technological development and SC methods enhancement accompanied by theoretical research will improve chance of implementation of continuous monitoring in olive orchards. The capacity of real-time continuous monitoring of the tree and fruit status by ground-based platforms distinguish them from other platforms. Moreover, the key point to promote continuous monitoring by ground-based platforms and provide agricultural services by them, is to integrate all type of sensor inputs (information) in a unique user-friendly platform.

References

Agam, N., Cohen, Y., Berni, J. A. J., Alchanatis, V., Kool, D., Dag, A., ... & Ben-Gal, A. (2013). An insight to the performance of crop water stress index for olive trees. Agricultural Water Management, 118, 79-86.

Agüero Alcaras, L.M., Rousseaux, M.C., Searles, P.S., 2016. Responses of several soil and plant indicators to post-harvest regulated deficit irrigation in olive trees and their potential for irrigation scheduling. Agricultural Water Management 171, 10e20.

Ahumada-Orellana, L. E., Ortega-Farías, S., Searles, P. S., & Retamales, J. B. (2017). Yield and water productivity responses to irrigation cut-off strategies after fruit set using stem water potential thresholds in a super-high density olive orchard. Frontiers in Plant Science, 8, 1280

Alruwaili, M., Alanazi, S., El-Ghany, S. A., & Shehab, A. (2019). An efficient deep learning model for olive diseases detection. International Journal of Advanced Computer Science and Applications, 10(8), 486-492.

Al-Tarawneh, M. S. (2013). An empirical investigation of olive leave spot disease using auto-cropping segmentation and fuzzy C-means classification. World Appl Sci J, 23(9), 1207-1211.

Amanpour, A., Kelebek, H., & Selli, S. (2019). LC-DAD-ESI-MS/MS–based phenolic profiling and antioxidant activity in Turkish cv. Nizip Yaglik olive oils from different maturity olives. Journal of mass spectrometry, 54(3), 227-238.

Amato, D., Montanaro, G., Vurro, F., Coppedé, N., Briglia, N., Petrozza, A., ... & Nuzzo, V. (2021). Towards In Vivo Monitoring of Ions Accumulation in Trees: Response of an in Planta Organic Electrochemical Transistor Based Sensor to Water Flux Density, Light and Vapor Pressure Deficit Variation. Applied Sciences, 11(11), 4729.

Amatya, S., Karkee, M., Gongal, A., Zhang, Q., & Whiting, M. D. (2016). Detection of cherry tree branches with full foliage in planar architecture for automated sweet-cherry harvesting. Biosystems engineering, 146, 3-15.

Berni, J. A. J., Zarco-Tejada, P. J., Sepulcre-Cantó, G., Fereres, E., & Villalobos, F. (2009). Mapping canopy conductance and CWSI in olive orchards using high resolution thermal remote sensing imagery. Remote Sensing of Environment, 113(11), 2380-2388.

Brunetti, C., Alderotti, F., Pasquini, D., Stella, C., Gori, A., Ferrini, F., ... & Centritto, M. (2022). On-line monitoring of plant water status: Validation of a novel sensor based on photon attenuation of radiation through the leaf. Science of the Total Environment, 817, 152881

Burgess, S. S., & Dawson, T. E. (2008). Using branch and basal trunk sap flow measurements to estimate whole-plant water capacitance: a caution. Plant and Soil, 305(1), 5-13.

Calderón, R., Navas-Cortés, J. A., Lucena, C., & Zarco-Tejada, P. J. (2013). High-resolution airborne hyperspectral and thermal imagery for early detection of Verticillium wilt of olive using fluorescence, temperature and narrow-band spectral indices. Remote Sensing of Environment, 139, 231-245.

Camposeo, S., Vivaldi, G.A., Gattullo, C.E., 2013. Ripening indices and harvesting times of different olive cultivars for continuous harvest. Sci. Hortic. (Amsterdam). 151, 1–10. https://doi.org/10.1016/j.scienta.2012.12.019.

Cardim Ferreira Lima, M., Damascena de Almeida Leandro, M. E., Valero, C., Pereira Coronel, L. C., & Gonçalves Bazzo, C. O. (2020). Automatic detection and monitoring of insect pests—A review. Agriculture, 10(5), 161.

Clark, N. A., Wynne, R. H., & Schmoldt, D. L. (2000). A review of past research on dendrometers. Forest Science, 46(4), 570-576.
Connor, D.J., Gómez-del-Campo, M., Rousseaux, M.C., Searles, P.S., 2014. Structure, management and productivity of hedgerow olive orchards. A review. Sci. Hortic. 169, 71–93. https://doi.org/10.1016/j.scienta.2014.02.010.
Corell, M., Martín-Palomo, M. J., Pérez-López, D., Centeno, A., Girón, I., Moreno, F., ... & Moriana, A. (2017). Approach for using trunk growth rate (TGR) in the irrigation scheduling of table olive orchards. Agricultural Water Management, 192, 12-20.
Corell, M., Martín-Palomo, M. J., Girón, I., Andreu, L., Trigo, E., López-Moreno, Y. E., ... & Moriana, A. (2019). Approach using trunk growth rate data to identify water stress conditions in olive trees. Agricultural Water Management, 222, 12-20.
Coppedè, N., Janni, M., Bettelli, M., Maida, C. L., Gentile, F., Villani, M., ... & Zappettini, A. (2017). An in vivo biosensing, biomimetic electrochemical transistor with applications in plant science and precision farming. Scientific reports, 7(1), 1-9.
Crist, E., Mora, C., Engelman, R., 2017. The interaction of human population, food production, and biodiversity protection. Science 356 (6335), 260–264. https://science.sciencemag.org/content/356/6335/260.
Cruz, A. C., Luvisi, A., De Bellis, L., & Ampatzidis, Y. (2017). X-FIDO: An effective application for detecting olive quick decline syndrome with deep learning and data fusion. Frontiers in plant science, 8, 1741.
Cuevas, M. V., Torres-Ruiz, J. M., Álvarez, R., Jiménez, M. D., Cuerva, J., & Fernández, J. E. (2010). Assessment of trunk diameter variation derived indices as water stress indicators in mature olive trees. Agricultural Water Management, 97(9), 1293-1302.
Cuevas, M. V., Martín-Palomo, M. J., Diaz-Espejo, A., Torres-Ruiz, J. M., Rodriguez-Dominguez, C. M., Perez-Martin, A., ... & Fernández, J. E. (2013). Assessing water stress in a hedgerow olive orchard from sap flow and trunk diameter measurements. Irrigation Science, 31(4), 729-746.
Das, I., Gogoi, B., Sharma, B., & Borah, D. (2022). Role of metal-nanoparticles in farming practices: an insight. 3 Biotech, 12(11), 1-18.
Díaz-Espejo, Antonio, Thomas N. Buckley, John S. Sperry, Maria V. Cuevas, Aa de Cires, Sheren Elsayed-Farag, María José Martin-Palomo et al. "Steps toward an improvement in process-based models of water use by fruit trees: a case study in olive." Agricultural Water Management 114 (2012): 37-49.
Dangare, P., Mhizha, T., & Mashonjowa, E. (2018). Design, fabrication and testing of a low cost Trunk Diameter Variation (TDV) measurement system based on an ATmega 328/P microcontroller. Computers and Electronics in Agriculture, 148, 197-206.
Ding, W., & Taylor, G. (2016). Automatic moth detection from trap images for pest management. Computers and Electronics in Agriculture, 123, 17-28.
Egea, G., Fernández, J. E., & Alcon, F. (2017). Financial assessment of adopting irrigation technology for plant-based regulated deficit irrigation scheduling in super high-density olive orchards. Agricultural Water Management, 187, 47-56.
Feng, J., Zeng, L., & He, L. (2019). Apple fruit recognition algorithm based on multispectral dynamic image analysis. Sensors (Basel, Switzerland), 19(4), 949. https://doi.org/10.3390/s19040949.
Ferreira, M.I., Conceição, N., David, T.S., Nadezhdina, N., 2013. Role of lignotuber versus roots in the water supply of rainfed olive. Acta Horticulturae 991, 181e188.

Fernandes, R. D. M., Cuevas, M. V., Diaz-Espejo, A., & Hernandez-Santana, V. (2018). Effects of water stress on fruit growth and water relations between fruits and leaves in a hedgerow olive orchard. Agricultural water management, 210, 32-40.

Fernández, J. E., Palomo, M. J., Dıaz-Espejo, A., Clothier, B. E., Green, S. R., Girón, I. F., & Moreno, F. (2001). Heat-pulse measurements of sap flow in olives for automating irrigation: tests, root flow and diagnostics of water stress. Agricultural water management, 51(2), 99-123.

Fernández, J. E., Moreno, F., Martín-Palomo, M. J., Cuevas, M. V., Torres-Ruiz, J. M., & Moriana, A. (2011a). Combining sap flow and trunk diameter measurements to assess water needs in mature olive orchards. Environmental and Experimental Botany, 72(2), 330-338.

Fernández, J. E., Rodriguez-Dominguez, C. M., Perez-Martin, A., Zimmermann, U., Rüger, S., Martín-Palomo, M. J., ... & Diaz-Espejo, A. (2011b). Online-monitoring of tree water stress in a hedgerow olive orchard using the leaf patch clamp pressure probe. Agricultural Water Management, 100(1), 25-35.

Fernández, J. E. (2014). Plant-based sensing to monitor water stress: Applicability to commercial orchards. Agric. Water Manag. 142, 99–109. doi: 10.1016/j.agwat. 2014.04.017.

Fernández, J. E. (2017). Plant-based methods for irrigation scheduling of woody crops. Horticulturae 3:35. doi: 10.3390/horticulturae3020035.

Fernández, J. E., Diaz-Espejo, A., Romero, R., Hernandez-Santana, V., García, J. M., Padilla-Díaz, C. M., & Cuevas, M. V. (2018). Precision irrigation in olive (Olea europaea L.) tree orchards. In Water scarcity and sustainable agriculture in semiarid environment (pp. 179-217). Academic Press.

Forster, M. A. (2017). How reliable are heat pulse velocity methods for estimating tree transpiration?. Forests, 8(9), 350.

Garrido, A., Fernández-González, M., Álvarez-López, S., González-Fernández, E., & Rodríguez-Rajo, F. J. (2020). First phenological and aerobiological assessment of olive orchards at the Northern limit of the Mediterranean bioclimatic area. Aerobiologia, 36(4), 641-656.

Gates, D. M. (1964). Leaf temperature and transpiration 1. Agronomy Journal, 56(3), 273-277.

Gené-Mola, J., Vilaplana, V., Rosell-Polo, J. R., Morros, J.-R., Ruiz-Hidalgo, J., & Gregorio, E. (2019). Multi-modal deep learning for Fuji apple detection using RGB-D cameras and their radiometric capabilities. Computers and Electronics in Agriculture, 162, 689–698. https://doi.org/10.1016/j.compag.2019.05.016.

Gentile, F., Vurro, F., Picelli, F., Bettelli, M., Zappettini, A., & Coppedè, N. (2020). A mathematical model of OECTs with variable internal geometry. Sensors and Actuators A: Physical, 304, 111894.

Girón, I. F., Corell, M., Martín-Palomo, M. J., Galindo, A., Torrecillas, A., Moreno, F., & Moriana, A. (2015a). Feasibility of trunk diameter fluctuations in the scheduling of regulated deficit irrigation for table olive trees without reference trees. Agricultural Water Management, 161, 114-126.

Girón, I. F., Corell, M., Galindo, A., Torrecillas, E., Morales, D., Dell'Amico, J., ... & Moriana, A. (2015b). Changes in the physiological response between leaves and fruits during a moderate water stress in table olive trees. Agricultural Water Management, 148, 280-286.

Green, S., Clothier, B., & Jardine, B. (2003). Theory and practical application of heat pulse to measure sap flow. Agronomy Journal, 95(6), 1371-1379.

Green, S.R., Romero, R., 2012. Can we improve heat-pulse to measure low and reverse flows? Acta Horticulturae 951, 19e22.

Hamed, S., Ibba, P., Petrelli, M., Ciocca, M., Lugli, P., & Petti, L. (2021, November). Transistor-based plant sensors for agriculture 4.0 measurements. In 2021 IEEE International Workshop on Metrology for Agriculture and Forestry (MetroAgriFor) (pp. 69-74). IEEE.

Hannah, R. L., & Reed, S. E. (Eds.). (1992). Strain gage users' handbook. Springer Science & Business Media.

Hernández-Santana, V., Fernández, J. E., Rodriguez-Dominguez, C. M., Romero, R., & Diaz-Espejo, A. (2016). The dynamics of radial sap flux density reflects changes in stomatal conductance in response to soil and air water deficit. Agricultural and Forest Meteorology, 218, 92-101.

Hernandez-Santana, V., Fernandes, R. D., Perez-Arcoiza, A., Fernández, J. E., Garcia, J. M., & Diaz-Espejo, A. (2018). Relationships between fruit growth and oil accumulation with simulated seasonal dynamics of leaf gas exchange in the olive tree. Agricultural and Forest Meteorology, 256, 458-469.

Hernandez-Santana, V., Perez-Arcoiza, A., Gomez-Jimenez, M. C., & Diaz-Espejo, A. (2021). Disentangling the link between leaf photosynthesis and turgor in fruit growth. The Plant Journal, 107(6), 1788-1801.

Herrera, J.M., Costa, P., Medinas, D., Marques, J.T., Mira, A., 2015. Community composition and activity of insectivorous bats in Mediterranean olive farms. Anim. Conserv. 18, 557–566. https://doi.org/10.1111/acv.12209.

Infante-Amate, J., Villa, I., Aguilera, E., Torremocha, E., Guzmán, G., Cid, A., González, M., 2016. The making of olive landscapes in the south of Spain. A history of continuous expansion and intensification. In: In: Agnoletti, M., Emanueli, F. (Eds.), Biocultural diversity in Europe. Environmental History, vol. 5 Springer, Cham. https://link.springer.com/chapter/10.1007/978-3-319-26315-1_8.

Jiang, J. A., Tseng, C. L., Lu, F. M., Yang, E. C., Wu, Z. S., Chen, C. P., ... & Liao, C. S. (2008). A GSM-based remote wireless automatic monitoring system for field information: A case study for ecological monitoring of the oriental fruit fly, Bactrocera dorsalis (Hendel). Computers and electronics in agriculture, 62(2), 243-259.

Khosravi, H., Saedi, S. I., & Rezaei, M. (2021a). Real-time recognition of on-branch olive ripening stages by a deep convolutional neural network. Scientia Horticulturae, 287, 110252.

Khosravi, A., Zucchini, M., Giorgi, V., Mancini, A., & Neri, D. (2021b). Continuous Monitoring of Olive Fruit Growth by Automatic Extensimeter in Response to Vapor Pressure Deficit from Pit Hardening to Harvest. Horticulturae, 7(10), 349.

Khosravi, A., Zucchini, M., Mancini, A., & Neri, D. (2022). Continuous Third Phase Fruit Monitoring in Olive with Regulated Deficit Irrigation to Set a Quantitative Index of Water Stress. Horticulturae, 8(12), 1221.

Klepper, B., Browing, V.D., Taylor, H.M., 1971. Stem diameter in relation to plant water status. Plant Physiol. 48, 683–685.

Kozlowski, T.T., 1967. Diurnal variations in stem diameters of small trees. Bot. Gaz. 128, 60–68.

Link, S. O., Thiede, M. E., & Bavel, M. V. (1998). An improved strain-gauge device for continuous field measurement of stem and fruit diameter. Journal of Experimental Botany, 49(326), 1583-1587.

López-Bernal, Á., Alcántara, E., Testi, L., & Villalobos, F. J. (2010). Spatial sap flow and xylem anatomical characteristics in olive trees under different irrigation regimes. Tree Physiology, 30(12), 1536-1544.

López-Bernal, Á., Testi, L., & Villalobos, F. J. (2012). Using the compensated heat pulse method to monitor trends in stem water content in standing trees. Tree physiology, 32(11), 1420-1429.
López-Bernal, Á., Testi, L., & Villalobos, F. J. (2017). A single-probe heat pulse method for estimating sap velocity in trees. New Phytologist, 216(1), 321-329.
Mahlein, A. K. (2016). Plant disease detection by imaging sensors–parallels and specific demands for precision agriculture and plant phenotyping. Plant disease, 100(2), 241-251.
Mancuso, S., Fiorino, P., & Pasquali, G. (2002). Phenology modelling and forecasting in olive (Olea europaea L.) using artificial neural networks. Phenology modelling and forecasting in olive (Olea europaea L.) using artificial neural networks, 1000-1010.
Marino, G., Scalisi, A., Guzmán-Delgado, P., Caruso, T., Marra, F. P., & Lo Bianco, R. (2021). Detecting mild water stress in olive with multiple plant-based continuous sensors. Plants, 10(1), 131.
Marino, G., Caruso, T., Ferguson, L., & Marra, F. P. (2018). Gas exchanges and stem water potential define stress thresholds for efficient irrigation management in olive (Olea europea L.). Water, 10(3), 342.
Martín-Palomo, M. J., Corell, M., Andreu, L., López-Moreno, Y. E., Galindo, A., & Moriana, A. (2021). Identification of water stress conditions in olive trees through frequencies of trunk growth rate. Agricultural Water Management, 247, 106735.
Measham, P. F., Wilson, S. J., Gracie, A. J., & Bound, S. A. (2014). Tree water relations: flow and fruit. Agricultural Water Management, 137, 59-67.
Michelakis, N., 1997. Daily stem radius variations as indicators to optimise olive tree irrigation scheduling. Acta Hort. 449, 297–304.
Milicevic, M., Zubrinic, K., Grbavac, I., & Obradovic, I. (2020). Application of deep learning architectures for accurate detection of olive tree flowering phenophase. Remote Sensing, 12(13), 2120.
Miranda, M. Á., Barceló, C., Valdés, F., Feliu, J. F., Nestel, D., Papadopoulos, N., ... & Alorda, B. (2019). Developing and implementation of decision support system (DSS) for the control of olive fruit fly, Bactrocera oleae, in Mediterranean olive orchards. Agronomy, 9(10), 620.
Moreira, F., Herrera, J.M., Beja, P., 2019. Making olive oil sustainable. Science 365 (6456) 873-873. https://science.sciencemag.org/content/365/6456/873.1.
Moreno, F., Fernández, J.E., Clothier, B., Green, S., 1996. Transpiration and root water uptake by olives. Plant and Soil 184, 85e96.
Moriana, A., Girón, I. F., Martín-Palomo, M. J., Conejero, W., Ortuño, M. F., Torrecillas, A., & Moreno, F. (2010). New approach for olive trees irrigation scheduling using trunk diameter sensors. Agricultural Water Management, 97(11), 1822-1828.
Moriana, A., Pérez-López, D., Prieto, M. H., Ramírez-Santa-Pau, M., and PérezRodriguez, J. M. (2012). Midday stem water potential as a useful tool for estimating irrigation requirements in olive trees. Agric. Water Manag. 112, 43–54. doi: 10.1016/j.agwat.2012.06.003.
Morgado, R., Santana, J., Porto, M., Sánchez-Oliver, J. S., Reino, L., Herrera, J. M., ... & Moreira, F. (2020). A Mediterranean silent spring? The effects of olive farming intensification on breeding bird communities. Agriculture, Ecosystems & Environment, 288, 106694.
Nadezhdina, N., Nadezhdin, V., Ferreira, M. I., & Pitacco, A. (2007). Variability with xylem depth in sap flow in trunks and branches of mature olive trees. Tree Physiology, 27(1), 105-113.
Nadezhdina, N., David, T.S., David, J.S., Nadezhdin, V., Cermak, J., Gebauer, R., Ferreira, M.I., Conceição, N., Dohnal, M., Tesar, M., Gartner, K., Ceulemans, R., 2012. Root function: in

situ studies through sap flow research. In: Mancuso, S. (Ed.), Measuring Roots: An Updated Approach. Springer, pp. 267e290 (Chapter 14).
Ortuño, M. F., Conejero, W., Moreno, F., Moriana, A., Intrigliolo, D. S., Biel, C., ... & Torrecillas, A. (2010). Could trunk diameter sensors be used in woody crops for irrigation scheduling? A review of current knowledge and future perspectives. Agricultural Water Management, 97(1), 1-11.
Osborne, C. P., Chuine, I., Viner, D., & Woodward, F. I. (2000). Olive phenology as a sensitive indicator of future climatic warming in the Mediterranean. Plant, Cell & Environment, 23(7), 701-710.
Pourreza, A., Lee, W. S., Ehsani, R., Schueller, J. K., & Raveh, E. (2015). An optimum method for real-time in-field detection of Huanglongbing disease using a vision sensor. Computers and Electronics in Agriculture, 110, 221–232. https://doi.org/ 10.1016/j.compag.2014.11.021.
Primicerio, J., Di Gennaro, S. F., Fiorillo, E., Genesio, L., Lugato, E., Matese, A., & Vaccari, F. P. (2012). A flexible unmanned aerial vehicle for precision agriculture. Precision Agriculture, 13(4), 517-523.
Rodriguez-Dominguez, C. M., Hernandez-Santana, V., Buckley, T. N., Fernández, J. E., & Diaz-Espejo, A. (2019). Sensitivity of olive leaf turgor to air vapour pressure deficit correlates with diurnal maximum stomatal conductance. Agricultural and Forest Meteorology, 272, 156-165.
Russo, C., Cappelletti, G.M., Nicoletti, G.M., Di Noia, A.E., Michalopoulos, G., 2016 Comparison of European olive production systems. Sustainability 8, 825. https://doi. org/10.3390/su8080825.
Sa, I., Ge, Z., Dayoub, F., Upcroft, B., Perez, T., & McCool, C. (2016). DeepFruits: A fruit detection system using deep neural networks. LID - 10.3390/s16081222 [doi] LID - E1222 [pii]. (1424-8220 (Electronic)).
Saedi, S. I., & Khosravi, H. (2020). A deep neural network approach towards real-time on-branch fruit recognition for precision horticulture. Expert Systems with Applications, 159, 113594.
Sánchez Martínez, J. D., & Paniza Cabrera, A. (2015). The olive monoculture in the south of Spain. European Journal of Geograph, 6(3), 16-29.
Scalisi, A., Bresilla, K., and Simões Grilo, F. (2017). Continuous determination of fruit tree water-status by plant-based sensors. Italus Hortus 24, 39–50. doi: 10.26353/j.itahort/2017.2.3950.
Scalisi, A., Marino, G., Marra, F. P., Caruso, T., & Lo Bianco, R. (2020). A Cultivar-Sensitive Approach for the Continuous Monitoring of Olive (Olea europaea L.) Tree Water Status by Fruit and Leaf Sensing. Frontiers in plant science, 11, 340.
Shafi, U., Mumtaz, R., García-Nieto, J., Hassan, S. A., Zaidi, S. A. R., & Iqbal, N. (2019). Precision agriculture techniques and practices: From considerations to applications. Sensors, 19(17), 3796.
Silveira, A., Ferrão, J., Munoz-Rojas Morenes, J., Pinto-Correia, T., Guimarães, M. H., & Schmidt, L. (2018). The sustainability of agricultural intensification in the early 21st century: insights from the olive oil production in Alentejo (Southern Portugal). Changing societies: legacies and challenges. Vol. 3. The diverse worlds of sustainability, 247-275.
Sishodia, R. P., Ray, R. L., & Singh, S. K. (2020). Applications of remote sensing in precision agriculture: A review. Remote Sensing, 12(19), 3136.
Smith, D. M., & Allen, S. J. (1996). Measurement of sap flow in plant stems. Journal of experimental Botany, 47(12), 1833-1844.

Steppe, K., De Pauw, D. J., Doody, T. M., & Teskey, R. O. (2010). A comparison of sap flux density using thermal dissipation, heat pulse velocity and heat field deformation methods. Agricultural and Forest Meteorology, 150(7-8), 1046-1056.

Testi, L., Villalobos, L., 2009. New approach for measuring low sap velocities in trees. Agriculture and Forest Meteorology 149 (3e4), 730e734.

Tjur, T., 2009. Coefficients of determination in logistic regression models—a new proposal: the coefficient of discrimination. Am. Stat. 63, 366–372. https://doi.org/10. 1198/tast.2009.08210.

Trentacoste, E. R., Puertas, C. M., and Sadras, V. O. (2015). Effect of irrigation and tree density on vegetative growth, oil yield and water use efficiency in young olive orchard under arid conditions in Mendoza, Argentina. Irrig. Sci. 33, 429–440. doi: 10.1007/s00271-015-0479-z.

Tzanakakis, M.E. Seasonal development and dormancy of insects and mites feeding on olive: A review. Netherlands. J. Zool. 2003, 52, 87–224.

Uğuz, S., & Uysal, N. (2021). Classification of olive leaf diseases using deep convolutional neural networks. Neural Computing and Applications, 33(9), 4133-4149.

Vandegehuchte, M. W., Braham, M., Lemeur, R., & Steppe, K. (2012). The importance of sap flow measurements to estimate actual water use of meski olive trees under different irrigation regimes in Tunisia. Irrigation and Drainage, 61(5), 645-656.

Vandegehuchte, M. W., & Steppe, K. (2013). Corrigendum to: Sap-flux density measurement methods: working principles and applicability. Functional Plant Biology, 40(10), 1088-1088.

Wang, C., Tang, Y., Zou, X., Luo, L., & Chen, X. (2017). Recognition and Matching of Clustered Mature Litchi Fruits Using Binocular Charge-Coupled Device (CCD) Color Cameras. Sensors, 17(11). https://doi.org/10.3390/s17112564.

Webber, H., Heyd, V., Horton, M., Bell, M., Matthews, W., & Chadburn, A. (2019). Precision farming and archaeology. Archaeological and Anthropological Sciences, 11(2), 727-734.

Wu, J., Zhang, B., Zhou, J., Xiong, Y., Gu, B., & Yang, X. (2019). Automatic recognition of ripening tomatoes by combining multi-feature fusion with a bi-layer classification strategy for harvesting robots. Sensors (Basel, Switzerland), 19(3), 612. https://doi.org/10.3390/s19030612.

Zadeh, L. A. (1998a). Roles of soft computing and fuzzy logic in the conception, design and deployment of information/intelligent systems. In Computational intelligence: soft computing and fuzzy-neuro integration with applications (pp. 1-9). Springer, Berlin, Heidelberg).

Zadeh, L. A. (1998b, May). Soft computing, fuzzy logic and recognition technology. In 1998 IEEE International Conference on Fuzzy Systems Proceedings. IEEE World Congress on Computational Intelligence (Cat. No. 98CH36228) (Vol. 2, pp. 1678-1679). IEEE.).

Zarco-Tejada, P. J., González-Dugo, V., & Berni, J. A. J. (2012). Fluorescence, temperature and narrow-band indices acquired from a UAV for water stress detection using a hyperspectral imager and a thermal camera. Remote Sensing of Environment, 117, 322–337.

Zarco-Tejada, P.J.; Hubbard, N.; Loudjani, P. Precision Agriculture: An Opportunity for EU Farmers—Potential Support with the CAP 2014–2020; Joint Research Centre (JRC) of the European Commission; Monitoring Agriculture ResourseS (MARS) Unit H04: Brussels, Belgium, 2014

Zhang, J., Huang, Y., Pu, R., Gonzalez-Moreno, P., Yuan, L., Wu, K., & Huang, W. (2019). Monitoring plant diseases and pests through remote sensing technology: A review. Computers and Electronics in Agriculture, 165, 104943.

Zimmermann, D., Reuss, R., Westhoff, M., Gessner, P., Bauer, W., Bamberg, E., ... & Zimmermann, U. (2008). A novel, non-invasive, online-monitoring, versatile and easy plant-based probe for measuring leaf water status. Journal of experimental botany, 59(11), 3157-3167.

Zude-Sasse, M., Fountas, S., Gemtos, T. A., & Abu-Khalaf, N. (2016). Applications of precision agriculture in horticultural crops.

Chapter 3.

Continuous Monitoring of Olive Fruit Growth by Automatic Extensimeter in Response to Vapor Pressure Deficit from Pit Hardening to Harvest

Arash Khosravi[1], Matteo Zucchini[1], Veronica Giorgi[1], Adriano Mancini[2] and Davide Neri[1],*

[1]Department of Agricultural, Food and Environmental Science, Marche Polytechnic University, 60131 Ancona, Italy; a.khosravi@pm.univpm.it (A.K.); m.zucchini@pm.univpm.it (M.Z.); v.giorgi@staff.univpm.it (V.G.)
[2]Department of Information Engineering, Marche Polytechnic University, 60131 Ancona, Italy; a.mancini@staff.univpm.it
* Correspondence: d.neri@staff.univpm.it

Published in Horticulturae 2021, 7, 349.
https:// doi.org/10.3390/horticulturae7100349

3.1 Abstract

Recently, several studies on olive fruit growth have focused on circadian monitoring as an important orchard management tool. The olive fruit growth trend is described by double sigmoid model with four growth phases, where the third phase spans from the end of pit hardening to initial fruit maturation, and the last phase includes olive maturation up to fruit drop. Environmental factors play an important role in fruit growth, with vapor pressure deficit (VPD) being a keystone factor. Our experiment was designed to hourly monitor olive (*Olea europaea* L. cv. 'Frantoio') fruit transversal diameter from approximately initial pit hardening (II Phase), extension (III Phase) until harvest time (IV Phase) in the attempt to determine whether fruit growth dynamically responds to environmental variables such as diurnal VPD change in different stages of fruit development. Automatic extensimeters were applied in open field and VPD was calculated from data of our weather station. Throughout the experiment period, the circadian model of fruit growth showed two steps: shrinkage and expansion. Almost in all days of the third phase of fruit growth, daily response of transversal diameter to VPD formed complete clockwise hysteresis loops. During the fourth phase of fruit growth, with increasing fruit maturation, the complete clockwise hysteresis loop experienced some abnormality. At the fourth stage of fruit growth there were incomplete and partial clockwise hysteresis loops. We conclude that hysteresis can be employed to detect the shift between the end of the third phase (cell expansion) and the beginning of the fourth phase (fruit maturation) of fruit growth. The disappearance of the complete clockwise hysteresis loop and the substitution with incomplete, or partial clockwise hysteresis loops was observable only in the fourth stage of fruit growth. These results can be valuable for any smart fruit management of olive fruit production.

Keywords: olive; fruit growth; hysteresis; transversal diameter; fruit maturation; vapor pressure deficit (VPD)

3.2 Introduction

Olive (*Olea europaea* L.) is an evergreen tree or shrub which was originally domesticated in the Fertile crescent region, from where it spread later on, to many parts of the world with Mediterranean climate. Maintaining constant and high olive yields requires an application of specific knowledge and techniques. Olive fruit growth and maturation is a combination of physiological and biochemical changes influenced by environmental and agronomic conditions (Conde et al ., 2008; Tombesi, 1994; Martinelli et al., 2011). Olive fruit growth can be described by a double-sigmoid growth curve (Fernández et al., 2018; Gucci et al., 2009), which is divided in four growth phases. The first phase (I Phase) is characterized by rapid cell division, which induces an exponential expansion of the volume; in the second phase (II Phase) the speed of cell division diminishes, while pit is hardening and fruit size increases slowly; in the third phase (III Phase) the fruit dimension increases with rapid and linear growth continues and leads to a beginning of fruit maturation; the fourth phase (IV Phase) finishes with full ripening and eventually fruit drop.

In addition to this, the growth of the fruit is the result of complex genetic, metabolic, hormonal and environmental interactions that determine the size, shape and oil composition (Gucci et al., 2009). It is influenced and regulated by endogenous factors such as genetic differences and fruit load, and exogenous factors such as water availability and ambient temperature (Corelli-Grappadelli and Lakso, 2002; Hammami et al., 2011). One of the most significant environmental variables is vapor pressure deficit (VPD). According to research of Amitrano et al. (2019), VPD is a driver for transpiration in plants and it is critical for plants' growth and productivity. Such degree of complexity in olive fruit growth demands a more accurate management in cultivating this crop.

Precision farming system is a management approach that has been implemented in agriculture in recent years. The 'precision farming' concept is based upon observing, measuring and responding to inter and intra-field variability in crops or in various aspects of animal husbandry (Zarco-Tejada et al., 2014). One of its main research foci in pomology consist in monitoring of fruit transversal diameter by an application of sensors, to represent fruit growth. Observation of circadian cycles applied to fruit growth contributes to gathering information regarding this phenological stage and to yield more data for developing precision farming technologies (Mariono et al., 2021; Zucchini et al., 2021).

Monitoring of fruit growth by following diurnal fluctuation of transversal diameter has been investigated in several species. For instance, Fishman and Génard (1998) simulated a model for seasonal and diurnal growth of peach (*Prunus persica* (L.) Batsch), whereas Brüggenwirth et al. (2016) showed the diurnal growth of sweet cherry (*Prunus avium* (L.) Sam). Monitoring fruit growth provided good estimations of fruit size and harvest date and granted better satisfaction of the target market in apple production (Manfrini et al., 2010). Olive fruits have been studied in this regard by Fernandes et al. (2018), that showed fruit growth and diurnal changes in olive (*Olea europaea* (L.) cv. 'Arbequina'), grown under different water regimes.

Production of highly precise instruments for accurate measurement of fruit growth has been developed and there are various experimental as well as commercial instruments (Morandi et al., 2007a). Nevertheless, Morandi et al. (2007a) described that, in most cases, the instrument consists of a sensor, supported by a frame, placed in contact with the epidermis

of the growing fruit. One aspect that bears considerably on the choice of sensor and of the materials used in constructing field probes is their ruggedness and accuracy under varying environmental conditions, including large temperature, precipitation, and air moisture changes (Morandi et al., 2007a).

Monitoring of fruit growth can help the Regulated Deficit Irrigation (RDI) index to optimize water consumption without diminishing yields or fruit quality. According to research of Goldhamer (1997), Tavor et al. (2002) and Tognetti et al. (2006), pit hardening is the best phenological phase for employing RDIs in olive trees but in many cases, differences among growth stages are not evident, neither easy to access (Alhaoui et al., 2015). Thus, in a smart farming approach, it is hence important to find physiological parameters that can be continuously measured by the sensors. A common challenge with tree-based sensors is to adjust their output to physiologically meaningful parameters in a consistent manner (Marino et al., 2021; Fernández, 2017; Jones, 2006).

The phenomenon of hysteresis in plant systems has been known for a long time, attracting the attention of many investigators for years (Mayergoyz, 2003). The root of the word hysteresis is Greek and means to “lag behind”. Hysteresis is non-linear loop like behavior that does not show affine similarity with respect to time (Phillips, 2003; O’kane, 2005). In other words, when the time argument of an input function is stretched or compressed, the corresponding output function is not stretched in the same way (O’kane, 2005; Zhang et al., 2014). For instance, hysteresis as a relation between environmental factor (e.g., meteorological factors) and sap flow has been investigated in various eco systems in different geographical regions (Zhang et al., 2014; Ewers et al., 2005; Meinzer et al., 2005; O’Brien et al., 2004; O’Grady et al., 2008; Unswoeth et al., 2004; Wullschleger et al., 1998; Zeppel et al., 2004); hysteresis was found also in the relationship between canopy conductance and temperature (Bai et al., 2017). Furthermore, Scalisi et al. (2020), examined two different olive cultivars under different irrigation regimes and explained hysteresis between fruit diameter and leaf pressure on two different olive cultivars. According to this research, there was a completely different mechanism of leaf and fruit water exchange in response to increasing water deficit in the two cultivars, which might be driven by different osmotic adjustments, cell-wall elasticity and tissue water content (Scalisi et al., 2020). Recently, in the cherry fruit growth relationship with VPD, full hysteresis was found only during the maturation phase while during fruit extension phase the hysteresis was null or partial (Zucchini et al., 2021).

This work examined olive fruit transversal diameter versus VPD and evaluated the presence of hysteresis curves. The specific objective is to continuously describe the 'Frantoio' olive growth by automatic extensimeter. Besides, the fruit color ‘veraison’ was used to detect the transition between fruit growth phases. It was automatically recorded the by time-lapse video. To our knowledge, no other studies have yet evaluated the hysteresis curve of diurnal variation of olive fruit dimensions vs. VPD.

3.3 Materials and Methods

3.3.1. Site Description and Phenology

The study was conducted in 2019 in the olive grove (*Olea europaea* L., cv. 'Frantoio') of the experimental research station and botanical garden of Polytechnic University of Marche at Gallignano of Ancona (AN), Italy (43◦34006.200 N 13◦25024.200 E). Trees were planted 6 × 6 m and trained as free open vase. These were about 40 years old at the time of experiment. The agricultural operations, pest control and fertilization practices were accomplished following organic agricultural methods. Olive trees were grown in rainfed condition and with permanent grass cover, with mowing 3–4 times during the growing season. According to Köppen–Geiger climate classification, Gallignano is classified in the Cfb category and this is characterized by warm temperature, highly humid and warm summer (Kottek et al., 2006).

3.3.2. Fruit Growth

In 2019, the transversal diameter (synonym of equatorial diameter) of two olive fruits (fruit A and fruit B) was measured from August 6th to October 24th (DOY (Day Of the Year) 118 to DOY 297), from the phase of pit hardening, about 55 days after full bloom (DAFB), until harvest. The two different fruits were selected on one representative tree. Fruit diameter was measured with highly precise DEX20 extensimeters (Dynamax Inc., Houston, TX, USA). DEX20 extensimeters measure the size of small fruits (0–25 mm). This is a caliper style device with a full bridge strain gage attached to a flexible arm. The accuracy of the extensimeter was 0.05 mm at 20 ◦C and the output signal expressed in millivolt varied with a range of ±5 mV. The sensor output showed both diurnal and long-term growth of fruit. Data were recorded by CR1000X data logger (Campbell scientific, Inc., Logan, UT, USA) every hour and sent to our own cloud service base on Amazon Web Service (AWS) twice per day (Figure 3.1). The measured daily data were normalized by Min-Max method through the equation:

$$x' = 0.9 \times ((x - x_{min})/x_{max} - x_{min}) + 0.05 \quad (1)$$

where x' is the normalized value, x is the value of the existing data, and x_{min} and x_{max} are the minimum and maximum values of the data, respectively (Zucchini et al., 2021).

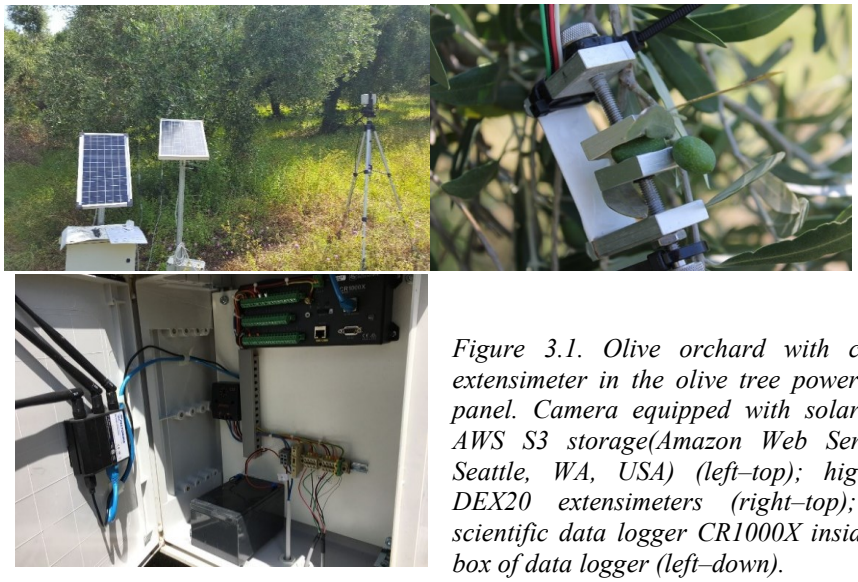

Figure 3.1. Olive orchard with camera and extensimeter in the olive tree powered by solar panel. Camera equipped with solar panel and AWS S3 storage(Amazon Web Services, Inc., Seattle, WA, USA) (left–top); highly precise DEX20 extensimeters (right–top); Campbell scientific data logger CR1000X inside the metal box of data logger (left–down).

3.3.3 Time-Lapse Video

The camera acquisition system was based on a custom 5Mpix RGB camera (Raspberry Pi Foundation, Cambridge, UK) with S-mount camera lens option. The device was attached to the mini-CSI port of a Raspberry Pi Zero W module (Raspberry Pi Foundation, Cambridge, UK). An IP65 enclosure ensured protection from water. Vision system was powered by a 10 W solar panel. A dedicated scheduler ensured the acquisition of images at the desired time. The acquired data were then synchronized to AWS S3 storage. Data connection was ensured by a Wi-Fi 3.5/4G powered by the solar panel. The camera was set on the orchard near to the tree to take pictures hourly (Figure 3.1). The images from the camera were labeled by olive maturation experts using Labelbox platform (Labelbox Inc., San Francisco, CA, USA); for each olive, the experts assigned a ripening stage according to 0–4 of Jaen index (International Olive Council (COI/OH/Doc. No1 November 2011)). Labelbox is fully configurable platform which enables us to create and manage machine learning training data. It is able to label data accurately with automated labeling workflows. Moreover, all data and processes are connected through a single platform with a central system of record. It accelerates model training and increases performance with faster iterations (https://labelbox.com/product/platform, accessed on 15 September 2021). The ripening index yielded by the camera images illustrated the maturity phase of the population of olive fruits. On the contrary, the extensimeter did not represent data of population of olive fruits; it represented single olive fruit data. Meanwhile, the single olive fruit data was inside the data of the population of olive fruits. Therefore, the parameter of 50% ripening of population of olive fruits was employed to approve maturation phase; monitoring of population of olive fruits was performed until countable full black fruits reached 50% of all countable fruit on the picture.

3.3.4. Meteorological Data

Meteorological data were recorded by a Vantage pro2 precision weather station (Davis Instruments Corporation, Hayward, CA, USA) located in the olive orchard. Vantage pro2 consists of weather-link software and data logger, which transfer weather data to a computer. For the calculation of vapor pressure deficit (VPD), air temperature (T) and relative humidity (RH) data were collected from our weather station. Vapor pressure deficit was calculated as:

$$VPD = (1 - (RH/100)) \times SVP \quad \text{and} \quad SVP\ (Pascals) = 610.7 \times 10^{\wedge 7.5T/(237.3+T)} \qquad (2)$$

The VPD formula was recommended by Monteith and Unsworth (2013); where RH is relative humidity, SVP is saturated vapor pressure and T is temperature (◦C). Our instrument was set to legal Rome time. In some part of analysis for better comparison between VPD and diameter, normalized VPD was considered. Data were normalized by Min-Max method and the equation was like Equation (1). Moreover, the other parameter used was VPD daily variation, expressed as the percentage of changing VPD in comparison with the same measured the day before. The VPD daily variation was employed to describe the possible daily different growth trend of fruit.

3.3.5.Hysteresis Curves

In this research, we studied the hysteresis curve of transversal diameter versus VPD. The latter has been shown to be especially important in woody plants, where it is the main variable affecting their diurnal evolution of transpiration (Perez-Martin et al., 2009). For description of the hysteresis curve, the terms of clockwise and anticlockwise loops (or curves) were used. To obtain the whole-day picture of the hysteresis curve, the best starting point for drawing each circadian graph was sunrise, due to the physiological effect of solar energy and its role in the photosynthesis and fruit growth. Consequently, our day started from sunrise and continued for 24 h. According to the data of our weather station, sunrise time from 6th of August to 5th of September (DOY 218 to 248) was set to 6 AM, from 6th of September to 24th of October (DOY 249 to 297) was set to 7 AM. Furthermore, the graphic representation of daily fruit growth and its fluctuations were reported from the time of sunrise. To obtain the seasonal model of hysteresis, the data should be categorized dividing the growing season into different stages (Bai et al., 2017). Therefore, with consideration of fruit growth trend in 24 h and its response to VPD, the experiment data were divided in two periods. The first period was from August 6th to October 3th (DOY 218–276) and the second period was from October 4th until end of experiment, on October 24th (DOY 277–297).

3.3.6. Data Analysis and Presentation

Data were analyzed using correlation and regression analysis. Pearson correlation test was used in order to determine the association between fruit diameter and VPD. From DOY 253 to 276, linear regression analyses between sensor output and time were performed to separate different slopes of fruit diameter in the third step of fruit growth. All data analyses

and graph design were carried out by Sigmaplot 14.5 (Systat Software, Inc., San Jose, CA, USA).

3.4 Results

3.4.1. Fruit Growth

The transversal diameters of the two different fruits (fruit A and fruit B) are reported (Figure 3.2). Transversal diameter of fruit A started at 10.71 mm and reached 11.55 mm at harvest time, whereas for fruit B started from 8.64 mm up to 9.66 mm. Fruit transversal diameter growth was described as continuous increase with diurnal fluctuation.

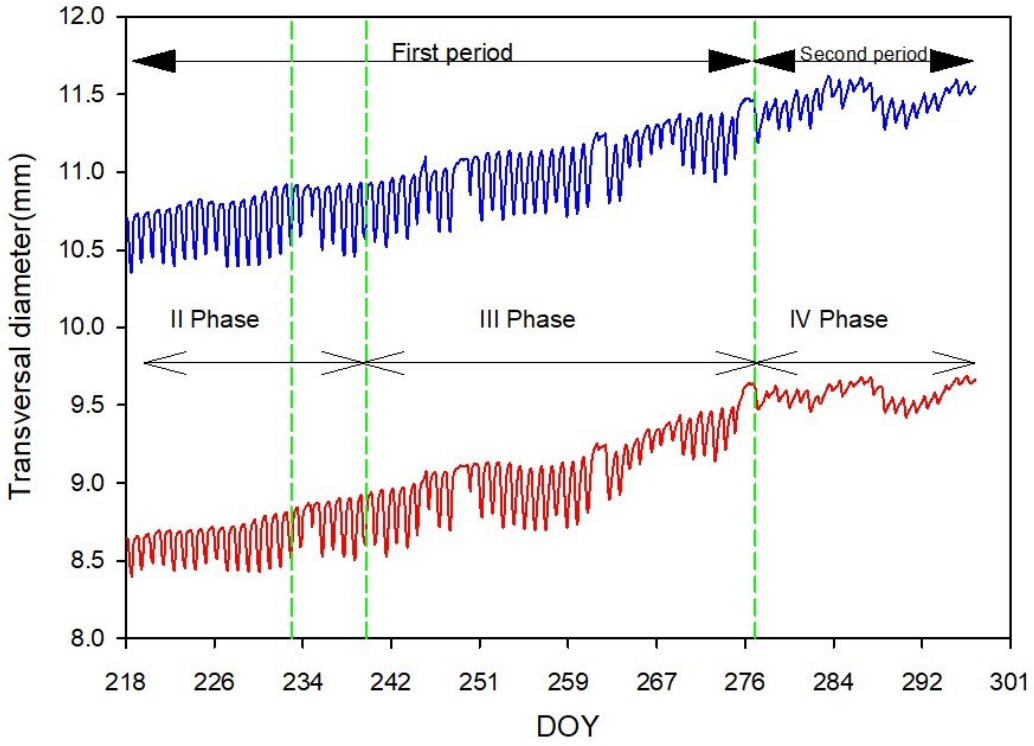

Figure 3.2. Continuous measurements of transversal diameter of fruit A (blue) and B (red). The first period of the study was from DOY 218 to 276 in 2019 and the second period of the study was from DOY 277 to 298 in 2019. Green dashed lines were drawn to separate fruit growth phases. An interval period of one week separated the end of the II phase from the following one. For this reason, there are two green dashed lines for ending the II phase of fruit growth.

The fruit's growth phase was divided in two periods. The first period (DOY 218–276) included II phase and the whole III phase of fruit growth. In this period, there was a

sequence of fruit diameter stability, followed by a decrease and finally by a fruit diameter increase (Figure 3.3). Fruit transversal diameter daily trend can be described with a three steps model: stability, decreasing and increasing. Fruit transversal diameter at the end of each day was bigger than at the starting point of the same day. Nevertheless, there were 3 days (DOY 246, 263, 274) for fruit A and 1 day (DOY 263) for fruit B in which transversal diameter at the end of the day was smaller than at the starting point of same day and categorized as a day with significant transversal diameter reduction. When normalized transversal diameter of fruit at the ending point of the day had at least 0.05 units reduction in comparison with the starting point of the same day, then it was considered as a significant transversal diameter reduction. The first step of fruit growth started at sunrise, but it was different throughout the days. At the second step, the diameter downsized with dissimilar duration and slope in different days. The last step was continuous growth of diameter and continued till the end of the 24th hour of one experimental day. During this step, the diameter increased with two different slopes from DOY 218 to 252, with a steep slope followed by flatter slope. However, from DOY 253 to 276 just the steep slope was observed (Figure 3.3). As starting point of each experimental day was set by sunrise, there is time lag aspect which should be considered. In other words, the real time argument of sunrise should be considered with a delay. According to the findings of Novick et al. (2016), it could be hypothesized that the first step of fruit growth was the sequence of fruit growth step from the day before, consequently the daily fruit growth could be explainable with two real steps (decreasing and increasing diameter), in the transversal diameter. In this first period, there were only 3 days (DOY 249, 262, 276) which did not show similar daily growth trends (Figure 3.4). There was no unique pattern for description of the three exception days (DOY 249, 262, 276).

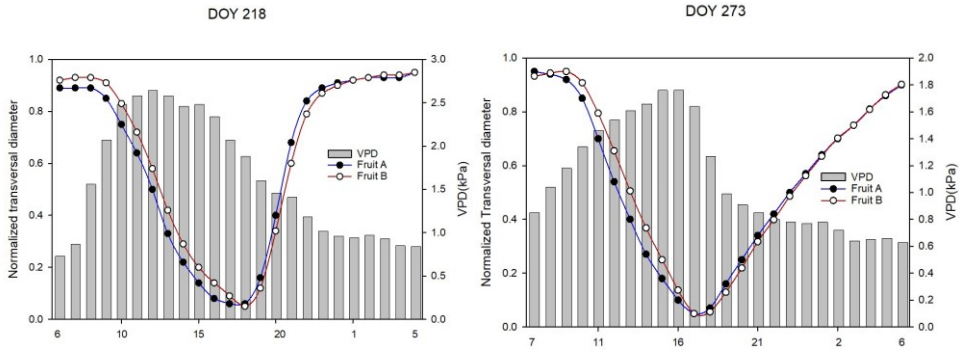

Figure 3.3. Continuous measurements of transversal diameter of fruit A and fruit B at selected days during the first period of the experiment.

In the second period of the experiment (DOY 277–297) which corresponded to the IV phase of fruit growth, daily trends of fruit growth for both fruits A and B were similar. It can be described in three steps: increasing diameter followed by decreasing diameter and again increasing diameter. Here, it also could be hypothesized that the first step of fruit growth represents a sequence of fruit growth steps from the day before, and daily fruit growth could be explainable with two real steps (decreasing and increasing growth).

Moreover, data of transversal diameter at the beginning point of the day and ending point of the same day showed that there were 11 days for fruit A and 9 days for fruit B in which transversal diameter at the end of the day was smaller than the starting point of the same day. All days of the second period showed a similar pattern, two example days are shown in Figure 3.5.

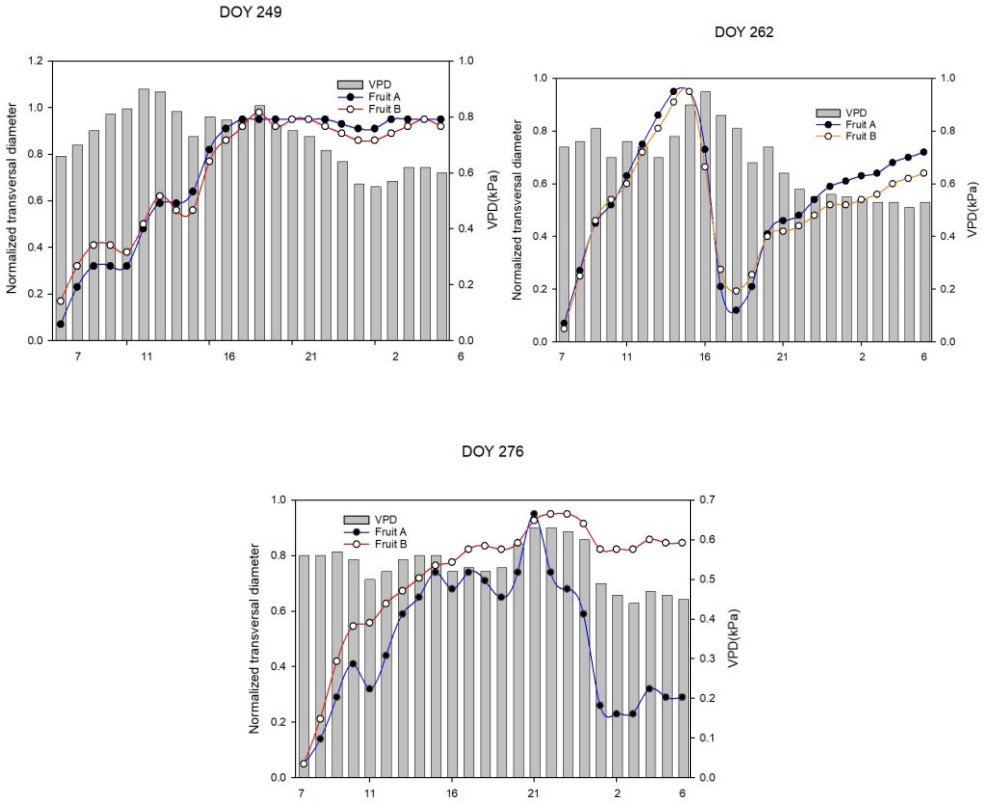

Figure 3.4. Continuous measurements of transversal diameter of fruit A and fruit B in exceptional days of the first period of experiment.

3.4.2. Analysis of Diameter Growth versus VPD and Hysteresis Curves

In the first period of experiment (DOY 218 to 276), daily growth of fruit transversal diameter versus VPD formed a model which was same for both fruit A and fruit B. The model was explainable with 3 steps. After sunrise, the value of transversal diameter decreased nonlinearly, and VPD had opposite trend and increased. Then there was a period of stability of the transversal diameter, during which VPD decreased. The final step consisted of a rapid increase of transversal diameter with decreasing VPD. In 84.75% of cases (50 out of 59), the mentioned 3 steps model formed a loop, which appeared as a complete clockwise hysteresis curve throughout the day (Figure 3.6a). The magnitude of

hysteresis loops differed from day to day, but a complete clockwise hysteresis was observed, all the time. There were nine exceptional days of a total of 59 days in which it did not appear complete clockwise hysteresis. In 10.17% of cases (6 out of 59), the clockwise hysteresis curve appeared in some part of the day and was not representative of the whole day, so it is called partial clockwise hysteresis (Figure 3.6c). In 1.69% of cases (1 out of 59), the ending point of the hysteresis loop did not reach the same level of the starting point of the loop, so the loop was not completely closed, and it was hence called incomplete clockwise hysteresis curve. Hysteresis loops were considered incomplete when the loop "opening" was less than 0.05 points (Figure 3.6d). Only in 3.39% of cases (2 out of 59), the pattern of daily transversal diameter versus VPD was not related to any noticeable model (Figure 3.6b). Figure 3.7 shows all 59 (from DOY 218 to 276) circadian measure series of transversal diameter versus VPD, providing an overall view of the first period of the experiment. The magnitude and shape of graphs for fruits A and B were similar.

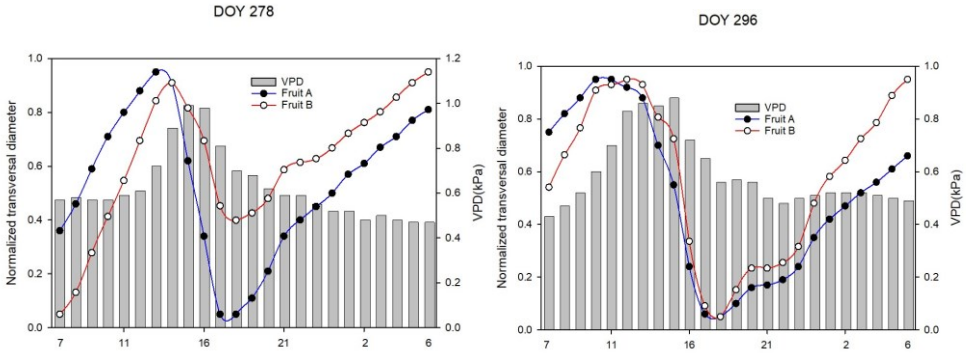

Figure 3.5. Continuous measurements of transversal diameter of fruit A and fruit B at example days of the second period of the experiment.

In the second period of the experiment (DOY 277 to 297) trends of daily fruit transversal diameter versus VPD formed partial clockwise hysteresis and incomplete clockwise hysteresis (Figure 3.8a-c). There were 7 days where the hysteresis pattern of fruit A and B was not the same. In fact, fruit A in 71.43% of cases (15 out of 21) showed incomplete clockwise hysteresis and in 28.57% of cases (6 out of 21) showed partial clockwise hysteresis. The percentage of incomplete clockwise hysteresis and partial clockwise hysteresis in fruit B was 47.62 (10 out of 21) for each one. The only exception from these 2 models was in fruit B which showed complete clockwise hysteresis in 4.76% of cases (1 out of 21) (Figure 3.8d). The average of VPD at the second period of experiment was 0.85 ± 0.37 (kPa). It showed 58.2% reduction in comparison with first period of experiment. There were 9 days with daily average of VPD lower than periodic average(average of second period of experiment) of VPD. Meanwhile, just three days (DOY 285, 296 and 297) for fruit A and two days (DOY 285 and 297) for fruit B were days with reduction of transversal diameter at the end of day. Besides there were two days (DOY 286 and 287) with normalized diameter smaller than 0.1. Finally, changing VPD in comparison with previous day did not demonstrate any specific results (Table 3.1). Consequently, the VPD alone was not able to explain the changing pattern of fruit growth in this second period in comparison with the first period, because in some situations decreasing VPD scores caused

an increase of fruit transversal diameter. The whole pattern of transversal diameter versus VPD for the second period of the experiment is shown in Figure 3.9, where 21 circadian measure series (DOY 277 to 297) of transversal diameter versus VPD are displayed. The shape of the graph was dissimilar from the one obtained from the first period of the experiment; besides fruit A and fruit B showed diverse growth patterns.

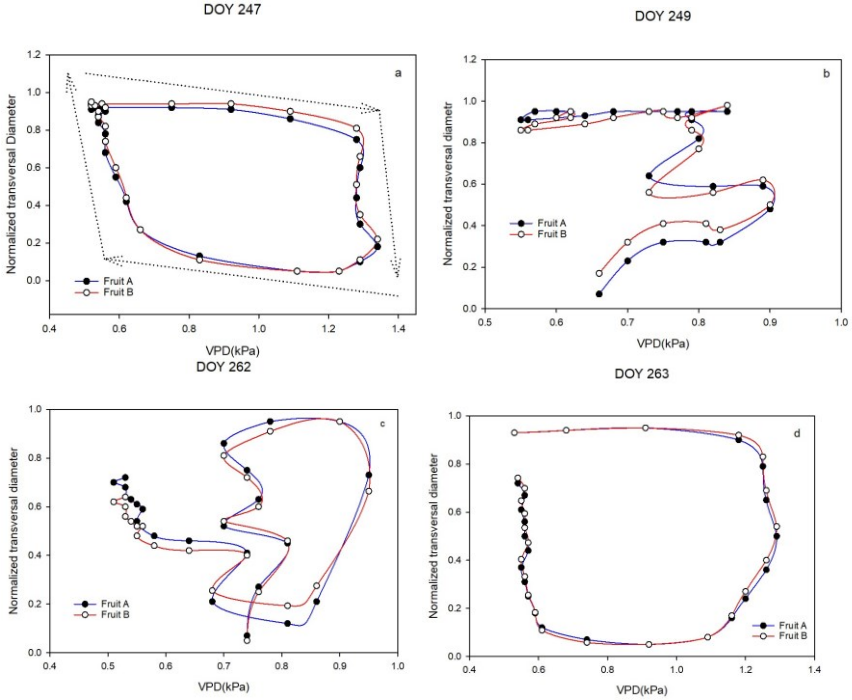

Figure 3.6. Correlation between transversal diameter and VPD for fruit A and B in four example days of the first period of the experiment: (a) complete clockwise hysteresis curve; (b) no noticeable model of hysteresis curve; (c) partial clockwise hysteresis curve; (d) incomplete clockwise hysteresis curve.

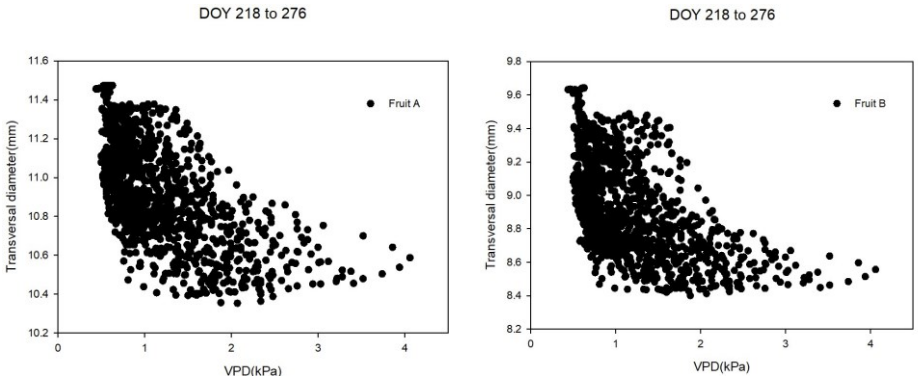

Figure 3.7. Transversal diameter versus VPD in all days of the first period of the experiment.

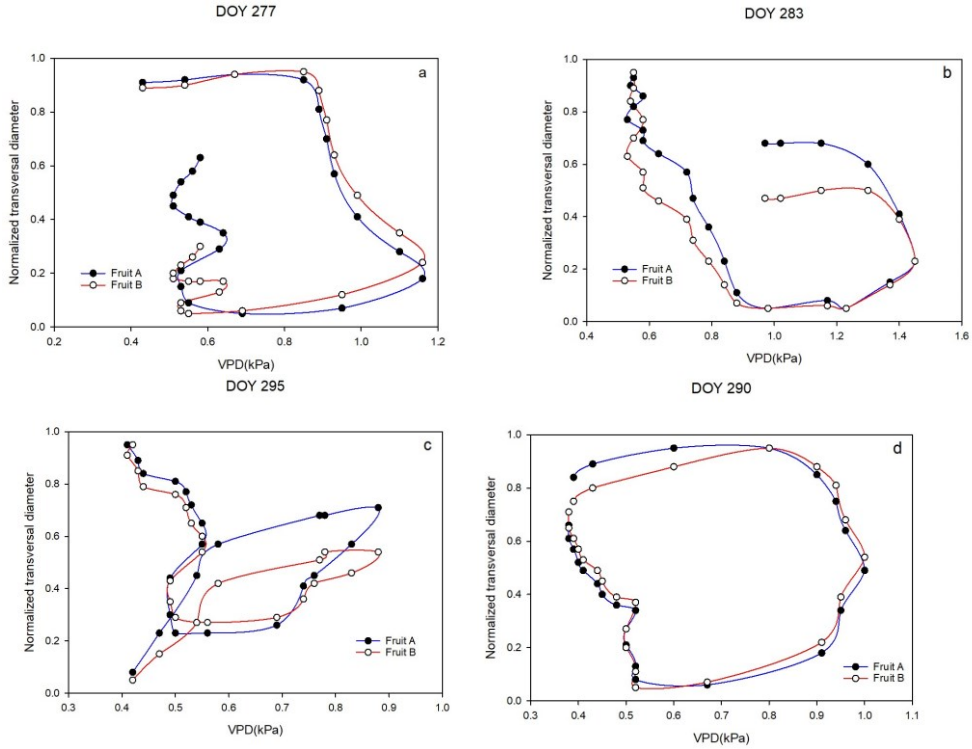

Figure 3.8. Correlation between transversal diameter and VPD for fruit A and B in four example days of the second period of the experiment: (a) incomplete clockwise hysteresis loop; (b) hysteresis loop which is near partial clockwise hysteresis loop; (c) partial clockwise hysteresis loop; (d) incomplete clockwise hysteresis loop for fruit A and complete clockwise hysteresis for fruit B.

The correlation coefficients of fruit A diameter versus VPD at the first and second period of the experiment were −0.527 and −0.286 and for fruit B were −0.453 and −0.232. The data showed moderate negative relationships between VPD and fruit diameter at the first period of the experiment and very weak negative relationships at the second period of the experiment. Furthermore, correlation data for the first part (DOY 218–252) and the second part (DOY 253–276) of the first period of the experiment were −0.608 and −0.377 for fruit A and −0.541 and −0.256 for fruit B, showing that correlations between fruit diameter and VPD decreased during the experiment, as fruits completed their development.

Table 3.1. VPD raw data. DOY 218 was beginning of experiment. So, the percentage of changing VPD in comparison with the same measured the day before (VPD daily variation) was exclude from table.

DOY	VPD(kPa)	VPD daily variation (%)	Normalized VPD	DOY	VPD(kPa)	VPD daily variation (%)	Normalized VPD	DOY	VPD(kPa)	VPD daily variation (%)	Normalized VPD
218	2.48	*	0.78	245	0.98	-33.33	0.25	272	1.58	-13.19	0.46
219	1.96	-21.00	0.59	246	0.90	-8.16	0.22	273	1.85	17.09	0.56
220	1.53	-21.91	0.44	247	1.47	63.33	0.42	274	1.28	-30.81	0.36
221	1.54	0.75	0.45	248	1.64	11.56	0.48	275	0.80	-37.50	0.19
222	2.57	66.99	0.81	249	0.41	-75.00	0.05	276	0.47	-41.25	0.07
223	2.97	15.56	0.95	250	0.66	60.98	0.14	277	0.93	97.87	0.37
224	2.72	-8.42	0.86	251	2.02	206.06	0.62	278	0.48	-48.39	0.10
225	1.65	-39.34	0.49	252	1.45	-28.22	0.42	279	1.15	139.58	0.50
226	1.41	-14.55	0.40	253	1.19	-17.93	0.32	280	0.94	-18.26	0.37
227	1.88	33.33	0.57	254	1.10	-7.56	0.29	281	0.97	3.19	0.39
228	1.65	-12.23	0.49	255	1.18	7.27	0.32	282	1.92	97.94	0.95
229	1.99	20.61	0.61	256	1.10	-6.78	0.29	283	1.08	-43.75	0.46
230	2.66	33.67	0.84	257	1.27	15.45	0.35	284	0.53	-50.93	0.13
231	2.83	6.39	0.90	258	0.99	-22.05	0.25	285	0.66	24.53	0.21
232	2.79	-1.41	0.89	259	1.52	53.54	0.44	286	0.46	-30.30	0.09
233	1.76	-36.92	0.52	260	2.18	43.42	0.67	287	0.39	-15.22	0.05
234	1.39	-21.02	0.39	261	1.58	-27.52	0.46	288	0.95	143.59	0.38
235	0.96	-30.94	0.24	262	0.51	-67.72	0.09	289	1.34	41.05	0.61
236	1.25	30.21	0.35	263	1.30	154.90	0.36	290	0.98	-26.87	0.40
237	1.03	-17.60	0.27	264	1.19	-8.46	0.32	291	1.02	4.08	0.42
238	1.25	21.36	0.35	265	0.69	-42.02	0.15	292	0.88	13.73	0.34
239	1.58	26.40	0.46	266	0.51	-26.09	0.09	293	0.93	5.68	0.37
240	1.64	3.80	0.48	267	0.72	41.18	0.16	294	0.83	-10.75	0.31
241	1.43	-12.80	0.41	268	0.86	19.44	0.21	295	0.40	-51.81	0.06
242	1.70	18.88	0.50	269	0.62	-27.91	0.12	296	0.51	27.50	0.12
243	1.42	-16.47	0.41	270	0.88	41.94	0.22	297	0.51	0.00	0.12
244	1.47	3.52	0.42	271	1.82	106.82	0.55				

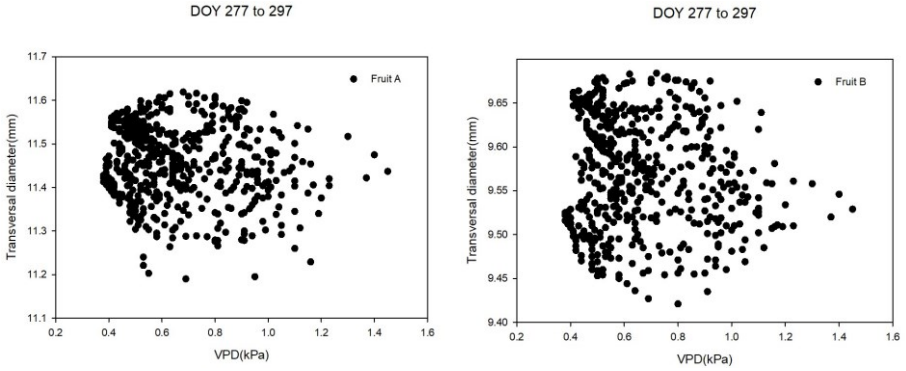

Figure 3.9. Transversal diameter versus VPD in all days of the second period of the experiment.

Additionally, the magnitude of hysteresis loops changed and became more compact during the experiment, flattening along the VPD axes, due to a reduction of VPD (Figure 3.10). Normalized graphs (Figure 3.10) show that the trend of transversal diameter versus VPD in the first period of the experiment was different from the second period. In both time intervals in the first period (i.e., 219–252 and 253–276 DOYs), maximum transversal diameter almost occurred at the minimum range of VPD, however, in the second period this trend was not observable.

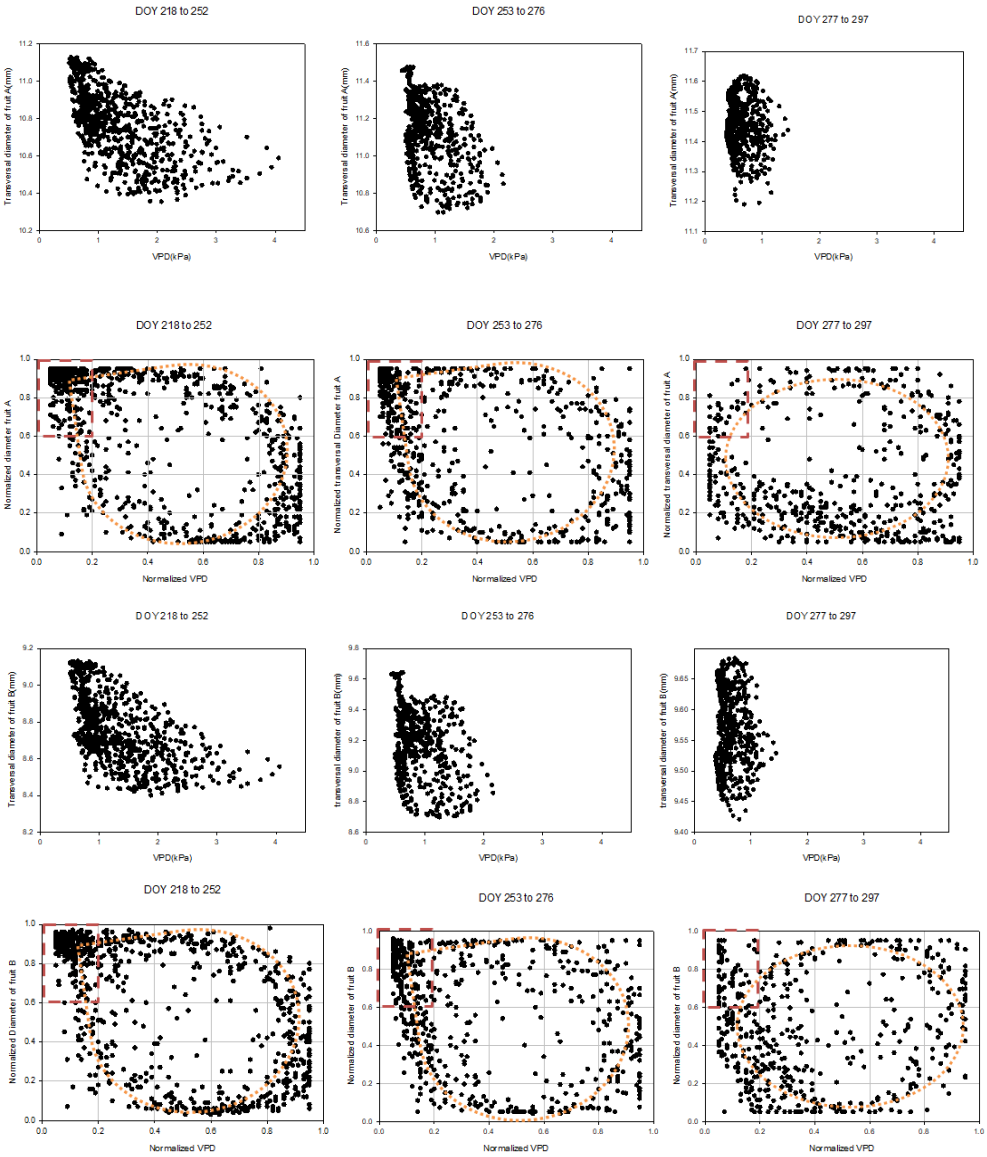

Figure 3.10. VPD versus transversal diameter for fruits A and B in both periods (first and second) of the experiment. The red box shows the area with minimum VPD and maximum transversal diameter. The orange dotted line shows almond shapes for both parts of the first period of the experiment and oval shapes for the second part.

3.4.3. Fruit Monitoring by Time-Lapse Camera

Figure 3.11 shows the fruit information such as countable fruits and ripening stage at random days of the first period of the experiment. According to camera images, fruits ripening started at DOY 259 (Figure 3.12), when the percentage of black olive fruits in the picture reached 5%. At the end of the first period, the ripening (population of countable black olive fruits) was 50% (Figure 3.11).

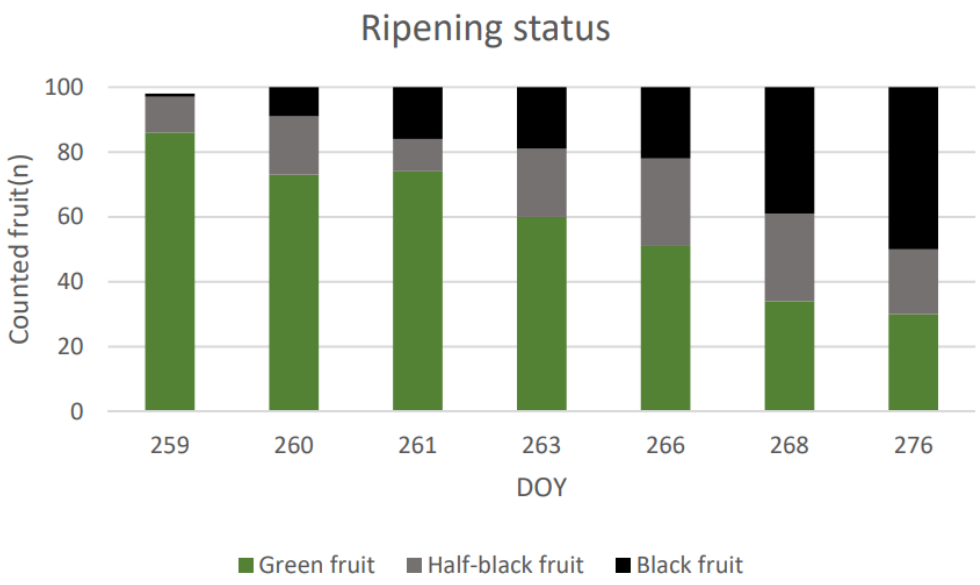

Figure 3.11. Fruit ripening data extracted from images of time-lapse video.

Figure 3.12. Pictures taken by automatic camera at three days of the experiment. The days are related to 2 weeks before, starting point and the day after ripening status assessment which has been demonstrated in figure 3.11. September 3rd (DOY 246) (left–top); 17th of September (DOY 259) (right–top); October 4th (DOY 277) (left–down). The image covering area was designed to represent the same fruit situation as fruits that were installed in the extensimeters. The collected images represented the canopy situation at the selected area.

3.5 Discussion

Dendrometers have been recently used in other research works for continuous monitoring of olive fruit, in correlation with water stress and scheduling the irrigation method such as regular deficit irrigation (RDI). For instance, Fernandes et al. (2018) explored the effect of water relations between leaves and fruits on fruit growth in a high-density olive orchard (cv. 'Arbequina') in southern Spain. Recent research (Marino et al., 2021) demonstrated that fruits acted as sinks of water during the night and as water sources during the day, leading to a strong daily shrinkage and swelling pattern in response to plant stress. This discovery highlights the important and still unrevealed role that fruits have as water storage compartments in drought resistance mechanisms of olives. Fruit daily diameter variation according to this research followed the same trend as our experiment, as reported in Figure 3.2. Additionally, Scalisi et al. (2020) performed continuous monitoring of two Sicilian olive cultivars (Nocellara del Belice and Olivo di Mandanici), in phases two and three of fruit development. They aimed at detecting whether fruit and leaf water dynamics of two different olive cultivars were differently affected by water deficit and their response to changes of midday stem water potential. This showed anti-clockwise hysteretic relationships between relative rates of fruit diameter change and relative rates of leaf pressure change. Besides, the results highlighted the advantages of the integration of fruit and leaf water dynamics to estimate plant water status and the need for genotype-specific models in olive. To the best of our knowledge, our work presents the first study on continuous measurement of transversal diameter of olive fruit with the description of fruit hysteresis according to daily variation of VPD. This study represents the results obtained only in 'Frantoio' cultivar in a specific range of environmental conditions, and it provides

innovative information about detecting the fourth phase of fruit growth by hysteresis phenomenon.

3.5.1. Diurnal Transversal Diameter Change and Its Influencing Factor

In the first period of the experiment, daily fruit growth followed a two steps cycle (decrease and increase). Due to the research of Fernandes et al. (2018) and Marino et al. (2021), the daily variations in fruit transversal diameters can be expounded as changes in flows of water into and out of the fruit hence, these can be connected to VPD and tree water status. Furthermore, Morandi et al. (2007b) explained that water and assimilates were translocated to the fruit via phloem and xylem streams, while fruit epidermis transpiration and fruit respiration were the main outgoing fluxes. This study described that fruit diameter variation in a finite time interval can be viewed as the net contribution of phloem import, which is always positive, whereas xylem flow, may be positive or negative and transpiration through the cuticle, which is always negative. However, the olive species (Olea europaea L.) has a very wide genetic pool, which can respond to drought using different leaf and fruit physiological and morphological mechanisms (Scalisi et al., 2020; Lo Bianco and Scalisi, 2016). It includes genotypes that can respond to drought using different mechanisms of leaf dehydration tolerance and leaf morphological and structural adaptations (Scalisi et al., 2020). Lo Bianco and Scalisi (2016) found different leaf stomatal regulation among olive cultivars.

We could monitor three exception days that did not show the daily trend of diameter decrease and increase (Figure 3.4). The ripening assessment data showed that the fruits in these 3 days where in different phenological phases. DOY 249 in the III phase and DOYs 262 and 276 in the IV phase of the fruit growth curve. The mean VPD in these 3 days was lower than periodic average of VPD (Table 3.1). Nevertheless, there were other days with average VPD lower than periodical average that did not show a different daily growth curve. Data of normalized VPD showed that all of these days had normalized VPD lower than 0.1. There was one day (DOY 266) which had normalized VPD lower than 0.1 but did not show a diverse daily growth curve. For the days with the exception daily pattern of diameter variation, the VPD daily variation was more than −41.2%; all the other days had much lower decrease percentage. Consequently, low daily average of VPD plus sudden decrease of VPD daily variation may have caused a different growth pattern during these 3 days.

In the first period of the experiment, the transversal diameter increased at the end of each day in comparison with starting point of same day. Only 5.1% of days for fruit A and 1.7% for fruit B showed an opposite pattern (lower diameter than the start of the day). The decreasing of the fruit transversal diameter can be caused by depletion of water reserves in fruit exposed to water stress. Considering meteorological data during all these days, the daily average of VPD was lower than periodic average of VPD (Table 3.1), however, there were other days with same weather condition which did not show daily reduction of transversal diameter.

In the second period of the experiment, daily growth pattern was described as a decrease followed by an increase of fruit transversal diameter. Besides, increasing transversal diameter at the end of each day in comparison with starting point of same day was not

observable in all days. Indeed, percentage of days in which transversal diameter reduced at the end of the day with comparison of starting point of the same day was 52.38% for fruit A and 42.85% for fruit B. According to Kong et al. (2019), decreasing transversal diameter for *Olea europaea* L. cv. 'Frantoio' could happen in the ripening stage. Data of Figure 3.10 shows that all days of the second period of the experiment had ripening percentage more than 50%, when fruits were in the IV phase of fruit growth. Consequently, fruit ripening caused increasing percentage of the days with reduction of transversal diameter at the ending point of each day. It could be hypothesized that variation of fruit growth trend between the first and second period of the experiment (the deformity on graph pattern) resulted from biotic parameters of fruit maturation, together with a high fluctuation of VPD and low periodic average of VPD at the second period of the experiment (Figure 3.2).

3.5.2. Hysteresis Loop, Challenges and Variations

Hysteresis is an indirect response of vegetation to diurnal changes in the external environment, because changes in such environmental controls often lead to complex physiological responses (Zhang et al., 2019). Under these environmental circumstances, VPD has been shown to be the major factor affecting the diurnal hysteresis loops (Ewers et al., 2005; O'Grady et al., 2008; Wullschleger et al ., 1998; Zeppel et al., 2004). Additionally, hysteresis can be seen as a way of self-protection for plants to avoid the overlapping of peak transpiration and peak VPD, thus preventing excessive extraction of water from the stem (Chen et al., 2011). Indeed, as a self-protective mechanism to avoid extremely high transpiration rates and adapt to tough weather (Chen et al., 2011). Therefore, the reaction time of plants is earlier than declines of meteorological variables which directly cause a hysteresis curve of fruit growth (transversal diameter) versus VPD.
In the first period of experiment (DOY 218–276) and from DOY 218 to 259, the percentage of complete clockwise hysteresis was 92.86 which declined to 35.3 in the period of DOY 260–276. This showed that with increasing fruit ripening, the percentage of complete clockwise hysteresis declined. Furthermore, in the same period data showed that the percentage of partial clockwise hysteresis and incomplete clockwise hysteresis increased from 2.38 to 29.4. The percentage for both kinds of hysteresis was the same. Therefore, with enhancing ripening percentage the partial clockwise hysteresis and incomplete clockwise hysteresis showed a reverse trend in comparison with complete clockwise hysteresis.
In the second period of the experiment (DOY 277–297) the percentage for complete clockwise hysteresis was 2.4, for incomplete hysteresis 64.3 and for partial hysteresis was 33.3. From Figure 3.10 it is observable that the percentage of ripening in the second period of experiment is 50%, so the fruit was at IV phase. Limitations to fruit growth and different fruit growth patterns at the ripening stage could be linked to changing in daily growth trends. In fact, with increasing fruit maturation the complete hysteresis loop started to show abnormality which appeared with incomplete or partial daily hysteresis loop, or with no daily hysteresis loop. When the percentage of black fruits is near 50%, the presence of a complete clockwise hysteresis loop diminished sensibly. Detecting the moment of disappearance of the complete clockwise hysteresis curve could be useful to evaluate more

precisely the IV phase of the double sigmoid growth curve of olives. Several studies (O'Grady et al., 2008; Bai et al., 2015; Janssen et al., 2008) showed that the magnitude of hysteresis loops is affected by biotic factors and abiotic factors. Additionally, findings by Scalisi et al. (2020) suggested that an overall decrease of the hysteretic loop area occurred from the II phase to the III phase of fruit growth. This is probably driven by the different fruit growth pattern at II and III phases (Scalisi et al., 2020).
Moreover, changing of graph form from almond shape to oval shape (Figure 3.10) was the outcome of diverse growth patterns in the third and fourth stages of fruit growth. Monitoring hysteretic loops and detecting the magnitude change could be used as a method for detecting the growth stages. Further investigations need to be done to promote models that evaluate hysteretic loops of olive daily growth versus VPD in different cultivars and range of environmental conditions. Nevertheless, our research produced viable data for an identification of different growth phases in the 'Frantoio' cultivar.

3.6 Conclusions

This study investigated the continuous transversal diameter growth of the olive fruit from pit hardening to harvest. The results demonstrated that almost in all days of the II phase of fruit growth the response of fruit transversal diameter to VPD formed a complete clockwise hysteresis curve. With the beginning of the IV phase of fruit growth, the complete clockwise hysteresis curve showed significant abnormality and became rare. The disappearance of complete clockwise hysteresis loop could be a good indicator of fruit maturation stage. A visualization of hysteresis curve, in normalized diameter vs. VPD, can be a tool to translate measured data to precise phenological phases of fruit growth and can be used for orchard management. These results will be useful for creating more robust and precise models for olive fruit growth and to gather useful outputs for precision agriculture methods.

References

Alhaoui, N.; Gómez-Caravaca, A.M.; Leon, L.; De la Rosa, R.; Fernandez-Gutierrez, A.; Segura-Carretero, A. Pattern of variation of fruit traits and phenol content in olive fruits from six different cultivars. J. Agric. Food Chem. 2015, 63, 10466–10476.

Amitrano, C.; Arena, C.; Rouphael, Y.; De Pascale, S.; De Micco, V. Vapour pressure deficit: The hidden driver behind plant morphofunctional traits in controlled environments. Ann. Appl. Biol. 2019, 175, 313–325.

Bai, Y.; Zhu, G.; Su, Y.; Zhang, K.; Han, T.; Ma, J.; Wang, W.; Ma, T.; Feng, L. Hysteresis loops between canopy conductance of grapevines and meteorological variables in an oasis ecosystem. Agric. For. Meteorol. 2015, 214-215, 319–327.

Bai, Y.; Li, X.; Liu, S.; Wang, P. Modelling diurnal and seasonal hysteresis phenomena of canopy conductance in an oasis forest ecosystem. Agric. For. Meteorol. 2017, 246, 98–110.

Bianco, R.L.; Scalisi, A. Water relations and carbohydrate partitioning of four greenhouse-grown olive genotypes under long-term drought. Trees 2016, 31, 717–727.

Brüggenwirth, M.; Winkler, A.; Knoche, M. Xylem, phloem, and transpiration flows in developing sweet cherry fruit. Trees 2016, 30, 1821–1830.

Chen, L.; Zhang, Z.; Li, Z.; Tang, J.; Caldwell, P.; Zhang, W. Biophysical control of whole tree transpiration under an urban environment in Northern China. J. Hydrol. 2011, 402, 388–400.

COI (International Olive Council). Guide for the Determination of the Characteristics of Oil Olives, COI/OH/Doc. No 1 November 2011. Available online: http://www.internationaloliveoil.org (accessed on 15 September 2021).

Conde, C.; Delrot, S.; Gerós, H. Physiological, biochemical and molecular changes occurring during olive development and ripening. J. Plant Physiol. 2008, 165, 1545–1562. https://doi.org/10.1016/j.jplph.2008.04.018.

Corelli-Grappadelli, L.; Lakso, A.N. Fruit development in deciduous tree crops as affected by physiological factors and environmental conditions (keynote). In Proceedings of the XXVI International Horticultural Congress: Key Processes in the Growth and Cropping of Deciduous Fruit and Nut Trees 636, Toronto, Canada, 11–17 August 2002; pp. 425–441.

Ewers, B.E.; Gower, S.T.; Bond-lamberty, B.; Wang, C.K. Effects of stand age and tree species on canopy transpiration and average stomatal conductance of boreal forests. Plant Cell Environ. 2005, 28, 660–678.

Fernandes, R.D.M.; Cuevas, M.V.; Diaz-Espejo, A.; Hernandez-Santana, V. Effects of water stress on fruit growth and water relations between fruits and leaves in a hedgerow olive orchard. Agric. Water Manag. 2018, 210, 32–40.

Fernández, J. Plant-based methods for irrigation scheduling of woody crops. Horticulturae 2017, 3, 35.

Fernández, F.J.; Ladux, J.L.; Hammami, S.B.; Rapoport, H.F.; Searles, P.S. Fruit, mesocarp, and endocarp responses to crop load and to different estimates of source: Sink ratio in olive (cv. Arauco) at final harvest. Sci. Hortic. 2018, 234, 49–57.

Fishman, S.; Génard, M. A biophysical model of fruit growth: Simulation of seasonal and diurnal dynamics of mass. Plant Cell Environ. 1998, 21, 739–752.

Goldhamer, D.A. Regulated deficit irrigation for California canning olives. In Proceedings of the III International Symposium on Olive Growing 474, Chania, Greece, 12–26 September 1997; pp. 369–372.

Gucci, R.; Lodolini, E.M.; Rapoport, H.F. Water deficit-induced changes in mesocarp cellular processes and the relationship between mesocarp and endocarp during olive fruit development. Tree Physiol. 2009, 29, 1575–1585.
Hammami, S.B.; Manrique, T.; Rapoport, H.F. Cultivar-based fruit size in olive depends on different tissue and cellular processes throughout growth. Sci. Hortic. 2011, 130, 445–451.
Janssen, R.H.H.; Meinders, M.B.J.; van Nes, E.H.; Scheffer, M. Microscale vegetation-soil feedback boosts hysteresis in a regional vegetation-climate system. Glob. Change Biol. 2008, 14, 1104–1112.
Jones, H.G. Monitoring plant and soil water status: Established and novel methods revisited and their relevance to studies of drought tolerance. J. Exp. Bot. 2006, 58, 119–130.
Kong, W.; Rui, H.; Na, L.; Wanming, B.; Junyi, M.; Xiaoyong, B.; Junyu, L.; Junlong, W.; Ji, Z. Dynamic assessment of the fruit quality of olives cultivated in Longnan (China) during ripening. Sci. Hortic. 2019, 253, 8–16.
Kottek, M.; Grieser, J.; Beck, C.; Rudolf, B.; Rubel, F. World map of the Köppen-Geiger climate classification updated. Meteorol. Z. 2006, 15, 259–263.
Tombesi, A. Olive fruit growth and metabolism. Acta Hortic. 1994, 356, 225–232. https://doi.org/10.17660/ActaHortic.1994.356.49.
Manfrini, L.; Pierpaoli, E.; Taylor, J.A.; Morandi, B.; Losciale, P.; Zibordi, M.; Grappadelli, L.C.; Bastías, R.M. Precision fruit growing: How to collect and interpret data on seasonal variation in apple orchards. In Proceedings of the XXVIII International Horticultural Congress on Science and Horticulture for People (IHC2010): International Symposium on Plant 932, Lisbon, Portugal, 22–27 August 2010; pp. 461–469.
Marino, G.; Scalisi, A.; Guzmán-Delgado, P.; Caruso, T.; Marra, F.P.; Lo Bianco, R. Detecting Mild Water Stress in Olive with Multiple Plant-Based Continuous Sensors. Plants 2021, 10, 131.
Martinelli, F.; Sebastiani, L.; Tonutti, P.; d'Andria, R. Molecular and metabolic analyses in developing olive fruit in relation to different water regimes. Acta Hortic. 2011, 888, 163–168. https://doi.org/10.17660/ActaHortic.2011.888.17.
Mayergoyz, I.D. Mathematical Models of Hysteresis and Their Applications, 2nd ed.; Electromagnetism; Academic Press: Cambridge, MA, USA, 2003; ISBN 978-0-12-480873-7.
Meinzer, F.C.; Goldstein, G.; Franco, A.C.; Bustamante, M.; Igler, E.; Jackson, P.; Caldas, L.; Rundel, P.W. Atmospheric and hydraulic limitations on transpiration in Brazilian cerrado woody species. Funct. Ecol. 1999, 13, 273–282.
Monteith, J.; Unsworth, M. Principles of Environmental Physics: Plants, Animals, and the Atmosphere; Academic Press: Cambridge, MA, USA, 2013.
Morandi, B.; Manfrini, L.; Zibordi, M.; Noferini, M.; Fiori, G.; Grappadelli, L.C. A Low-cost Device for Accurate and Continuous Measurements of Fruit Diameter. HortScience 2007a, 42, 1380–1382.
Morandi, B.; Rieger, M.; Grappadelli, L.C. Vascular flows and transpiration affect peach (Prunus persica Batsch.) fruit daily growth. J. Exp. Bot. 2007b, 58, 3941–3947.
Novick, K.A.; Miniat, C.F.; Vose, J.M. Drought limitations to leaf-level gas exchange: results from a model linking stomatal optimization and cohesion-tension theory. Plant Cell Environ. 2016, 39, 583–596.

O'Brien, J.J.; Oberbauer, S.F.; Clark, D.B. Whole tree xylem sap flow responses to multiple environmental variables in a wet tropical forest. Plant Cell Environ. 2004, 27, 551–567.
O'Grady, A.P.; Worledge, D.; Battaglia, M. Constraints on transpiration of Eucalyptus globulus in southern Tasmania, Australia. Agric. Meteorol. 2008, 148, 453–465.
O'Kane, J.P. Hysteresis in hydrology. Acta Geophys. Pol. 2005, 53, 373–383.
Perez-Martin, A.; Flexas, J.; Ribas-Carbó, M.; Bota, J.; Tomàs, M.; Infante, J.M.; Diaz-Espejo, A. Interactive effects of soil water deficit and air vapour pressure deficit on mesophyll conductance to CO2 in Vitis vinifera and Olea europaea. J. Exp. Bot. 2009, 60, 2391–2405.
Phillips, J.D. Sources of nonlinearity and complexity in geomorphic systems. Prog. Phys. Geogr. 2003, 27, 1–23.
Scalisi, A.; Marino, G.; Marra, F.P.; Caruso, T.; Lo Bianco, R. A Cultivar-Sensitive Approach for the Continuous Monitoring of Olive (Olea europaea L.) Tree Water Status by Fruit and Leaf Sensing. Front. Plant Sci. 2020, 11, 340.
Tognetti, R.; d'Andria, R.; Lavini, A.; Morelli, G. The effect of deficit irrigation on crop yield and vegetative development of Olea europaea L.(cvs. Frantoio and Leccino). Eur. J. Agron. 2006, 25, 356–364.
Tovar, M.J.; Romero-Fabregat, M.-P.; Alegre, S.M.; Girona, J.; Motilva, M.J. Composition and organoleptic characteristics of oil fromArbequina olive (Olea europaea L.) trees under deficit irrigation. J. Sci. Food Agric. 2002, 82, 1755–1763.
Unsworth, M.H.; Phillips, N.; Link, T.; Bond, B.J.; Falk, M.; Harmon, M.E.; Hinckley, T.M.; Marks, D.; Paw, U.K.T. Components and controls of water flux in an old-growth douglas-fir-western hemlock ecosystem. Ecosystems 2004, 7, 468–481.
Wullschleger, S.D.; Hanson, P.J.; Tschaplinski, T.J. Whole-plant water flux in understory red maple exposed to altered precipitation regimes. Tree Physiol. 1998, 18, 71–79.
Zarco-Tejada, P.J.; Hubbard, N.; Loudjani, P. Precision Agriculture: An Opportunity for EU Farmers—Potential Support with the CAP 2014–2020; Joint Research Centre (JRC) of the European Commission; Monitoring Agriculture ResourseS (MARS) Unit H04, Brussels, Belgium, 2014.
Zeppel, M.J.B.; Murray, B.R.; Barton, C.; Eamus, D. Seasonal responses of xylem sap velocity to VPD and solar radiation during drought in a stand of native trees in temperate Australia. Funct. Plant Biol. 2004, 31, 461–470.
Zhang, Q.; Manzoni, S.; Katul, G.; Porporato, A.; Yang, D. The hysteretic evapotranspiration—Vapor pressure deficit relation. J. Geophys. Res. Biogeosciences 2014, 119, 125–140.
Zhang, R.; Xu, X.; Liu, M.; Zhang, Y.; Xu, C.; Yi, R.; Luo, W.; Soulsby, C. Hysteresis in sap flow and its controlling mechanisms for a deciduous broad-leaved tree species in a humid karst region. Sci. China Earth Sci. 2019, 62, 1744–1755.
Zucchini, M.; Khosravi, A.; Giorgi, V.; Mancini, A.; Neri, D. Is There Daily Growth Hysteresis versus Vapor Pressure Deficit in Cherry Fruit? Horticulturae 2021, 7, 131.

Chapter 4.

Continuous Third Phase Fruit Monitoring in Olive with Regulated Deficit Irrigation to Set a Quantitative Index of Water Stress

Arash Khosravi[1], Matteo Zucchini[1], Adriano Mancini[2] and Davide Neri[1],*

[1]Department of Agricultural, Food and Environmental Science, Marche Polytechnic University, 60131 Ancona, Italy; a.khosravi@pm.univpm.it (A.K.); m.zucchini@pm.univpm.it (M.Z.); v.giorgi@staff.univpm.it (V.G.)
[2]Department of Information Engineering, Marche Polytechnic University, 60131 Ancona, Italy; a.mancini@staff.univpm.it
* Correspondence: d.neri@staff.univpm.it

Published in Horticulturae 2022, 8, 1221.
https://doi.org/10.3390/ horticulturae8121221

4.1 Abstract

The transversal fruit diameter (FD) was monitored continuously by automatic extensimeters (fruit gauges) in order to monitor fruit growth dynamics under deficit irrigation treatments. The daily diameter fluctuation (ΔD, mm), the daily growth (ΔG, mm), the cumulative fruit growth (CFG, mm), and the fruit relative growth rate (RGR, mm mm^{-1} h^{-1}) of four olive cultivars ('Ascolana dura', 'Piantone di Falerone', 'Arbequina', and 'Lea') were studied during the third phase of fruit growth. Two regulated deficit irrigation treatments DI-20 (20% of ET_c) and DI-10 (10% of ET_c) were applied. The daily hysteretic pattern of FD versus the environmental variable of vapor pressure deficit (VPD) was evaluated using the data of a local weather station. The assessment of fruit growth parameters showed cultivar-specific response to water stress. For instance, after performing deficit irrigation, minimum RGR in different cultivars downsized with various slopes which suggested a very different response of the cultivars to dehydration. On the other hand, the daily hysteretic pattern of FD versus VPD was detected in all the studied cultivars, and a quantitative index (height of hysteresis curves) used for explanation of hysteresis magnitude's changed according to the deficit irrigation treatments. The results showed a significant reduction of height of hysteresis curves by irrigation treatments which were not cultivar-specific. The quantitative index for hysteresis curve magnitude's change in the four olive cultivars of 'Ascolana dura', 'Piantone di Falerone', 'Arbequina' and 'Lea' can efficiently estimate the plant water response to irrigation treatment in olive orchards. However, further investigation needs to be done to implement precise irrigation systems.

Keywords: *Olea europaea* L.; fruit diameter; hysteresis; deficit irrigation; vapor pressure deficit (VPD); water stress index; continuous fruit-based index; extensimeter (fruit gauge)

4.2 Introduction

The importance of olive (*Olea europaea* L.) as essential for human diet and landscape management is undeniable in areas with Mediterranean climate. Olive production has been affected by increasing global demand (table olive and olive oil), which has imposed a greater need for agricultural inputs as we address resource scarcity and climate change (Seifi et al., 2015; Rodrigues et al., 2018; Fraga et al., 2020). One of the key inputs of olive production is water. Around 70% of the world surface of olive groves is irrigated (Romero-Triqueros et al., 2019), therefore, the development of appropriate methods and strategies of sustainable water use in olive groves is fundamental (Fernández, 2014). The most common technique for optimizing water efficiency is Regulated Deficit Irrigation (RDI), in which water deficits are imposed during phenological periods when the tree is most insensitive to water stress (Ahumada-Orellana et al., 2017; Romero-Triqueros et al., 2017; Lodolini et al., 2011a), and complementary irrigation (Lodolini et al., 2014 and 2016). Furthermore, the results of Goldhamer (1999) and Gómez-del Campo (2013) showed that RDI strategies resulted in a saving of about 20% of the total amount of water applied without reducing the yield, fruit and oil content. Moreover, numerous studies show that deficit irrigation avoids or minimizes the negative impact of irrigation on erosion, in particular by reducing surface runoff and contributing less to the infiltration of pollutants (herbicides and pesticides) into groundwater (Rodríguez Sousa et al., 2019). In the classical method, the calculation of irrigation amount is based on multiplying reference evapotranspiration (ET0) by grass-reference-based crop-specific coefficients (Kc). Nevertheless, the traditional method of estimation of Kc for olive orchards could be inaccurate. Kc is affected by some aspects such as canopy architecture, ground cover, and the interactions of climatic conditions, soil type, cultivars, and irrigation management practices (Ahumada-Orellana et al., 2017).

To achieve precise irrigation results, some recent research suggested continuous assessment of plant water status indices (Scalisi et al., 2020; Marino et al., 2021; Caruso et al., 2022a and 2022b). In fact, in Soil Plant Atmosphere Continuum (SPAC), plant plays an interface role between soil and the environment, and its physiological response is a combination of results (Scalisi et al., 2020; Measham et al., 2017; Fernández, 2017). Furthermore, the continuous measurement of plant water status indices would provide a solid base for precision irrigation management, by real time response to water stress. However, the olive species (*Olea europaea*) has a very wide genetic pool, which can respond to drought using different leaf and fruit physiological and morphological mechanisms (Scalisi et al., 2020; Lo Bianco and Scalisi, 2017). It includes genotypes that can respond to drought using different tolerances to leaf dehydration and morphological and structural adaptations of the leaves (Scalisi et al., 2020). Lo Bianco and Scalisi 2017) found a different leaf stomatal regulation among the olive cultivars. Due to this difficulty, the correct choice of the water status index of the plant is essential. The most common suggested indices are midday stem water potential (Ψstem), trunk diameter variation (TDV), sap flow (SF), leaf turgor pressure (LTP), as well as fruit diameter (FD), which can be used alone or in combination. A combination of indices (sensors) could provide robust data, however, increased the complexity. Moreover, considering the difficulty of replicating continuous measurements on a large number of trees, the need to obtain an accurate index has become more essential. The midday stem water potential (Ψstem) is accurate and reliable, however, not only it is a

destructive method, but also not suitable for continuous measurement (Scalisi et al., 2019 and 2020; Marino et al., 2018). The stem/trunk diameter variation (by trunk dendrometer) is another useful index. However, the trunk diameter fluctuations are affected by plant age and size, crop load, environmental variables, and growth patterns (Fernández, 2017). The sap flow (SF) methods are particularly demanding in terms of installation; most of the SF methods suitable for fruit trees are invasive, such that sensors must be installed within the trunk of the trees (Fernández, 2014). Moreover, the sap flow rate demonstrates transpiration dynamics that depend on stomatal activity and environmental variables (Scalisi et al., 2019). The leaf turgor pressure (LTP) measurement method is carried out by probe which is a cheap and handy method but does not allow for continuous measurement (Boini et al., 2019). The advanced LTP measurement method employed leaf patch clamp pressure (LPCP) probes is able to continuously monitor the pressure, but the different initial condition of the leaf related to age (especially in evergreen species) and exposure to light inside the canopy leads to obtaining partial information from LPCP (Marino et al., 2021; Scalisi et al., 2019). In addition, findings by Jones (2004) suggested that LTP in the isohydric species is not very useful in the early detection of plant water deficiency. The other innovative plant water status index is fruit diameter (FD). The daily fruit growth dynamics can be expounded as changes in flows of water into and out of the fruit, rather than carbon gains; thus, the daily fruit diameter variation responds to water deficit (Marino et al., 2021; Scalisi et al., 2017; Fernandes et al., 2018; Khosravi et al., 2021). Fruits represent the actual goal of production but fruit growth is the result of several genetic, metabolic, hormonal, and environmental interactions (Gucci et al., 2009), therefore, optimal fruit growth can be determined only by the efficient physiological manipulation of the condition tree (Boini et al., 2019). In the olive tree, the root response to localized application systems of organic residues, nutrients, and water reveal an enormous plasticity of the root system (Giorgi et al., 2008; Lodolini et al., 2011b; Polverigiani et al., 2012) which can compensate for local stress. Although olive tree root systems are highly capable and could supply a constant water flow, fruit daily growth trend is described by periods of shrinkage and then after expansion, which usually lead to increase in fruit size at the end of the day (Boini et al., 2019; Khosravi et al., 2021). Due to the research of Fernandes et al. (2018) and Marino et al. (2021), the daily variations in fruit transversal diameters can be expounded as changes in flows of water into and out of the fruit hence, these can be connected to vapor pressure deficit (VPD) and tree water status. Furthermore, Scalisi et al. (2020) explained that fruit growth (measured by FD) is strictly related to soil water availability and plant water status, it is also influenced by environmental variables, crop load, genetic factors, and phenology. Consequently, fruit growth monitoring (by FD) could represent a sensitive indicator of plant water and physiological status of the trees, especially during cell expansion phase, when fruit growth rate is constant and truly decisive for productive performances (Boini et al., 2019; Lakso et al., 1995). FD monitoring has been investigated in several studies by researchers to measure daily fluctuation in the volume of selected fruits, including pears (Morandi et al., 2014), sweet cherry (Brüggenwirth et al., 2016; Mancini et al., 2021; Zucchini et al., 2021), mango (Carella et al., 2021), apple (Boini et al., 2019), nectarine (Scalisi et al., 2019), orange (Grilo et al., 2019), and olive (Scalisi et al., 2020; Marino et al., 2021; Fernandes et al., 2018; Khosravi et al., 2021). The continuous FD monitoring provides robust data but water management protocols based on FD measurements need further study to develop field applicable models (Marino et al.,

2021; Boini et al., 2019; Khosravi et al., 2021). A common challenge with tree-based sensors is to adjust their output to physiologically meaningful parameters in a consistent manner (Fernández, 2017; Khosravi et al., 2021; Zucchini et al., 2021).
In order to translate outputs of plant-based sensors, the phenomenon of hysteresis should be further considered. Explaining the causes of hysteretic phenomenon appears fraught with complex interactions between exogenous and endogenous factors to the plant system [39]. The root of the word hysteresis is Greek and means to "lag behind" (Zhang et al., 2014; Khosravi et al., 2021). Hysteresis is non-linear loop-like behavior that has been known in plant systems for a long time (Zhang et al., 2014; Mayergoyz, 2003). In hysteresis, when the time argument of an input function is stretched or compressed, the corresponding output function is not stretched in the same way, so the hysteresis does not show affine similarity with respect to time (Zhang et al., 2014; Phillips, 2003; O'Kane, 2005). For example, a diurnal hysteresis between evapotranspiration (ET) (or transpiration) and vapor pressure deficit (VPD) has been studied [40]; hysteresis as a relationship between environmental factor (e.g., meteorological factors) and sap flow (Zhang et al., 2014; Zappel et al., 2004; O'Brein, 2004); hysteresis was found also in the relationship between canopy conductance and temperature (Bai et al., 2017); hysteresis between fruit diameter and leaf pressure on two different olive cultivars (Scalisi et al., 2020). Furthermore, in the cherry fruit growth relationship with VPD, complete hysteresis was found only during the maturation phase while during fruit extension phase the hysteresis was null or partial (Zucchini et al., 2021). Recently Khosravi et al. (2021) examined the 'Frantoio' olive cultivar and explained the different hysteresis curves of the diameter versus the VPD during the second, third, and fourth phases of olive fruit development. According to this research, monitoring hysteretic loops and detecting the magnitude change could be used as a method for detecting the growth phases. In this research, the form, magnitude, and rotational pattern of hysteresis curve (loop) of transversal diameter versus VPD were investigated. It has been shown that VPD is especially important in woody plants, where it is the main variable affecting their diurnal evolution of transpiration (Perez-Martin et al., 2009).
The aim of this work was to describe third phase of olive fruit development by continuous monitoring with extensimeter under regulated deficit irrigation regimes. Furthermore, we hypothesized the presence of hysteresis curves by examining the olive fruit diameter (FD) compared to VPD. We intended to provide some indexes for smart irrigation in relation to the regulated deficit irrigation in a key phenological stage of the fruit.

4.3 Materials and Methods

4.3.1. Site Description and Phenology

The experiment was carried out in 2021 at the experimental farm of the Polytechnic University of Marche, located in Agugliano (Marche, Italy) (latitude 43°54′ N, longitude 13°36′ E, altitude 85 m), in a high-density olive orchard in four self-rooted olive (Olea europaea L.) cultivars of 'Ascolana dura', 'Piantone di Falerone', 'Arbequina' and 'Lea'. The trees were planted 4 × 2 m (1250 tree ha^{-1}) in May 2012, about 9 years old at the time of experiment. Each cultivar was displayed in a separate row. The olive trees were initially trained as a central leader, the tree canopy was afterwards flattened according to a

hedgerow, removing long branches toward the interrow (Assirelli et al., 2021). Integrated agricultural methods were adopted for the agricultural operations, pest control, and fertilization practices according to regional guidelines (Agenzia Servizi Settore Agroalimentare delle Marche (ASSAM). The irrigation was localized and used to perform different irrigation treatments during experiment (see Section 4.3.2. Irrigation). The soil was managed with permanent grass cover in the inter-row alley, with mowing 3–4 times during the growing season and with tillage along the row (Khosravi et al., 2021).

4.3.2. Irrigation

The olive trees were irrigated by a drip irrigation system with a flow of 8 (L h^{-1}) per tree. Two deficit irrigation levels were performed and the higher dose (DI-20) was supplied to big fruit varieties while the lower dose (DI-10) was supplied to medium-small fruit varieties. DI-20 had 20% of the amount of ET_c and was supplied to Ascolana dura and Piantone di Falerone trees, while DI-10 had 10% of the amount of ET_c and was supplied to Lea and Arbequina trees. The crop evapotranspiration ET_c was estimated according to FAO56 equation which is:

$$(ET_c = ET_0 \times K_c) \quad (1)$$

where the evapotranspiration (ET_0) was calculated by the local weather station automatically via FAO Penman–Monteith equation and K_c was the crop coefficient (Ahumada-Orellana et al., 2017). Moreover, effective rainfall (R) was calculated as:

$$R = (Pp - 5) * 0.75 \quad (2)$$

where Pp = rainfall obtained from the local weather station (Ahumada-Orellana et al., 2017). The irrigation treatment was performed according to the randomized block with three replications, and each block consisted of at least five adjacent trees on the same row. The irrigation was done three times during the experiment period, 17th August (Day of the Year, DOY, 229), 19th August (DOY 231), and 16th September (DOY 259). The DI-20 irrigated cultivars received 62 mm of water during all fruit growth phases which 17.5 mm was during the third growth phase. For the DI-10 irrigated cultivars the amount of received water during all fruit growth phases and third growth phase were 31 and 8.75 mm, respectively. For big fruit varieties of Ascolana dura and Piantone di Falerone, the no irrigated fruit (DI-0) was considered as a reference point for detecting the effect of the deficit irrigation treatment on fruit growth. The rationale behind using DI-0 against fully irrigated treatment comes from the idea of analyzing the effect of deficit irrigation on fruit growth (daily and periodical growth) which should be discovered in comparison with normal growth conditions (without irrigation). The changes in the daily olive fruit growth pattern by irrigation has been explained by some research previously (Scalisi et al., 2020; Marino et al., 2021).

4.3.3. Fruit Maturation Monitoring

From 19th September (DOY 262) to 26th October (DOY 299) the fruits, which were placed inside the extensimeter, were photographed by Canon EOS 1100D Camera (Canon Inc., Tokyo, Japan) weekly. In the case of adverse weather conditions, taking images was postponed to the next possible day. The ripening status of each olive fruit was assessed according to the first five (0–4) classes of Jaen index (International Olive Council (COI) COI/OH/Doc. No 1 November 2011) (Table 4.1). Up to DOY 276, fruits inside the extensimeter were in the third phase of fruit development, and maturity index ranged from 0 to 2. Consequently, DOY 276 was considered the ending day of the third phase of fruit development.

Table 4.1. Data of ripening index for the fruits, which were mounted on the extensimeters. Data were collected weekly from 262 to 299 days of the year (DOY). Maturation indexes were performed according to the first five (0 to 4) categories of the Jaen index. Arb1(DI-10) and Arb2(DI-10) represent fruit 1 and 2 of "Arbequina" at 10% deficit irrigation, respectively. Lea1(DI-10) and Lea2(DI-10) represent fruit 1 and 2 of "Lea" at 10% deficit irrigation, respectively. Asc1(DI-20) and Asc2(DI-20) represent fruit 1 and 2 of "Ascolana dura" at 20% deficit irrigation, respectively. Asc3(DI-0) represents fruit 3 of non-irrigated "Ascolana dura". Fal1(DI-20) and Fal2(DI-20) represent fruit 1 and 2 of "Piantone di Falerone" at 20% deficit irrigation, respectively. Fal4(DI-0) represents fruit 4 of non-irrigated "Piantone di Falerone".

DOY	Arb1(DI-10)	Arb2(DI-10)	Lea1(DI-10)	Lea2(DI-10)	Asc1(DI-20)	Asc2(DI-20)	Asc3(DI-0)	Fal1(DI-20)	Fal2(DI-20)	Fal4(DI-0)
262	0	0	0	0	0	0	0	0	0	0
269	0	0	0	1	0	0	0	0	0	2
276	0	0	0	2	0	0	0	2	1	2
284	0	0	1	3	1	1	1	3	2	2
291	1	1	1	3	1	1	1	3	3	3
299	1	1	2	4	3	2	2	4	3	3

4.3.4. Fruit Measurement and Experimental Design

The fruit transversal diameter (synonym to equatorial diameter) of ten fruits were monitored by automatic extensimeters (synonym to fruit gauge) from 12th August (DOY 224) to 3rd October (DOY 276) in 2021. We used two kinds of extensimeters; one model was Winet (Winet s.r.l. Cesena, Italy) and another model was DEX20 (Dynamax Inc., Houston, TX, USA). The Winet experimental extensimeter consisted of a variable linear resistance transducer sensor (model MM(R)10-12) (Megatron Elektronik GmbH & Co., Munich, Germany) supported by a stainless steel frame. The extensimeters were connected to the wireless data-logger system (Winet s.r.l. Cesena, Italy) which collected data at 10

min intervals. Data has been sent through the wireless nodes to a central network node, which transmits information via general packet radio service (GPRS) modem to the server. Second model of extensimeter (DEX20) was a caliper style device with a full bridge strain gage attached to a flexible arm; data were recorded by CR1000X data logger (Campbell scientific, Inc., Logan, UT, USA) every hour and sent to our own cloud service based on Amazon Web Service (AWS) twice per day. Both models of extensimeters were examined and showed accurate functionality (Khosravi et al., 2021; Morandi et al., 2007a).
The full bloom day occurred for Arbequina and Ascolana dura on the 24th and 28th of May, and for Piantone di Falerone and Lea on the 31st of May. So, the experiment started almost 11 weeks after full bloom (WAFB). Moreover, the BBCH scale was employed to obtain a phenological phase. In this scale, the end of the second phase of fruit development (pit-hardening) was determined when it was no longer possible to cut the fruit (Ahumada-Orellana et al., 2017). For each cultivar, 15 fruits were sampled randomly. Sampling was repeated every 10 days and pit resistance to cutting were examined by blade. The ending day of the second phase of fruit development was observed on the 13th of August (DOY 225). Consequently, our experiment period started from the third phase (cell expansion) of fruit development.
Eight fruits were mounted on Wi-net extensimeter which consisted of three fruits of Ascolana dura (two with DI-20 and one DI-0 (without irrigation) that from here called Asc1 (DI-20), Asc2 (DI-20) and Asc3 (DI-0), three fruits of Piantone di Falerone (two with DI-20 and one DI-0 (without irrigation) that from here called Fal1 (DI-20), Fal2 (DI-20) and Fal3 (DI-0) and two fruits of Lea with DI-10 irrigation level that from here called Lea1 (DI-10) and Lea2 (DI-10). In the middle of the experiment the fruit of Fal3 (DI-0) felt down and was substituted with Fal4 (DI-0). Two fruits of Arbequina with DI-10 irrigation level were mounted on DEX20 extensimeter (Arb1 (DI-10) and Arb2 (DI-10)). The representative trees according to irrigation level were selected in the center of the experimental block to avoid border effect. Moreover, all extensimeters of the same cultivar-irrigation level were installed together on one representative tree.
According to the importance and physiological effect of daylight on fruit growth and its role in photosynthesis, the graphic representation of daily fruit growth and its fluctuations were reported from the time of sunrise (Scalisi et al., 2020; Khosravi et al., 2021). In fact, the day started from sunrise and continued for 24 h. Based on data from our weather station, sunrise time from 12th of August to 5th of September (DOY 224 to 248) was estimated at 6 AM, from 6th of September to 3rd of October (DOY 249 to 276) was estimated at 7 AM.

4.3.5. Fruit Growth Parameters

In correspondence with the days in which irrigation treatment (DI-20 and DI-10) were performed (DOYs 229, 231 and 259), 6 day intervals were selected for assessment of deficit irrigation effect on fruit growth. The mentioned window (6 days) consisted of the 2 days before irrigation up to 3 days after irrigation day. The parameters calculated for each intervals were: 1) daily diameter fluctuation (ΔD, mm) which was calculated as the maximum diameter minus the minimum diameter of same day, 2) daily growth (ΔG, mm) which was calculated as the diameter of ending point of day minus the diameter of starting

point of same day, 3) cumulative fruit growth (CFG, mm) as the maximum daily diameter of the fruit subtracted from maximum diameter of the previous day (Fernandes et al., 2018), 4) fruit relative growth rate (RGR, mm mm^{-1} h^{-1}) was calculated using the following equation:

$$RGR = [(\ln D_2 - \ln D_1)/(t_2 - t_1)] \quad (3)$$

where D_1 and D_2 are fruit diameters at times t_1 and t_2, respectively (Scalisi et al., 2020; Marino et al., 2021). And the daily range of RGR (RGRrange, mm mm^{-1} h^{-1}) was calculated as the difference between the minimum value and the maximum value of RGR in one day.

In addition, unitless (standardized) data have been used to allow comparisons among fruits with different initial diameter when extensimeters were installed. The data of sensors was standardized for each day by using:

$$x' = x/x_0 \quad (4)$$

where x' is the standardized value, x is the value of the existing data, and x_0 is the initial values of the data at starting point of same day.

4.3.6. Meteorological Data

According to Köppen–Geiger climate classification, Agugliano is classified in the Cfa category and this is characterized by warm temperature, highly humid and warm summer (Kottek et al., 2006) but in recent years the classification is moving toward Csa (hot summer Mediterranean). Meteorological data were recorded with a MeteoSense 4.0 weather station (Netsense S.r.l Florence, Italy) located in the olive orchard. For the calculation of vapor pressure deficit (VPD), air temperature (T), and relative humidity (RH) data were collected from our weather station. Vapor pressure deficit was calculated as:

$$VPD = (1-(RH/100)) \times SVP \text{ and } SVP \text{ (Pascals)} = 610.7 \times 10^{\wedge(7.5T/(237.3 + T))} \quad (5)$$

The VPD formula was recommended by Monteith and Unsworth (Monteith and Unsworth, 2013); where RH is the relative humidity, SVP is saturated vapor pressure, and T is temperature (°C). Our instrument was set to legal Rome time.

4.3.7. Hysteresis Curves

To explore the circadian pattern of hysteresis curve (loop), hourly collected data of transversal fruit diameter (FD) versus VPD were considered. For description of the hysteresis rotational pattern, the terms of clockwise and anticlockwise curve were employed. Furthermore, for characterization of hysteresis form, three concepts of partial, incomplete, and complete were used. When the hysteresis curve appeared in some part of the day and was not representative of the whole day, it was called partial. When the ending point of the hysteresis loop reached the same level of the starting point of the loop, it was defined as complete. Lastly, when the ending point of the hysteresis loop did not reach the same level of the starting point of the loop, so the loop was not completely closed, it was

called incomplete hysteresis curve. For detection of incomplete clockwise hysteresis, normalized data of diameter were employed. Hysteresis loops were considered incomplete when the loop "opening" was more than 0.05 units. In the case of loop opening, less than 0.05 is considered as complete (Khosravi et al., 2021).
The measured daily data were normalized by Min-Max method through the equation:

$$x' = 0.9 \times ((x - x_{min})/x_{max} - x_{min}) + 0.05 \quad (6)$$

where x' is the normalized value, x is the value of the existing data, and x_{min} and x_{max} are the minimum and maximum values of the data, respectively (Khosravi et al., 2021; Zucchini et al., 2021).

4.3.8. Data Analysis and Presentation

One-way repeated measures analysis of variance (ANOVA) was performed for assessing significant differences. The significant differences among the treatments were assessed using Student–Newman–Keuls's test ($p < 0.05$). All data analyses and graph design were performed using Sigmaplot 14.5 (Systat Software, Inc., San Jose, CA, USA).

4.4 Results

4.4.1. Environmental Data Analysis and VPD Evolution

Figure 4.1 shows the data of VPD, temperature (T), ET0, and rainfall during the experiment (DOY 224 to DOY 276). The highest measured hourly VPD was 5.4 (kPa) on 16th of August (DOY 228) and the lowest was 0.05 (kPa) on 23rd and 24th of August (DOYs 235 and 236). The highest daily average of VPD was 3.0 (kPa) on the 16th of August (DOY 228) and the lowest was 0.12 (kPa) on the 27th of September (DOY 270). The daily mean of VPD during the experiment was 0.91 ± 0.56 (kPa). The daily mean of temperature during experiment was 21.30 ± 3.43 (°C), with a minimum daily temperature of 15.76 (°C) on the 1st of October (DOY 274) and maximum daily temperature of 32.26 (°C) reached on 17th of August (DOY 229). The maximum and minimum hourly temperatures were 39.0 and 9.5 (°C) which reached on 16th of August (DOY 228) and 1st of October (DOY 274), respectively. The total reference ET_0 was 173.9 (mm) for the experiment period. The maximum and minimum daily ET_0 was 6.3 (mm day^{-1}) on 16th of August (DOY 228) and 0.6 (mm day^{-1}) on 27th of September (DOY 270), respectively. The maximum hourly ET_0 was 0.7 (mm $hour^{-1}$) which reached on 14th, 15th, 16th of August (DOYs 226, 227, and 228). During the experiment period, the accumulated rainfall was 96.1 (mm), with maximum hourly and daily of 17.6 (mm $hour^{-1}$) and 39.5 (mm day^{-1}) reached on 23rd of August (DOY 235).

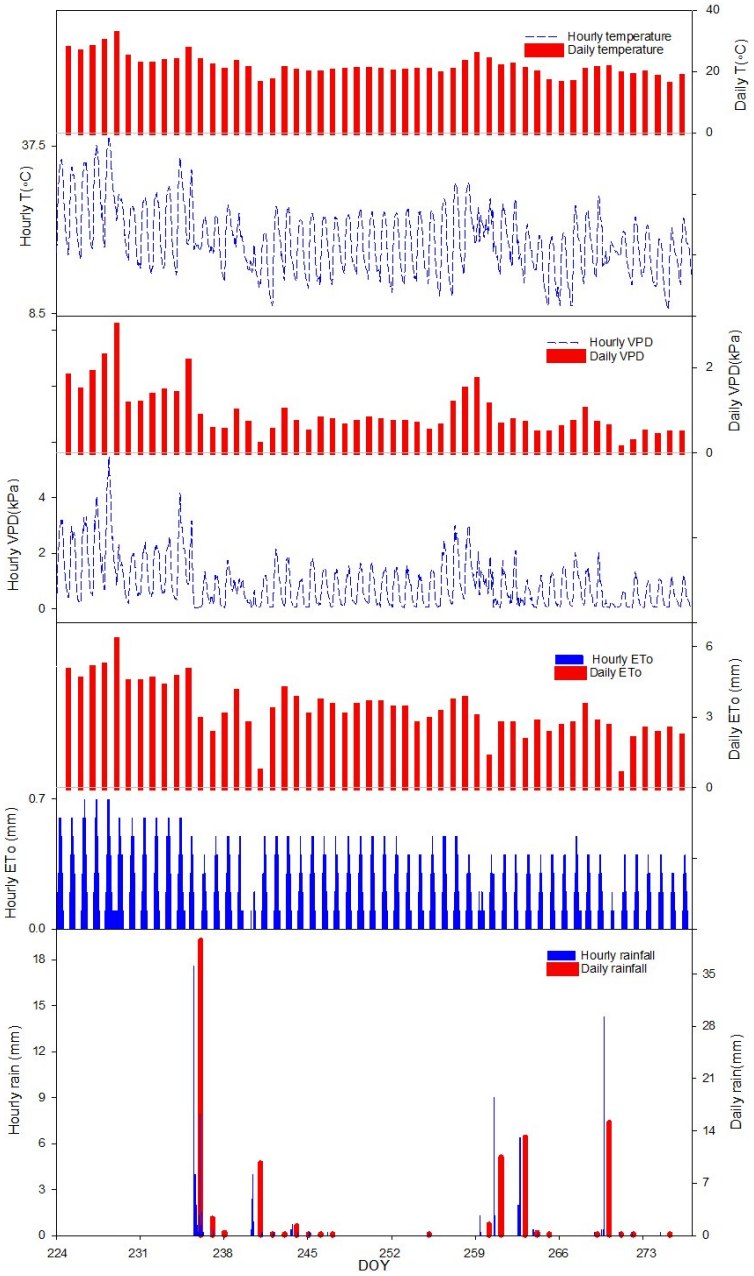

Figure 4.1. Trend of hourly and daily temperature (T), vapor pressure deficit (VPD), reference evapotranspiration (ET_0) and rainfall, during the experiment period (from 224 to 276 days of the year (DOY), obtained by MeteoSense 4.0 weather station.

4.4.2. Fruit Growth

Figure 4.2 reports the hourly transversal diameter of fruits for the four different cultivars from DOY 224 to DOY 276. The typical third phase of the fruit growth was observable in all four cultivars (Lea, Figure 4.2A; Arbequina, Figure 4.2B; Piantone di Falerone, Figure 4.2C; Ascolana dura Figure 4.2D); however, with dissimilar growth slope among different cultivars and a final relentless toward maturation (4th phase). The fruit growth showed a diameter increase with diurnal fluctuation. The diurnal fluctuation of olive fruit was detected as a shrinkage of fruit diameter from mid-morning to early afternoon followed by expansion of fruit diameter from late afternoon to early morning (Figure S4.1A). At the end of the day, the fruits reached a size larger than the initial point of the same day. In fact, Arbequina (DI-10) in 60.4% of cases (64 out of 106), Lea (DI-10) in 82.89% of cases (63 out of 76), Ascolana dura (DI-0) in 77.5% of cases (38 out of 49), Ascolana dura (DI-20) in 72.4% of cases (55 out of 76), Piantone di Falerone (DI-0) in 82.5% of cases (32 out of 39) and Piantone di Falerone (DI-20) in 87.7% of cases (86 out of 98) reached a size similar or larger than the initial point of same day.

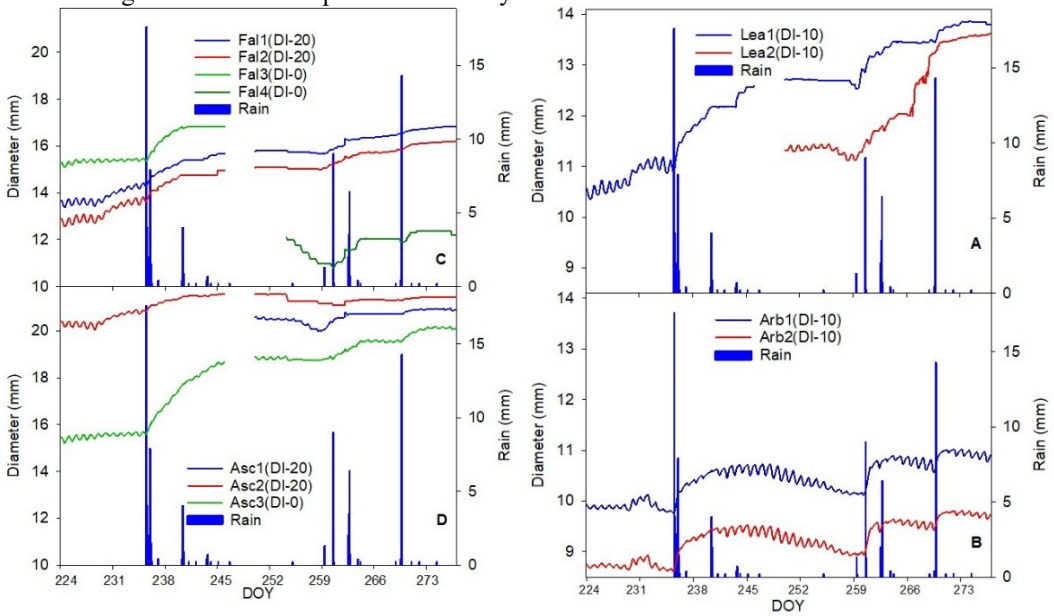

Figure 4.2. Continuous measurements of diameter of olive fruits during the experiment period (from 224 to 276 days of the year (DOY): (A) fruit 1 and 2 of "Lea" at 10% deficit irrigation (Lea1(DI-10) and Lea2(DI-10), respectively); (B) fruit 1 and 2 of "Arbequina" at 10% deficit irrigation (Arb1(DI-10) and Arb2(DI-10), respectively); (C) fruit 1 and 2 of "Piantone di Falerone" at 20% deficit irrigation (Fal1(DI-20) and Fal2(DI-20), respectively) and fruit 3 and 4 of non-irrigated "Piantone di Falerone" (Fal3(DI-0) and Fal4(DI-0), respectively) ; (D) fruit 1 and 2 of "Ascolana dura" at 20% deficit irrigation (Asc1(DI-20) and Asc2(DI-20), respectively) and fruit 3 of non-irrigated "Ascolana dura"

(Asc3(DI-0)). Missing data From 224 to 249 day of the year (DOY) for Lea2 (DI-10) and Asc1 (DI-20) and from 246 to 249 day of the year (DOY) for panel (A,C,D).

The duration, from beginning to finishing daily fruit shrinkage and expansion, did not show similarity among cultivar-irrigation level (Table S4.1). In addition, there were some exceptional days which showed different growth patterns (Figure S4.1B). There was no unique pattern for explanation of diameter (fruit growth) fluctuation of these days.

4.4.3. Irrigation Response

Monitoring the daily variation of fruit diameter at 6 days' window (from DOY 227 to 234) in correspondence with first and second irrigation days showed that diameter of Arb1(DI-10) downsized from 9.91 mm to 9.81 mm, whereas for Arb2 (DI-10) downsized from 8.76 mm to 8.65 mm, but for Lea1 (DI-10) started from 10.7 mm and increased to 11.1 mm. At the same period, diameter of Asc2 (DI-20) started from 20.4 mm up to 20.9 mm, Fal1 (DI-20) started from 13.7 mm up to 14.4 mm, and Fal2 (DI-20) started from 13.0 mm and reached 13.8 mm, whereas transversal diameter of Asc3 (DI-0) and Fal3 (DI-0) started from 15.6 mm and 15.4 mm up to 15.7 mm and 15.4 mm, respectively (Figure S4.2A–D). It showed diameter increase for both cultivar with and without irrigation treatment, nevertheless, standardized diameter (Table 4.2) showed different ratio of diameter growth. For irrigated Ascolana dura and Piantone di Falerone, the ratio of diameter growth was higher than non-irrigated treatment.

Table 4.2. Standardized data of diameter for period of 227 to 234 day of the year (DOY) and 257 to 262 day of the year (DOY). Data of DOY 227 and 257 is related to the starting point of day and for DOY 234 and 262 is related to the ending point of day. Arb1(DI-10) and Arb2(DI-10) represent fruit 1 and 2 of "Arbequina" at 10% deficit irrigation, respectively. Lea1(DI-10) and Lea2(DI-10) represent fruit 1 and 2 of "Lea" at 10% deficit irrigation, respectively. Asc1(DI-20) and Asc2(DI-20) represent fruit 1 and 2 of "Ascolana dura" at 20% deficit irrigation, respectively. Asc3(DI-0) represents fruit 3 of non-irrigated "Ascolana dura". Fal1(DI-20) and Fal2(DI-20) represent fruit 1 and 2 of "Piantone di Falerone" at 20% deficit irrigation, respectively. Fal3(DI-0) and Fal4(DI-0) represent fruit 3 and 4 of non-irrigated "Piantone di Falerone", respectively. Fal3 (DI-0) fell down and has been substituted with Fal4 (DI-0) for 257 to 262 day of the year (DOY). Missing data from 227 to 234 day of the year (DOY) for Lea2 (DI-10) and Asc1(DI-20).

DOY	Arb1 (DI-10)	Arb2 (DI-10)	Lea1 (DI-10)	Lea2 (DI-10)	Asc1 (DI-20)	Asc2 (DI-20)	Asc3(DI-0)	Fal1 (DI-20)	Fal2 (DI-20)	Fal3(DI-0)	Fal4(DI-0)
	First and second irrigation treatment (DOYs 229 &231)										
227	0.4	0.46	0.29	-	-	0.41	0.62	0.34	0.32	0.72	-
234	0.13	0.15	0.79	-	-	0.91	0.9	0.95	0.95	0.89	-
	Third irrigation treatment (DOY 259)									-	
257	0.19	0.2	0.23	0.24	0.38	0.95	0.1	0.17	0.08	-	0.81
262	0.95	0.91	0.95	0.83	0.89	0.95	0.95	0.92	0.92	-	0.95

In correspondence with the third irrigation day (from DOY 257 to 262), diameter of Arb1 (DI-10) started at 10.2 mm reached 10.8 mm, and for Arb2 (DI-10) started from 9.0 mm up to 9.6 mm. Diameter of Lea1 (DI-10) started from 12.7 mm and reached to 13.3 mm, and for Lea2 (DI-10) started from 11.3 mm up to 11.7 mm. About Asc1 (DI-20) diameter started from 20.3 mm and reached 20.7 mm and for Asc2 (DI-20) started from 21.3 mm and remained the same size. About Fal1 (DI-20), diameter started from 15.7 mm and reached 16.3, and Fal2 (DI-20) started from 15.0 mm and reached 15.5 mm. In the non-irrigated fruits, the diameter of Asc3 and Fal4 started from 18.77 mm and 11.4 mm up to 19.3 mm and 11.6 mm, respectively (Figure S4.2E–H). Data showed diameter increase for all the four cultivars with different irrigation levels and for two cultivars (Ascolana dura and Piantone di Falerone) without irrigation treatment. Data of standardized diameter explained that diameter growth ratio in irrigated Ascolana dura was lower than non-irrigated and for irrigated Piantone di Falerone was higher than non-irrigated (Table 4.2).

The daily growth (ΔG) (Table 4.3) provided more information related to diameter change in correspondence with irrigation days. On the first irrigation day (DOY 229), for both cultivars with DI-20, not only ΔG was positive, but it was higher than ΔG of the previous day. At the same time, ΔG for non-irrigated fruits did not show any growth in comparison with the previous day. In fact, ΔG of Ascolana dura (DI-0) was positive and the same as the previous day and for Piantone di Falerone (DI-0) was negative and lower than previous day. About cultivars with DI-10, ΔG was higher than the previous day but for Lea it was positive and for Arbequina it was negative. In all four irrigated cultivars (with DI-10 or DI-20), in the day after irrigation ΔG increased in comparison with the day before. The trend

of ΔG in the non-irrigated fruits at the day after Irrigation for Ascolana dura was downward, and for Piantone di Falerone did not show any changes.

Table 4.3. Standardized data of daily fruit growth (ΔG) in correspondence with irrigation days. Data was related to the 6 days window (2 days before and 3 days after irrigation day). Arb1(DI-10) and Arb2(DI-10) represent fruit 1 and 2 of "Arbequina" at 10% deficit irrigation, respectively. Lea1(DI-10) and Lea2(DI-10) represent fruit 1 and 2 of "Lea" at 10% deficit irrigation, respectively. Asc1(DI-20) and Asc2(DI-20) represent fruit 1 and 2 of "Ascolana dura" at 20% deficit irrigation, respectively. Asc3(DI-0) represents fruit 3 of non-irrigated "Ascolana dura". Fal1(DI-20) and Fal2(DI-20) represent fruit 1 and 2 of "Piantone di Falerone" at 20% deficit irrigation, respectively. Fal3(DI-0) and Fal4(DI-0) represent fruit 3 and 4 of non-irrigated "Piantone di Falerone", respectively. Fal3 (DI-0) fell down and has been substituted with Fal4 (DI-0) for 257 to 262 day of the year (DOY). Missing data from 227 to 234 day of the year (DOY) for Lea2 (DI-10) and Asc1(DI-20).

DOY	Arb1(DI-10)	Arb2(DI-10)	Lea1(DI-10)	Lea2(DI-10)	Asc1(DI-20)	Asc2(DI-10)	Asc3(DI-0)	Fal1(DI-20)	Fal2(DI-20)	Fal3(DI-0)	Fal4(DI-0)
227	0.0004	0.0021	0.0019	-	-	−0.0029	−0.0006	−0.0029	−0.0031	0.0000	-
228	−0.0005	0.0021	0.0028	-	-	0.0000	0.0013	−0.0044	−0.0054	0.0006	-
229	−0.0050	−0.0086	0.0102	-	-	0.0054	0.0013	0.0102	0.0139	−0.0013	-
230	−0.0076	−0.0066	0.0119	-	-	0.0063	−0.0013	0.0116	0.0144	−0.0013	-
231	−0.0034	−0.0029	0.0073	-	-	0.0048	−0.0006	0.0086	0.0097	0.0000	-
232	0.0158	0.0177	0.0027	-	-	0.0034	0.0006	0.0064	0.0074	0.0006	-
233	0.0134	0.0113	−0.0018	-	-	0.0029	0.0006	0.0049	0.0044	0.0006	-
234	0.0029	0.0029	−0.0090	-	-	−0.0010	0.0000	0.0021	0.0022	0.0000	-
257	0.0043	0.0059	0.0000	−0.0044	−0.0089	0.0000	−0.0011	−0.0032	0.0000	-	−0.0236
258	0.0030	0.0041	−0.0063	0.0018	−0.0045	−0.0042	0.0011	−0.0019	−0.0007	-	−0.0170
259	0.0008	−0.0017	0.0174	0.0116	0.0145	−0.0005	0.0048	0.0089	0.0100	-	−0.0009
260	−0.0395	−0.0408	0.0194	0.0159	0.0108	−0.0024	0.0058	0.0063	0.0072	-	0.0027
261	−0.0177	−0.0204	0.0076	0.0201	0.0015	0.0000	0.0074	0.0088	0.0098	-	0.0154
262	−0.0022	0.0020	0.0053	0.0009	0.0068	0.0071	0.0084	0.0137	0.0052	-	0.0294

On the second irrigation day (DOY 231), ΔG for both cultivars with DI-20 was positive, however, it was lower than ΔG of the previous day. Concurrently, ΔG of non-irrigated fruits was higher than the previous day. Although, ΔG of Ascolana dura (DI-0) was negative and for Piantone di Falerone (DI-0) was zero. About cultivars with DI-10, for Arbequina ΔG was greater than the previous day and with a negative amount and for Lea it was lower than the previous day with a positive amount. In both irrigated cultivars with DI-20, in the day after irrigation, ΔG decreased in comparison with the day before, whereas ΔG of non-irrigated fruits for both cultivars increased. About cultivars with DI-10, in the day after irrigation, for Arbequina ΔG increased and for Lea ΔG decreased in comparison with the previous day.

On the third irrigation day (DOY 259), ΔG for both cultivars of Ascolana dura and Piantone di Falerone (irrigated (DI-20) and non-irrigated (DI-0)) was higher than the previous day. About cultivars with DI-10, ΔG of Arbequina was lower than the previous

day but for Lea was higher. On the day after irrigation, ΔG for both cultivars with DI-20 was lower than the irrigation day, whereas ΔG of non-irrigated (DI-0) cultivars was higher than the irrigation day. About cultivars with DI-10, in the day after irrigation, for Arbequina ΔG reduced and for Lea ΔG enlarged in comparison with the previous day (Table 4.3).

The daily diameter fluctuation (ΔD) in the first irrigation day was reduced in both cultivars with DI-20 and reduction continued until the day after irrigation, whereas in both cultivars with DI-10, ΔD increased and the day after decreased. In the second irrigation day, ΔD in both cultivars with DI-20 was almost the same as the previous day, and in the day after irrigation, followed by slight increase for cultivar Piantone di Falerone and stability for Ascolana dura. In the second irrigation day, ΔD for cultivar with DI-10 followed the opposite trend, which was a reduction for Arbequina and an increase for Lea; however, in the day after irrigation ΔD for both DI-10 cultivars increased. In the third irrigation day, ΔD for Piantone di Falerone DI-20 increased and in the day after decreased. For the Ascolana dura DI-20, one fruit showed decreasing of ΔD followed by increasing in the day after, and other fruit showed increasing of ΔD followed by decreasing in the day after. About cultivar with DI-10, ΔD showed a different trend. Indeed, for Arbequina ΔD decreased and in the day after irrigation increased, but for Lea ΔD increased and in the day after irrigation one fruit showed ΔD reduction and other one showed ΔD increase (Figure S4.3A–D).

The cumulative fruit growth (CFG), for all irrigated cultivars (DI-20 and DI-10), in correspondence with the first irrigation day increased and the upward trend has continued in the day after irrigation (Figure 4.3A and B). In non-irrigated cultivars, a small growth of CFG was observed which was followed by a reduction in the day after irrigation (Figure 4.3B). In the second irrigation day, CFG for all irrigated cultivars (DI-20 and DI-10) decreased, the downward trend continued in the day after irrigation but with a slight slope (Figure 4.3A and B). In the same time, CFG of DI-0 treatments decreased but in the day after irrigation it increased (Figure 4.3B). On the third irrigation day, CFG for all irrigated (DI-20 and DI-10) and non-irrigated cultivars increased (Figure 4.3C and D). The only exception was one fruit of Ascolana dura (Asc2 (DI-20)) which CFG decreased (Figure 4.3D). On the day after irrigation, CFG of both cultivars with DI-20 was the same as irrigation day and did not show any change (Figure 4.3D), nevertheless CFG of both cultivars with DI-10 increased (Figure 4.3C). CFG for Ascolana dura (DI-0) was the same as the previous day and did not change, whereas, CFG of Piantone di Falerone (DI-0) increased (Figure 4.3D).

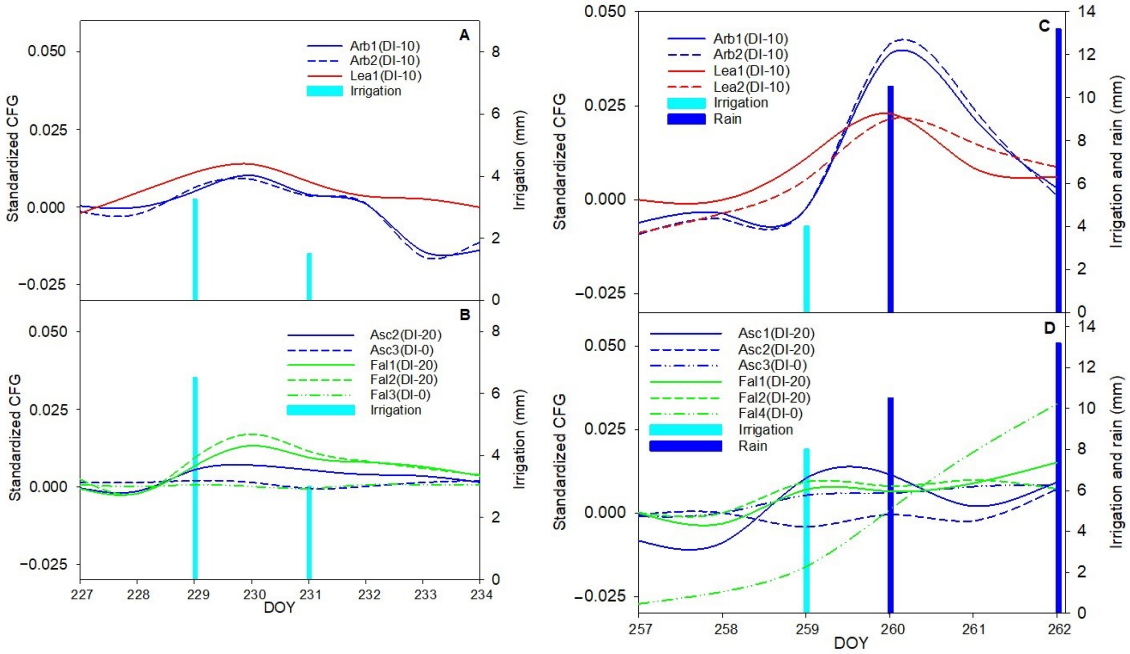

Figure 4.3. Standardized cumulative fruit growth (CFG). From 227 to 234 day of the year (DOY) (in correspondence with first and second irrigation days) for the olive cultivar Arbequina and Lea (A) and for the olive cultivars Ascolana dura and Piantone di Falerone (B). From 257 to 262 day of the year (DOY) (in correspondence with third irrigation day) for the olive cultivar Arbequina and Lea (C) and for the olive cultivars Ascolana dura and Piantone di Falerone (D). Arb1(DI-10) and Arb2(DI-10) represent fruit 1 and 2 of "Arbequina" at 10% deficit irrigation, respectively. Lea1(DI-10) and Lea2(DI-10) represent fruit 1 and 2 of "Lea" at 10% deficit irrigation, respectively. Asc1(DI-20) and Asc2(DI-20) represent fruit 1 and 2 of "Ascolana dura" at 20% deficit irrigation, respectively. Asc3(DI-0) represents fruit 3 of non-irrigated "Ascolana dura". Fal1(DI-20) and Fal2(DI-20) represent fruit 1 and 2 of "Piantone di Falerone" at 20% deficit irrigation, respectively. Fal3(DI-0) and Fal4(DI-0) represent fruit 3 and 4 of non-irrigated "Piantone di Falerone", respectively.

After the first and second irrigation day, daily fruit relative growth rate (RGR) changed significantly (Figure 4.4B–F). After the first irrigation day the minimum amount of RGR was near zero and then decreased continuously (dashed orange line). The minimum of RGR downsized with dissimilar slopes in different irrigation levels. Moreover, the trend of minimum RGR reduction in different cultivars with the same irrigation level was diverse too. The maximum amount of RGR for both cultivars with DI-20 increased slightly (dashed black line in Figure 4.4B,D), whereas cultivars with DI-10 did not show any consistent decreasing or increasing of maximum RGR (Figure 4.4E,F). At the same time, minimum RGR of Piantone di Falerone (DI-0) and Ascolana dura (DI-0) showed consistent decrease (dashed orange line in Figure 4.4A,C). The maximum RGR for Piantone di Falerone (DI-0)

did not show any specific patterns, however, for Ascolana dura (DI-0) was stable (dashed black line in Figure 4.4C).

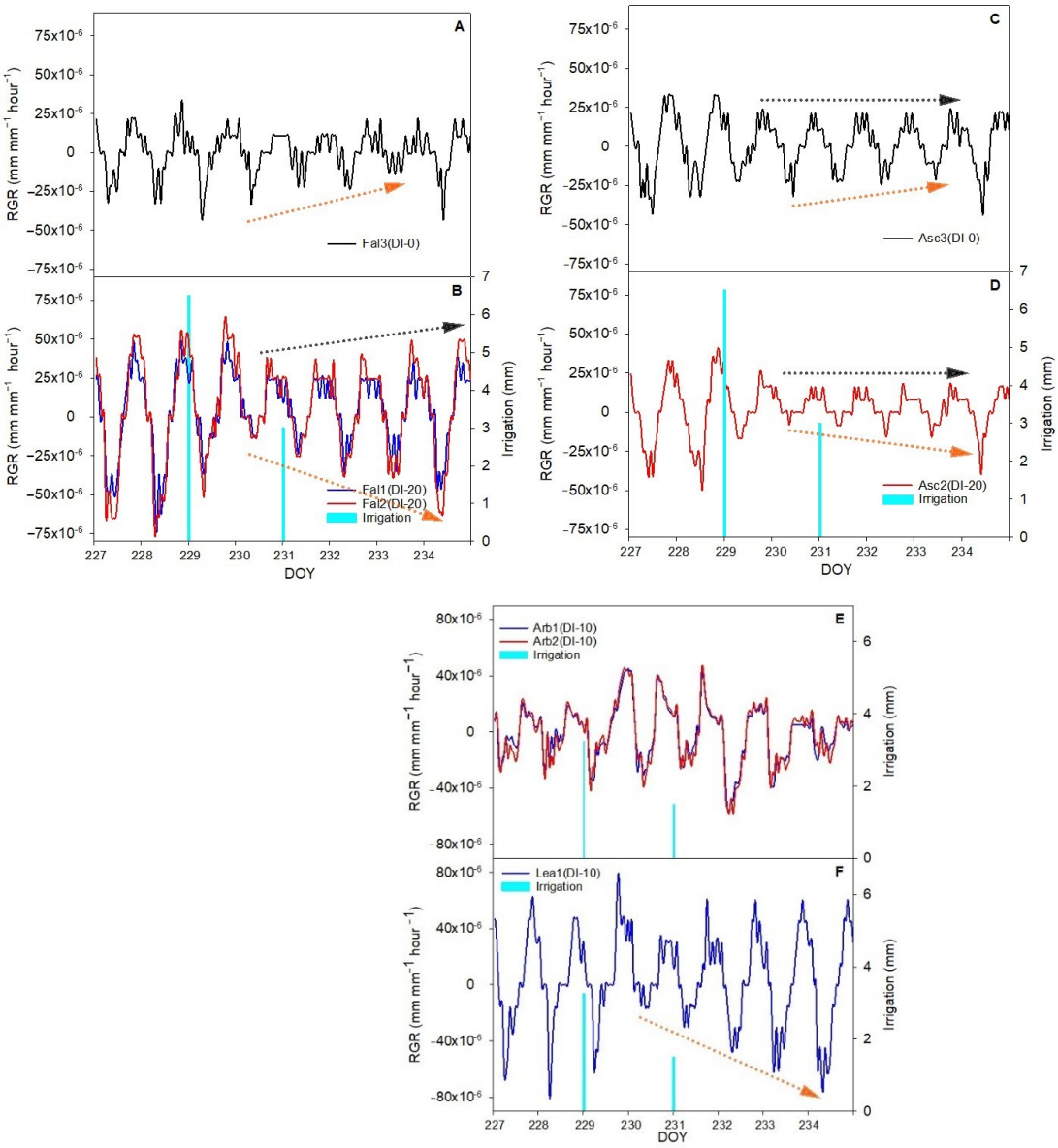

*Figure 4.4. Daily fruit relative growth rate (RGR) from 227 to 234 day of the year (DOY) (in correspondence with first and second irrigation days. The olive cultivar '**Piantone di Falerone**' (A,B); the olive cultivar '**Ascolana dura**' (C,D); the olive cultivar '**Arbequina**' (E); the olive cultivar '**Lea**' (F). Fal3(DI-0) represents fruit 3 of non-irrigated "Piantone di Falerone". Fal1(DI-20) and Fal2(DI-20) represent fruit 1 and 2 of "Piantone di Falerone"*

at 20% deficit irrigation, respectively. Asc3(DI-0) represents fruit 3 of non-irrigated "Ascolana dura". Asc2(DI-20) represents fruit 2 of "Ascolana dura" at 20% deficit irrigation. Arb1(DI-10) and Arb2(DI-10) represent fruit 1 and 2 of "Arbequina" at 10% deficit irrigation, respectively. Lea1(DI-10) represents fruit 1 of "Lea" at 10% deficit irrigation.

After irrigation withholding, RGR_{range} amount of two cultivars (Ascolana dura and Piantone di Falerone) with DI-20 irrigation treatment increased (Figure 4.5B). The RGR_{range} enlargement has been reported by other research as a water stress signal in olive (Scalisi et al., 2020; Marino et al., 2021; Fernandes et al., 2018). However, there is no defined threshold for RGR_{range} as a water stress index. The trend of RGR_{range} in the cultivars with DI-10 irrigation treatment was not same as each other. Indeed, the trend for cultivar Lea was more similar to DI-20 irrigation treated cultivars (Figure 4.5A), whereas, the trend of Arbequina up to the day after first irrigation treatment was close to Lea and then after followed dissimilar trend (Figure 4.5A). The trend of Asc3 (DI-0) was mismatched with Fal3 (DI-0), besides, both of them (DI-0s) showed diverse pattern in comparison with related irrigated cultivar (Figure 4.5C).

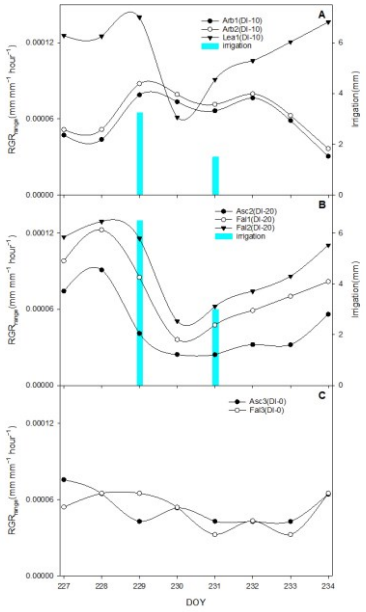

Figure 4.5. Relative growth rate range (RGR_{range}) from 227 to 234 day of the year (DOY) (in correspondence with first and second irrigation days: (A) fruit 1 and 2 of "Arbequina" at 10% deficit irrigation (Arb1(DI-10) and Arb2(DI-10), respectively) and fruit 1 of "Lea" at 10% deficit irrigation (Lea1(DI-10)); (B) fruit 1 and 2 of "Piantone di Falerone" at 20% deficit irrigation (Fal1(DI-20) and Fal2(DI-20), respectively) and fruit 2 of "Ascolana dura" at 20% deficit irrigation (Asc2(DI-20)); (C) fruit 3 of non-irrigated "Ascolana dura" (Asc3(DI-0)) and fruit 3 of non-irrigated "Piantone di Falerone" (Fal3(DI-0)).

After third irrigation treatment, fruit RGR dynamics did not show similarity to first and second irrigation treatment (Figure 4.6A–F). Moreover, the pattern of the fruit with the same cultivar-irrigation level was diverse too. For instance, minimum RGR of Piantone di Falerone (DI-20) for one fruit (Fal1) was stable and almost zero, but for other fruit (Fal2) followed oscillation and was negative, whereas maximum RGR for both Piantone di Falerone (DI-20) had same trend but without any progressive decrease or increase (Figure 4.6B). Maximum RGR for Ascolana dura (DI-20) in one fruit (Asc1) showed consistent reduction but for the other one was almost stable and near zero (Figure 4.6D).

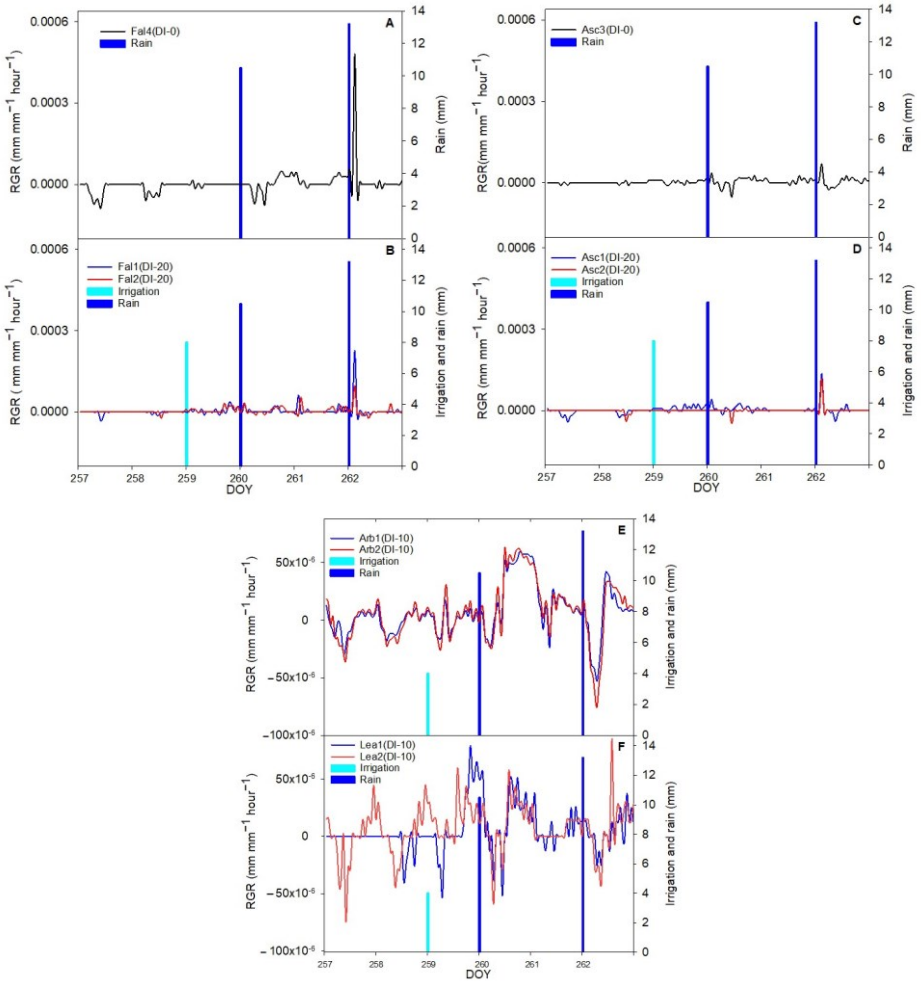

*Figure 4.6. Daily fruit relative growth rate (RGR) from 257 to 262 day of the year (DOY) (in correspondence with the third irrigation day). The olive cultivar '**Piantone di Falerone**' (A,B); the olive cultivar '**Ascolana dura**' (C,D); the olive cultivar '**Arbequina**' (E); the olive cultivar '**Lea**' (F). Fal4(DI-0) represents fruit 4 of non-irrigated "Piantone di Falerone".*

Fal1(DI-20) and Fal2(DI-20) represent fruit 1 and 2 of "Piantone di Falerone" at 20% deficit irrigation, respectively. Asc3(DI-0) represents fruit 3 of non-irrigated "Ascolana dura". Asc1(DI-20) and Asc2(DI-20) represent fruit 1 and 2 of "Ascolana dura" at 20% deficit irrigation, respectively. Arb1(DI-10) and Arb2(DI-10) represent fruit 1 and 2 of "Arbequina" at 10% deficit irrigation, respectively. Lea1(DI-10) and Lea2(DI-10) represent fruit 1 and 2 of "Lea" at 10% deficit irrigation, respectively.

After irrigation withholding up to first rainy day (DOY 260), RGR_{range} amount of Ascolana dura with DI-20 irrigation treatment increased (Figure 4.7B), whereas, in the Piantone di Falerone with DI-20 irrigation treatment, RGR_{range} amount in the one fruit increased and in other one decreased (Figure 4.7B). In addition, on the day after first rain the RGR_{range} amount of Ascolana dura with DI-20 irrigation treatment decreased and for Piantone di Falerone increased (Figure 4.7B). Finally, the increase of RGR_{range} in Ascolana dura and Piantone di Falerone (Figure 4.7B) in 2 rainy days (DOYs 260 and 262) was in contrast with our expectation. Nevertheless, it resulted from the time of rainfall. Data showed that rainfall in DOY 260 and 262 started at 16:00 and 15:00, respectively. Consequently, the fruit experienced water stress before rain fall, and RGR_{range} increased. RGR_{range} of Asc3 (DI-0) and Fal4 (DI-0) in correspondence with two rainy days showed the same results of DI-20 treated and confirmed the effect of time of rainfall happening (Figure 4.7C).

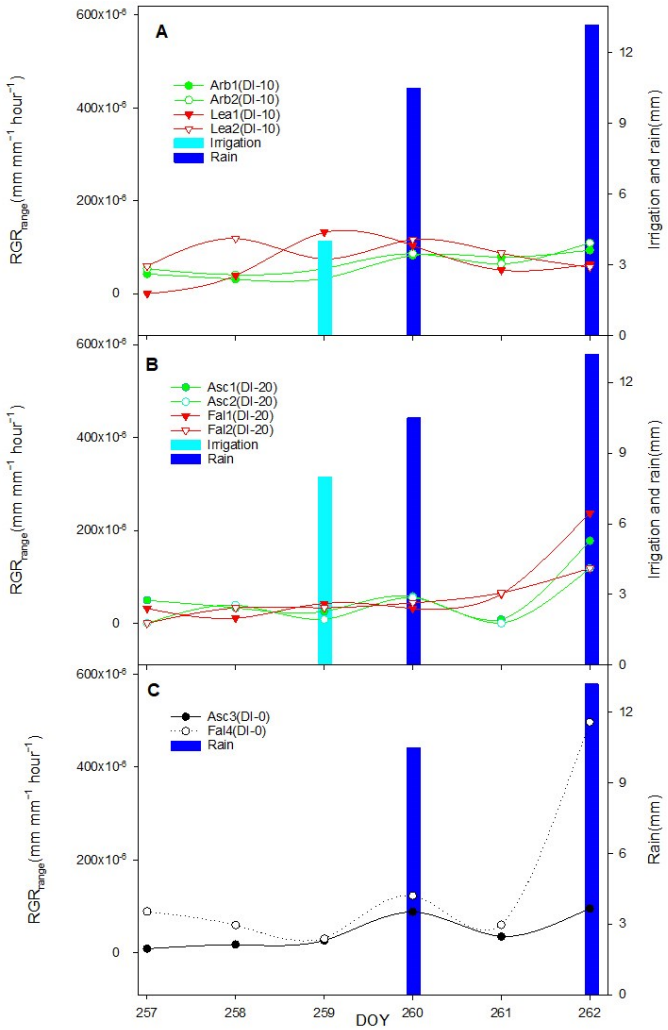

Figure 4.7. Relative growth rate range (RGR_{range}) from 257 to 262 day of the year (DOY) (in correspondence third irrigation day): (A) fruit 1 and 2 of "Arbequina" at 10% deficit irrigation (Arb1(DI-10) and Arb2(DI-10), respectively) and fruit 1 and 2 of "Lea" at 10% deficit irrigation (Lea1(DI-10) and Lea2(DI-10), respectively); (B) fruit 1 and 2 of "Ascolana dura" at 20% deficit irrigation (Asc1(DI-20) and Asc2(DI-20), respectively) and fruit 1 and 2 of "Piantone di Falerone" at 20% deficit irrigation (Fal1(DI-20) and Fal2(DI-20), respectively); (C) fruit 3 of non-irrigated "Ascolana dura" (Asc3(DI-0)) and fruit 4 of non-irrigated "Piantone di Falerone" (Fal4(DI-0)).

The RGR_{range} in the cultivars with DI-10 irrigation treatment did not show similarity to each other (Figure 4.7A). On the irrigation day, the RGR_{range} of Arbequina increased but for Lea

in Lea1 increased and in Lea2 decreased (Figure 4.7A). From irrigation day up to the end of 6 days window (DOY 262), the RGR_{range} trend of Arbequina (DI-10) was similar to Ascolana dura (DI-20) (including pattern in 2 rainy days (DOYs 260 and 262)). Whereas, Lea showed dissimilar trend in comparison with Arbequina. In addition, RGR_{range} trend of Lea1 and Lea2 was diverse too (Figure 4.7A).

4.4.4. Hysteresis Curves of Fruit Growth versus VPD

The hysteresis phenomenon is an indirect response of vegetation to diurnal changes in the external environment and the time lag is a major characteristic of hysteresis (Zhang et al., 2019). In our case hysteresis is formed by the time lag between VPD and fruit growth. To better capture the time lag between daily diameter and VPD, the normalized data of diameter and VPD have been used. The blue box showed a time lag between some example fruits diameter and VPD (Figure 4.8).

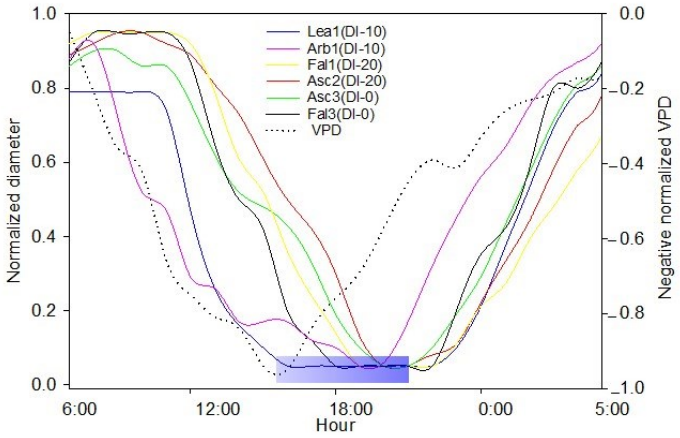

Figure 4.8. Normalized diameter of example fruits versus normalized vapor pressure deficit (VPD) in 228 day of the year (DOY). The blue box shows daily time lag between VPD and fruit diameter. In the blue box darkness of color shows increasing time lag. To better demonstrate time lag, a negative normalized amount of VPD has been employed. Lea1(DI-10) represents fruit 1 of "Lea" at 10% deficit irrigation. Arb1(DI-10) represents fruit 1 of "Arbequina" at 10% deficit irrigation. Fal1(DI-20) represents fruit 1 of "Piantone di Falerone" at 20% deficit irrigation. Fal3(DI-0) represents fruit 3 of non-irrigated "Piantone di Falerone". Asc2(DI-20) represents fruit 2 of "Ascolana dura" at 20% deficit irrigation. Asc3(DI-0) represents fruit 3 of non-irrigated "Ascolana dura".

In most periods of experiment, the daily growth of fruit transversal diameter versus VPD formed clockwise curves. The mentioned curves, according to their shape, were explainable as complete hysteresis (Figure 4.9A), incomplete hysteresis (Figure 4.9B), or partial hysteresis (Figure 4.9C). Although, different kinds of hysteresis curves have appeared by dissimilar frequency, shape, and magnitude in each cultivar-irrigation level (Table 4.4).

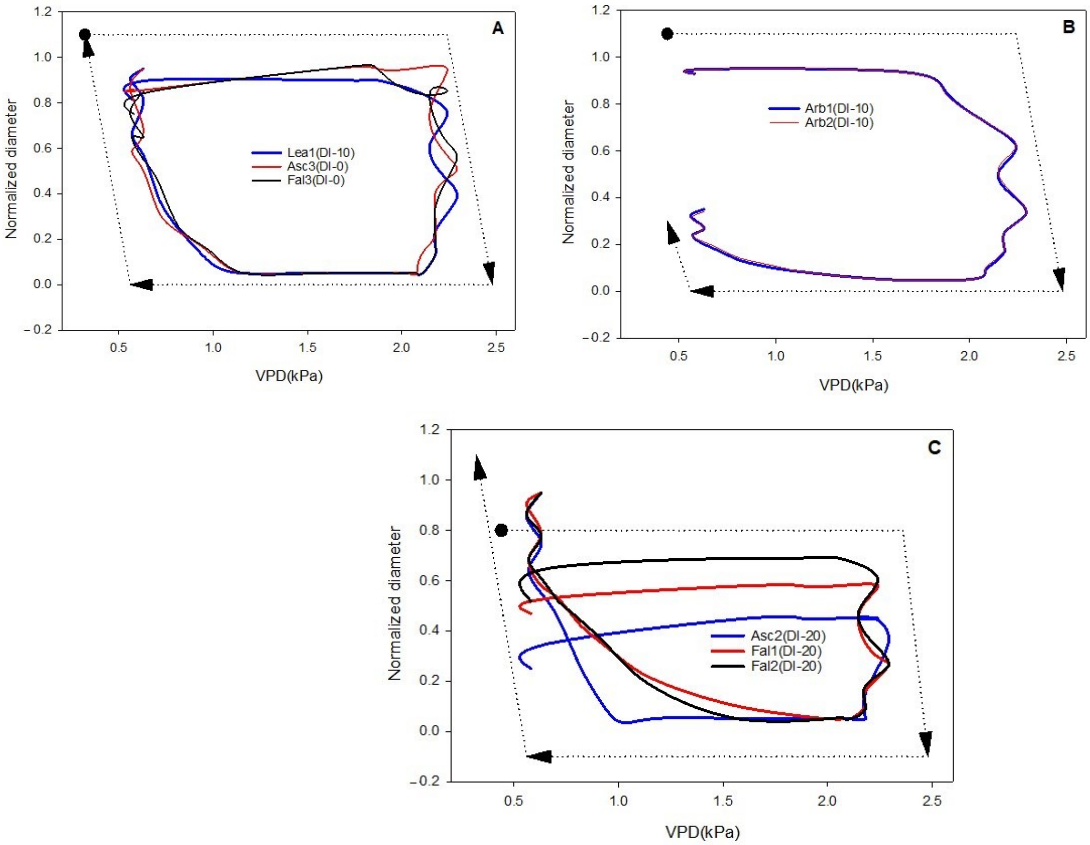

Figure 4.9. Hysteresis loops of diameter versus vapor pressure deficit (VPD) in one example day (232 day of the year (DOY)). (A) Complete clockwise hysteresis; (B) incomplete clockwise hysteresis; (C) partial clockwise hysteresis. Dotted black line shows the rotational pattern and starting and ending point of hysteresis loops. Arb1(DI-10) and Arb2(DI-10) represent fruit 1 and 2 of "Arbequina" at 10% deficit irrigation, respectively. Lea1(DI-10) represents fruit 1 of "Lea" at 10% deficit irrigation. Asc2(DI-20) represents fruit 2 of "Ascolana dura" at 20% deficit irrigation. Asc3(DI-0) represents fruit 3 of non-irrigated "Ascolana dura". Fal1(DI-20) and Fal2(DI-20) represent fruit 1 and 2 of "Piantone di Falerone" at 20% deficit irrigation, respectively. Fal3(DI-0) represents fruit 3 of non-irrigated "Piantone di Falerone".

Table 4.4. Data of percentage of appearance of different hysteresis curves. Invalid data were excluded from the table. Arb1(DI-10) and Arb2(DI-10) represent fruit 1 and 2 of "Arbequina" at 10% deficit irrigation, respectively. Lea1(DI-10) and Lea2(DI-10) represent fruit 1 and 2 of "Lea" at 10% deficit irrigation, respectively. Asc1(DI-20) and Asc2(DI-20) represent fruit 1 and 2 of "Ascolana dura" at 20% deficit irrigation, respectively. Asc3(DI-0) represents fruit 3 of non-irrigated "Ascolana dura". Fal1(DI-20) and Fal2(DI-20) represent fruit 1 and 2 of "Piantone di Falerone" at 20% deficit irrigation, respectively. Fal3(DI-0) and Fal4(DI-0) represent fruit 3 and 4 of non-irrigated "Piantone di Falerone", respectively.

Type of hysteresis	Arb1(DI-10)	Arb2(DI-10)	Lea1(DI-10)	Lea2(DI-10)	Asc1(DI-20)	Asc2(DI-20)	Asc3(DI-0)	Fal1(DI-20)	Fal2(DI-20)	Fal3(DI-0)	Fal4(DI-0)
Complete	27.45	15.69	19.05	12.50	15.00	12.82	27.66	6.67	10.26	35.29	0.00
Incomplete	41.18	50.98	23.81	62.50	50.00	25.64	19.15	42.22	15.38	17.65	33.33
Partial	23.53	25.49	42.86	16.67	15.00	30.77	34.04	26.67	48.72	23.53	50.00
No hysteresis	7.84	7.84	14.29	8.33	20.00	30.77	19.15	24.44	25.64	23.53	16.67

The trend of hysteresis curves in correspondence with irrigation days has been shown in Table 4.5. In the first and second irrigation day, in all irrigated cultivars (with DI-10 and DI-20), a partial clockwise hysteresis curve has appeared. Nevertheless, on the third irrigation day, it did not form any hysteresis pattern.

Table 4.5. Data of hysteresis curve types in correspondence with irrigation days. Arb1(DI-10) and Arb2(DI-10) represent fruit 1 and 2 of "Arbequina" at 10% deficit irrigation, respectively. Lea1(DI-10) and Lea2(DI-10) represent fruit 1 and 2 of "Lea" at 10% deficit irrigation, respectively. Asc1(DI-20) and Asc2(DI-20) represent fruit 1 and 2 of "Ascolana dura" at 20% deficit irrigation, respectively. Asc3(DI-0) represents fruit 3 of non-irrigated "Ascolana dura". Fal1(DI-20) and Fal2(DI-20) represent fruit 1 and 2 of "Piantone di Falerone" at 20% deficit irrigation, respectively. Fal3(DI-0) and Fal4(DI-0) represent fruit 3 and 4 of non-irrigated "Piantone di Falerone", respectively. From 227 to 234 day of the year (DOY), extensimeters of Lea2 (DI-10) and Asc1 (DI-20) were missing (marked by "-" in the table). In the 257 day of the year (DOY), data of extensimeters of Lea1 (DI-10), Asc2 (DI-20), and Fal2 (DI-20), and in 261 day of the year (DOY) data for Asc2 (DI-20) were incorrect and excluded from the table (marked by " # " in the table).

DOY	Arb1(DI-10)	Arb2(DI-10)	Lea1(DI-10)	Lea2(DI-10)	Asc1(DI-20)	Asc2(DI-20)	Asc3(DI-0)	Fal1(DI-20)	Fal2(DI-20)	Fal3(DI-0)	Fal4(DI-0)
227	Complete	Incomplete	Complete	-	-	Incomplete	Complete	Incomplete	Incomplete	Complete	-
228	Complete	Incomplete	Complete	-	-	Complete	Complete	Incomplete	Incomplete	Complete	-
229	Partial	Partial	Partial	-	-	Partial	Partial	Partial	Partial	Incomplete	-
230	Partial	Partial	Partial	-	-	Partial	Incomplete	Partial	Partial	Incomplete	-
231	Partial	Partial	Partial	-	-	Partial	Complete	Partial	Partial	Complete	-
232	Incomplete	Incomplete	Complete	-	-	Partial	Complete	Partial	Partial	Complete	-
233	Incomplete	Incomplete	Incomplete	-	-	Partial	Incomplete	Partial	Partial	Partial	-
234	Incomplete	Incomplete	Incomplete	-	-	Incomplete	Complete	Complete	Complete	Complete	-
257	Incomplete	Incomplete	#	Incomplete	Incomplete	#	Incomplete	Incomplete	#	-	Incomplete
258	Incomplete	Incomplete	Incomplete	Complete	Incomplete	Incomplete	Complete	Incomplete	Incomplete	-	Incomplete
259	No	No	No	No	No	No	No	No	No	-	No
260	Partial	Partial	No	Partial	No	No	Partial	No	No	-	Complete
261	No	No	Partial	Incomplete	Partial	#	Partial	Incomplete	Partial	-	Partial
262	Partial	Incomplete	Partial	Chaos	Partial	Partial	Partial	Partial	Partial	-	Partial

In the past decade, several researchers have developed indices to quantify the shape, size, and direction of hysteresis curves (Zuecco et al., 2016). In all indices or metrics, three main characteristics of hysteresis relation which are shape, direction, and the extent of loop should be considered (Zuecco et al., 2016). About hysteresis direction, according to our results all hysteresis curves were clockwise. In addition, all shapes of hysteresis were circular (i.e., eight-shaped or linear form has not been formed). Therefore, for detecting extent change, the loop's height was employed (blue, red, and green dotted lines in Figure 10). Loop's height was calculated as the maximum normalized diameter minus the minimum normalized diameter inside the loop. In addition, according to the employment of normalized diameter for calculation of loop's height, it is a normalized unitless parameter.

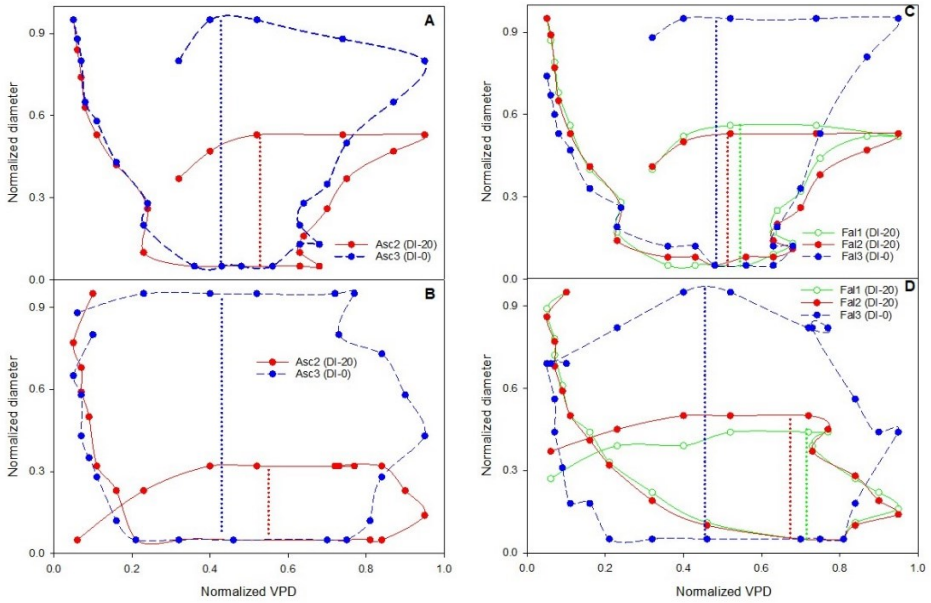

Figure 4.10. Hysteresis loops of diameter versus vapor pressure deficit (VPD) in first (229 day of the year (DOY)) and second (231 day of the year (DOY)) irrigation days. (A) 229 day of the year (DOY) for Ascolana dura; (B) 231 day of the year (DOY) for Ascolana dura; (C) 229 day of the year (DOY) for Piantone di Falerone; (D) 231 day of the year (DOY) for Piantone di Falerone. Asc2(DI-20) represents fruit 2 of "Ascolana dura" at 20% deficit irrigation. Asc3(DI-0) represents fruit 3 of non-irrigated "Ascolana dura". Fal1(DI-20) and Fal2(DI-20) represent fruit 1 and 2 of "Piantone di Falerone" at 20% deficit irrigation, respectively. Fal3(DI-0) represents fruit3 of non-irrigated "Piantone di Falerone". Dotted lines show the height of hysteresis curves.

In the first and second irrigation days, for the cultivar of Ascolana dura deficit irrigation treatment reduced height of hysteresis curve (red dotted line in Figure 4.10A,B) in comparison with non-irrigated treatment (blue dotted line in Figure 4.10A,B). In the same time, Piantone di Falerone (deficit irrigated) experienced the same magnitude change as Ascolana dura (Figure 4.10C, D).

The hysteresis height was tested by the repeated measures ANOVA test and the test revealed significant differences ($p = 0.005$ for Piantone di Falerone and $p = 0.019$ for Ascolana dura) among irrigated cultivars with their non-irrigated (Table 4.6). Indeed, multiple comparison tests of Student–Newman–Keuls showed significant differences between Fal1 (DI-20) and Fal3 (DI-0), Fal2 (DI-20), and Fal3 (DI-0) as well as Asc2 (DI-20) and Asc3 (DI-0).

Table 4.6. One way repeated measures ANOVA testing hysteresis height (mean) of different cultivar irrigation treatment from 227 to 234 day of the year (DOY). Asc2(DI-20) represents fruit 2 of "Ascolana dura" at 20% deficit irrigation. Asc3(DI-0) represents fruit 3 of non-irrigated "Ascolana dura". Fal1(DI-20) and Fal2(DI-20) represent fruit 1 and 2 of "Piantone di Falerone" at 20% deficit irrigation, respectively. Fal3(DI-0) represents fruit 3 of non-irrigated "Piantone di Falerone". Before performing repeated measures ANOVA test, selected data were examined by normality test and equal variance test (for the Fal1 (DI-20), Fal2 (DI-20), and Fal3 (DI-0) normality test (Shapiro–Wilk, passed p = 0.425) and equal variance test (Brown–Forsythe, passed p = 0.185); for the Asc2 (DI-20) and Asc3 (DI-0) normality test (Shapiro–Wilk, passed p = 0.325) and Equal variance test (Brown–Forsythe, passed p = 1.000)).

Treatment Name	N	Mean	Std Dev	SEM	Student-Newman-Keuls test
Fal1 (DI-20)	8	62.125	25.503	9.017	A
Fal2 (DI-20)	8	70	18.83	6.657	A
Fal3 (DI-0)	8	90	0	0	B
Asc2 (DI-20)	8	56.125	31.692	11.205	A
Asc3 (DI-0)	8	90	0	0	B

On the third irrigation day, the hysteresis curve did not appear (Table 4.5). As VPD were the input of hysteresis curve, appearance and characteristic of the hysteresis curve were affected by VPD, so disappearance of hysteresis curve can be related to different circadian cycles (daily pattern) of VPD. In the normal circadian cycle, VPD tended to peak in the early afternoon, but on the third irrigation day from 11 AM up to 1 PM the VPD decreased. Mentioned reduction of VPD suppressed formation of hysteresis curves. Fruit development is also a significant parameter which influences daily growth patterns and therefore the formation and characteristic of the hysteresis curve (Khosravi et al., 2021). Recent research explained disappearance of hysteresis curve in 'Frantoio' olive cultivar during fruit maturation, and finding by Scalisi et al. (2019) suggested hysteresis magnitude changes or disappearance of it in nectarine during different stages of fruit development. However, Table 4.1 did not show any fruit maturation during our experiment.

4.5 Discussion

The daily olive fruit growth patterns were detected through the continuous monitoring of FD. The FD increased with diurnal variations as it was observed in peach (*Prunus persica* (L.) Batsch) (Fishman and Génard, 1998), sweet cherry (*Prunus avium* L.) (Brüggenwirth et al., 2016; Zucchini et al., 2021), apple (*Malus* x *domestica* cv. 'Imperial Gala') (Boini et al., 2019), kiwi (*Actinidia deliciosa* cv. 'Summerkiwi 4605') (Morandi et al., 2010), and olive (*Olea europaea* L.) (Fernandes et al., 2018; Khosravi et al., 2021). Indeed, during the hottest hours (mid-morning to early afternoon) due to low xylem flow (low water potential) or/and xylem backflow and maximum transpiration rate, fruit faces with size reduction and shrinks, while from the late afternoon to early morning, xylem water potential restored and

fruit gradually expands and usually reaches size larger than the initial point of same day (Carella et al., 2021; Grilo et al., 2019).
On the other hand, there are some exceptional days with different growth patterns (Figure 4.S1B). Khosravi et al. (2021) already showed that for olive (*Olea europaea* (L.) cv. 'Frantoio' there were some days with different daily growth patterns related to the change in the daily VPD pattern.

4.5.1. Response of Fruit Growth to Deficit Irrigation and Rain

During the third phase of olive fruit development, the growth would be mainly driven by cell expansion with cell division processes becoming much less important (Hernandez-Santana et al., 2021). Therefore, the third phase of olive fruit development (fruit expansion) requires an adequate flow of water to the fruit and sufficient turgor to drive in cell enlargement (Ahumada-Orellana et al., 2017). Our results in first and second irrigation days (DOYs 229 and 231) were in line with what we would expect from increasing flow of water. Indeed, ΔG and CFG increased, but with dissimilar slope and amount in diverse cultivars (Table 4.3 and Figure 4.3A,B). With first and second irrigation days (DOYs 229 and 231), Ascolana dura and Piantone di Falerone, which are categorized as a table olive and treated with same irrigation regimes (DI-20), had the same CFG trend (Figure 4.3B), while Arbequina and Lea, which are categorized as oil varieties and treated with same irrigation regimes (DI-10), had the different CFG trend (Figure 4.3A). Dissimilarity in CFG trend is resulted by different irrigation treatments (DI-10 and DI-20), crop load, genetic factors, and phenology (Scalisi et al., 2020). In the 6 days in correspondence with first and second irrigation days, data of the standardized diameter (Table 4.2) showed that the ratio of diameter increase for both cultivars with DI-20 irrigation treatment is higher than non-irrigated, which confirmed the positive effect of irrigation.
On the other hand, the decreasing minimum of RGR after the first and second irrigation event (orange dashed line in Figure 4.4B,D–F) confirmed the positive effect of water flow too. Minimum RGR in different cultivars downsized with various slopes which suggested a very different response of cultivars to dehydration. Similar results were previously explained for two Sicilian olive cultivars of Nocellara del Belice and Olivo di Mandanici (Marino et al., 2021). On the contrary, minimum RGR for Ascolana dura (DI-0) and Piantone di Falerone (DI-0) increased (orange dashed line in Figure 4.4A,C). It could be hypothesized that with positive changes in the environmental condition (here was significant reduction of daily average of VPD from 3 (kPa) in DOY 228 to 1.14, 1.17, 1.34, 1.44 and 1.38 (kPa) in the days after, respectively), the minimum RGR increased.
In the 6 days in correspondence with the third irrigation day (DOY 259), flow of water to the fruit has been affected not only by irrigation, but also by rain. Therefore, diameter of both DI-20 irrigated and non-irrigated treatments increased, but with dissimilar ratios (Table 4.2), the only exception was Asc2 (DI-20) which did not show any changes in diameter. In addition, the CFG amount in both DI-20 irrigated and non-irrigated treatments increased too, the only exception was Asc2 (DI-20) which did not show any changes in irrigation day (Figure 4.3C,D). However, the effect of rain on CFG was not the same in different cultivars. For instance, in the first rainy day (DOY 260), CFG for Asc2 (DI-20), Asc3 (DI-0), and Fal4 (DI-0) increased, for Fal2 (DI-20) decreased, and for Asc1 (DI-20)

and Fal1 (DI-20) was constant. This dissimilarity of the CFG trend between cultivars and among different fruits of the same cultivar was detectable also in the second rainy day (DOY 262). The dissimilarity of CFG trend between cultivars could be resulted by crop load, genetic factors and phenology (Scalisi et al., 2020), and different cultivar specific drought resistance mechanisms and still unrevealed role that fruits have as water storage compartments in drought resistance mechanisms of olive (Marino et al., 2021).
Although, in the same time, RGR graphs show some similarity between cultivars of Ascolana dura and Piantone di Falerone, including pronounced maximum amount after second rainy day for both irrigated and non-irrigated treatments (Figure 4.6A–D), or sudden decreasing of minimum RGR for cultivars of Arbequina and Lea after the second rainy day; but RGR pattern did not show any sameness to the trend of first and second irrigation events (Figure 4.6A–F).
At the same time, RGR_{range} showed diverse patterns in different cultivars. Moreover, in some cases the pattern was different among fruits of the same cultivar (Figure 4.7A–C).
Overall, due to different responses of diverse cultivars to deficit irrigation, the use of common fruit development indices (i.e., RGR_{range}) as an indicator of water status should be cultivar-specific. Indeed, cultivar-specific thresholds should be adopted. In addition, fruit growth is affected by parameters such as fluctuation in environmental conditions, phenological stage, and crop load (Morandi et al., 2007b; Marino et al., 2021), therefore, the effects should be considered in threshold definition.

4.5.2. Hysteresis Curves Variations

VPD (input) and FD (output) time series (blue box in the Figure 4.8) formed FD-VPD loops, which are examples of hysteresis curves (Figure 4.9). The magnitude and characterization of hysteresis curves differed from day to day. Magnitude change of hysteresis curves was reported by other researchers as well (Scalisi et al., 2019; Khosravi et al., 2021; Zhang et al., 2014).
Interestingly, in our research, magnitude change of hysteresis curves versus VPD is not cultivar-specific (Figure 4.10), accordingly, acquired indices are not cultivar-specific. Zhang et al. (2014) suggested that the relation between the hysteresis magnitude and plant water potential provides a possible way to detect plant water stress. However, other factors are also involved since it has been shown that formation of hysteresis curves resulted from complex interactions between exogenous and endogenous factors (Zhang et al., 2014). Moreover, according to research by Zuecco et al. (2016), hysteresis can be thought of as the dependence of a response variable not only on the value of a driving variable but also on its past history. Here, height reduction of hysteresis curves (magnitude change) by irrigation treatment (reduction of water stress) (Figure 4.10), could be employed as an index for estimation of water status of plants.
With normal circadian pattern of VPD, the hysteresis height's change is influenced by fruit diameter change (daily fruit growth dynamics). In the third stage of the fruit development (cell expansion stage) the daily fruit growth dynamics can be explained as changes in flows of water into and out of the fruit, rather than carbon gains; thus, fruit diameter variation responds to water deficit (Marino et al., 2021; Boini et al., 2019; Scalisi et al., 2017; Fernandes et al., 2018; Khosravi et al., 2021; Lakso et al., 1995). Consequently, hysteresis

magnitude change is closely related to water status of fruit. Indeed, in the day with normal circadian pattern of VPD, with increasing water flow into the fruit (by irrigation), the hysteresis height's decreases. Therefore, increasing hysteresis height's is the sign of reduction of water flow into fruit and could be used for water stress detection (Figures 4.10A–D and S4.4).
Overall, results highlight the magnitude change of hysteresis curves (height of loop) as a non-cultivar-specific quantitative index in two cultivars of Ascolana dura and Piantone di Falerone which can be taken in order to estimate the water status. However, development of quantitative assessment of hysteresis curves using an index approach is vital in this regard.

4.6 Conclusions

The paper presents some physiological basis to better monitor deficit irrigation in olive in different varieties. In the four olive cultivars ('Ascolana dura', 'Piantone di Falerone', 'Arbequina' and 'Lea'), fruit growth parameters including CFG and RGR showed different response to irrigation treatment which resulted by cultivar specific drought response mechanisms and suggest cultivar-specific water stress detection strategy. Moreover, during the third phase of olive fruit development, the hysteresis pattern between FD and VPD were explained and for the first time the quantitative differences of hysteresis curves for two deficit irrigated cultivars of Ascolana dura and Piantone di Falerone were demonstrated and discussed. In addition, the height of the hysteresis curve was significantly affected by irrigation. In general, height of hysteresis curves is reduced by deficit irrigation treatment for all four olive cultivars. Hysteresis magnitude's change resulted in a non-cultivar-specific parameter that could enable it to monitor plant water status and perform better tuned irrigation treatment in olive orchards. However, further studies should be performed to develop this continuous fruit-based parameter. In particular, various percentage of deficit irrigation treatments on different cultivars and in the diverse environmental conditions should be examined to enhance non-cultivar-specific index derived from hysteresis magnitude's change. Moreover, fruit growth-related factors (i.e., crop load, previously experienced stress, and phenological stage) should be considered to establish an efficient index (Marino et al., 2021). These results can be useful for setting up more robust and precise indicators to detect water stress in olive orchards and improve precision irrigation methods.

Supplementary Materials

Table S4.1. Data for starting and finishing time of shrinkage and expansion for different cultivar-irrigation levels in 3 consecutive example days (from 228 to 230 day of the years (DOY)). The ending time of Expansion is on the next day. Arb(DI-10) represents average data of two fruits of 'Arbequina' at 10% deficit irrigation. Lea(DI-10) represents average data of two fruits of 'Lea' at 10% deficit irrigation. Asc(DI-20) represents average data of two fruits of 'Ascolana dura' at 20% deficit irrigation. Asc(DI-0) represents data of one non-irrigated fruit of 'Ascolana dura'. Fal(DI-20) represents average data of two fruits of 'Piantone di Falerone' at 20% deficit irrigation. Fal(DI-0) represents data of one non-irrigated fruit of 'Piantone di Falerone'.

DOY	Arb (DI-10)		Lea (DI-10)		Asc (DI-20)		Asc (DI-0)		Fal (DI-20)		Fal (DI-0)	
	Shrinkage	Expansion	Shrinkage	Expansion	Shrinkage	Expansion	Shrinkage	Expansion	Shrinkage	Expansion	Shrinkage	Expansion
228	7:00 to 18:00	19:00 to 7:00	9:00 to 15:00	21:00 to 7:00	9:00 to 19:00	21:00 to 9:00	10:00 to 19:00	20:00 to 7:00	10:00 to 18:00	21:30 to 8:00	10:00 to 17:00	21:00 to 7:00
229	7:00 to 17:30	19:00 to 8:00	9:00 to 16:00	21:00 to 8:00	10:00 to 16:00	21:00 to 9:00	8:00 to 18:00	21:00 to 7:00	9:30 to 13:30	21:00 to 8:30	10:00 to 17:00	19:00 to 7:00
230	9:00 to 18:00	19:00 to 7:00	11:00 to 16:00	21:00 to 8:00	13:00 to 14:00	21:00 to 8:00	11:00 to 18:00	22:00 to 7:00	12:30 to 16:00	20:00 to 8:30	10:00 to 17:00	23:00 to 8:00

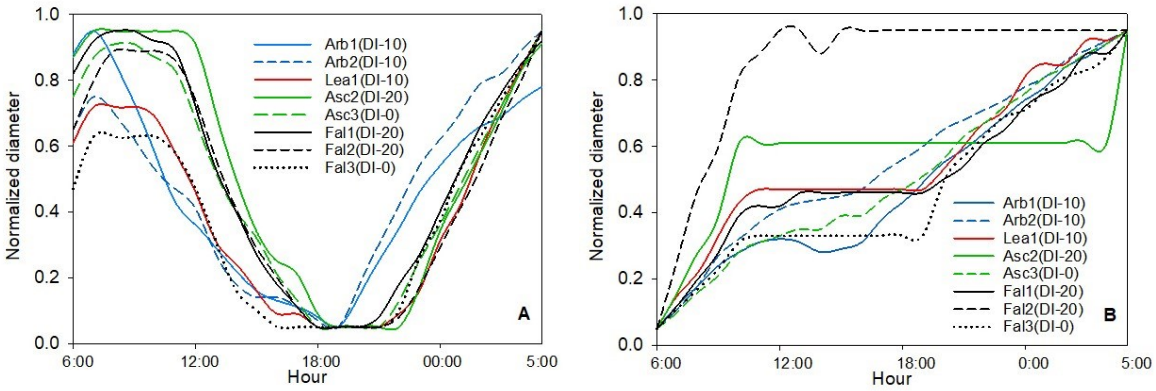

Figure S4.1. Continuous measurements of diameter of olive fruit in two example days of the experiment: (A) fruits with normal growth pattern in day of the year (DOY) 225; (B) fruit with exceptional growth pattern during rainy day (rainfall at beginning hours of the day) in day of the year (DOY) 236, in addition, it was the day after heavy rainfall. Arb1(DI-10) and Arb2(DI-10) represent fruit 1 and 2 of 'Arbequina' at 10% deficit irrigation, respectively. Lea1(DI-10) represents fruit 1 of 'Lea' at 10% deficit irrigation. Asc2(DI-20) represents fruit 2 of 'Ascolana dura' at 20% deficit irrigation. Asc3(DI-0) represents fruit 3 of non-irrigated 'Ascolana dura'. Fal1(DI-20) and Fal2(DI-20) represent fruit 1 and 2 of 'Piantone di Falerone' at 20% deficit irrigation, respectively. Fal3(DI-0) represents fruit 3 of non-irrigated 'Piantone di Falerone'.

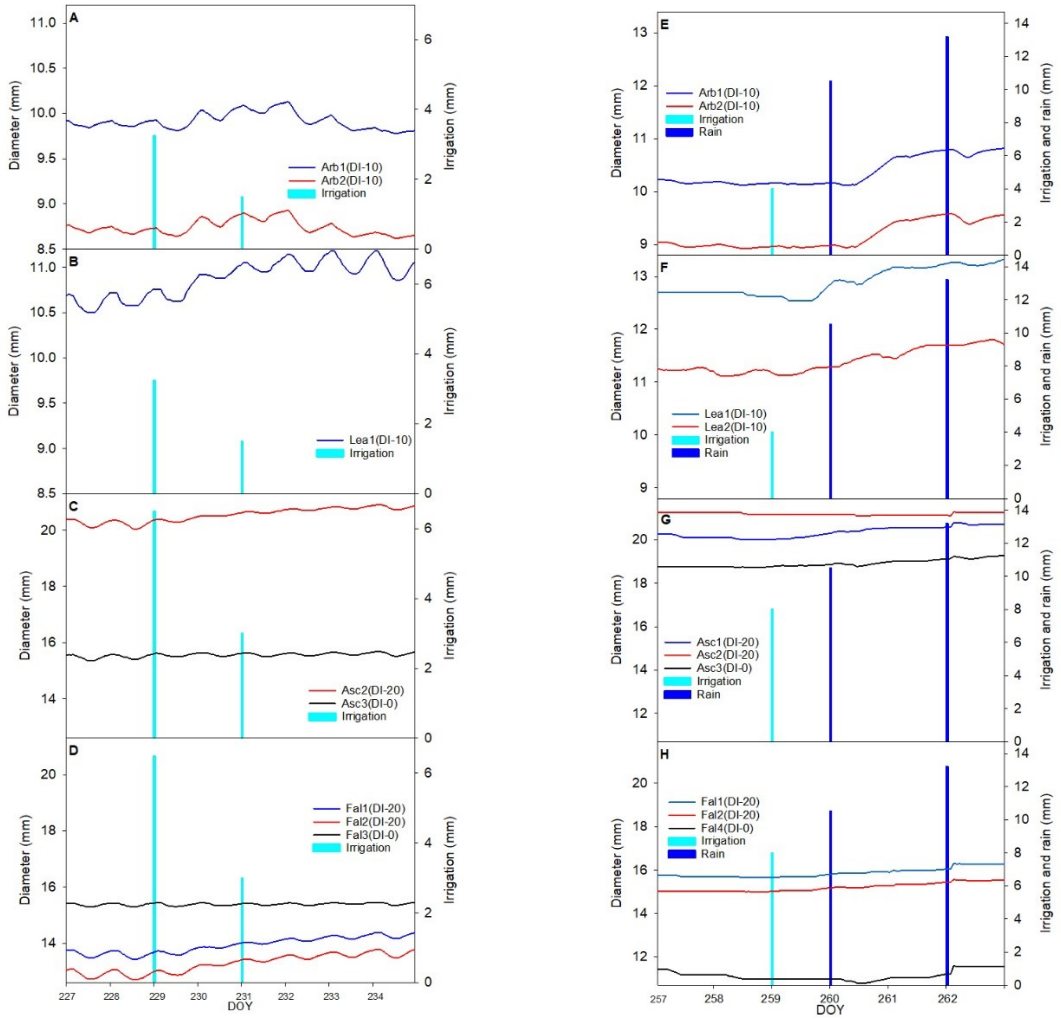

*Figure S4.2. Daily variation of fruit diameter from 227 to 234 day of the year (DOY) and from 257 to 262 day of the year (DOY). (A) cultivar of '**Arbequina**' in the first and the second irrigation days; (B) cultivar of '**Lea**' in the first and the second irrigation days; (C) cultivar of '**Ascolana dura**' in the first and the second irrigation days; (D) cultivar of '**Piantone di Falerone**' in the first and the second irrigation days; (E) cultivar of '**Arbequina**' in the third irrigation day; (F) cultivar of '**Lea**' in the third irrigation day; (G) cultivar of '**Ascolana dura**' in the third irrigation day; (H) cultivar of '**Piantone di Falerone**' in the third irrigation day. Arb1(DI-10) and Arb2(DI-10) represent fruit 1 and 2 of 'Arbequina' at 10% deficit irrigation, respectively. Lea1(DI-10) and Lea2(DI-10) represent fruit 1 and 2 of 'Lea' at 10% deficit irrigation, respectively. Asc1(DI-20) and Asc2(DI-20) represent fruit 1 and 2 of 'Ascolana dura' at 20% deficit irrigation, respectively. Asc3(DI-0) represents fruit 3 of non-irrigated 'Ascolana dura'. Fal1(DI-20)*

and Fal2(DI-20) represent fruit 1 and 2 of 'Piantone di Falerone' at 20% deficit irrigation, respectively. Fal3(DI-0) and Fal4(DI-0) represent fruit 3 and 4 of non-irrigated 'Piantone di Falerone', respectively.

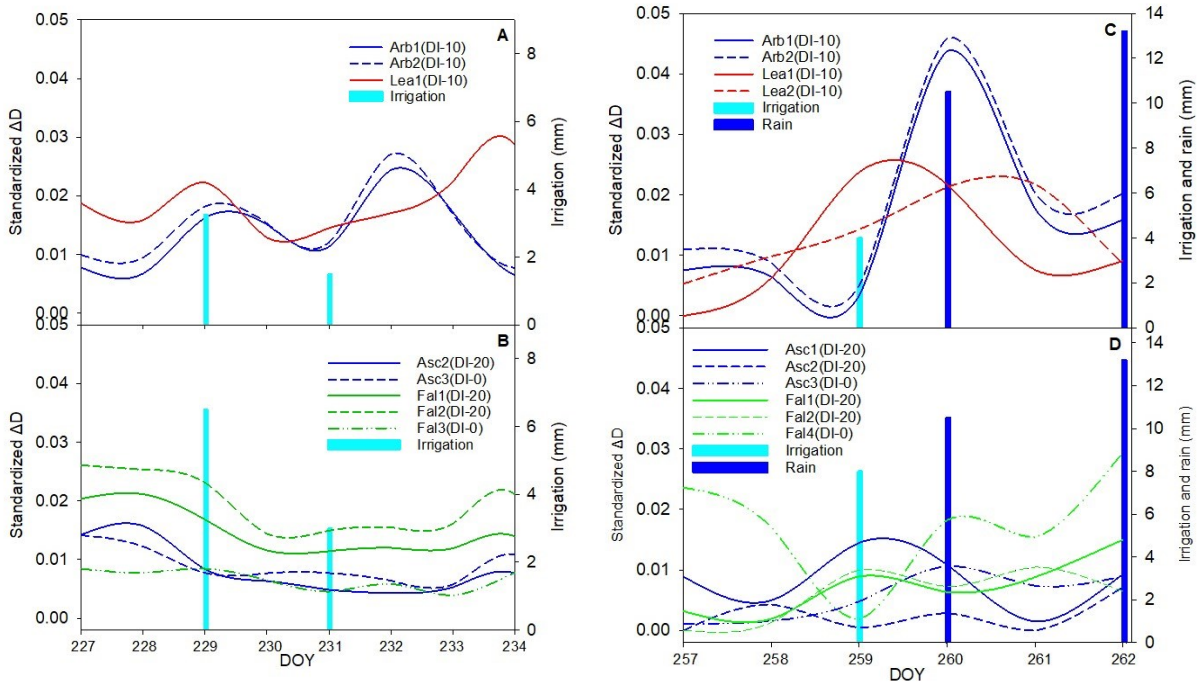

Figure S4.3. Standardized Fruit daily diameter fluctuation (ΔD). From 227 to 234 day of the year (DOY) (in correspondence with first and second irrigation days) for the olive cultivar Arbequina and Lea (A) and for the olive cultivars Ascolana dura and Piantone di Falerone (B); From 257 to 262 day of the year (DOY) (in correspondence with third irrigation day) for the olive cultivar Arbequina and Lea (C) and for the olive cultivars Ascolana dura and Piantone di Falerone (D). Arb1(DI-10) and Arb2(DI-10) represent fruit 1 and 2 of 'Arbequina' at 10% deficit irrigation, respectively. Lea1(DI-10) and Lea2(DI-10) represent fruit 1 and 2 of 'Lea' at 10% deficit irrigation, respectively. Asc1(DI-20) and Asc2(DI-20) represent fruit 1 and 2 of 'Ascolana dura' at 20% deficit irrigation, respectively. Asc3(DI-0) represents fruit 3 of non-irrigated 'Ascolana dura'. Fal1(DI-20) and Fal2(DI-20) represent fruit 1 and 2 of 'Piantone di Falerone' at 20% deficit irrigation, respectively. Fal3(DI-0) and Fal4(DI-0) represent fruit 3 and 4 of non-irrigated 'Piantone di Falerone', respectively.

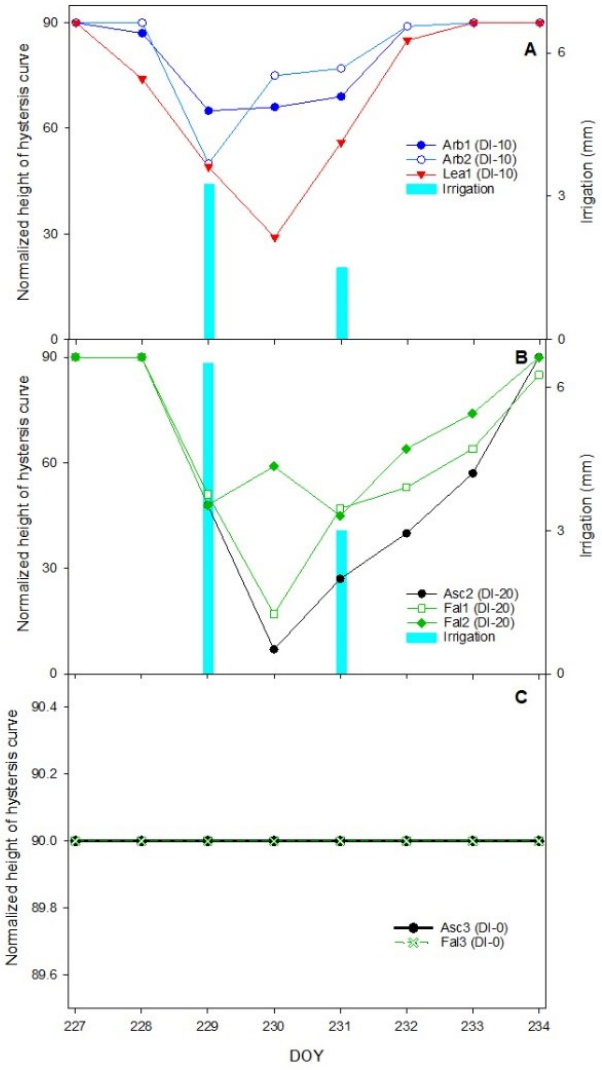

Figure S4.4. Height of hysteresis curves from 227 to 234 day of the year (DOY) (in correspondence with first and second irrigation days). (A) fruit 1 and 2 of 'Arbequina' at 10% deficit irrigation (Arb1(DI-10) and Arb2(DI-10), respectively) and fruit 1 of 'Lea' at 10% deficit irrigation (Lea1(DI-10)); (B) fruit 1 and 2 of 'Piantone di Falerone' at 20% deficit irrigation (Fal1(DI-20) and Fal2(DI-20), respectively) and fruit 2 of 'Ascolana dura' at 20% deficit irrigation (Asc2(DI-20)); (C) fruit 3 of non-irrigated 'Ascolana dura' (Asc3(DI-0)) and fruit 3 of non-irrigated 'Piantone di Falerone' (Fal3(DI-0)).

References

Agenzia Servizi Settore Agroalimentare delle Marche (ASSAM). Available online: http://www.meteo.marche.it/pi/#produzioneintegrata_discliplinare (accessed on 12 September 2022).

Ahumada-Orellana, L. E., Ortega-Farías, S., Searles, P. S., & Retamales, J. B. Yield and water productivity responses to irrigation cut-off strategies after fruit set using stem water potential thresholds in a super-high density olive orchard. Front. Plant Sci. 2017, 8, 1280. doi.org/10.3389/fpls.2017.01280.

Assirelli, A.; Romano, E.; Bisaglia, C.; Lodolini, E.M.; Neri, D.; Brambilla, M. Canopy Index Evaluation for Precision Management in an Intensive Olive Orchard. Sustainability 2021, 13, 8266. https:// doi.org/10.3390/ su13158266.

Bai, Y.; Li, X.; Liu, S.; Wang, P. Modelling diurnal and seasonal hysteresis phenomena of canopy conductance in an oasis forest ecosystem. Agric. For. Meteorol. 2017, 246, 98–110. doi.org/10.1016/j.agrformet.2017.06.006.

Boini, A., Manfrini, L., Bortolotti, G., Corelli-Grappadelli, L., & Morandi, B. Monitoring fruit daily growth indicates the onset of mild drought stress in apple. Sci. Hortic. 2019, 256, 108520. doi.org/10.1016/j.scienta.2019.05.047.

Brüggenwirth, M.; Winkler, A.; Knoche, M. Xylem, phloem, and transpiration flows in developing sweet cherry fruit. Trees 2016, 30, 1822–1830. doi.org/10.1007/s00468-016-1415-4.

Carella, A.; Gianguzzi, G.; Scalisi, A.; Farina, V.; Inglese, P.; Bianco, R.L. Fruit Growth Stage Transitions in Two Mango Cultivars Grown in a Mediterranean Environment. Plants 2021, 10, 1332. https://doi.org/10.3390/ plants10071332.

Caruso, G., Palai, G., Gucci, R., & Priori, S. Remote and Proximal Sensing Techniques for Site-Specific Irrigation Management in the Olive Orchard. Appl. Sci. 2022a, 12(3), 1309. doi.org/10.3390/app12031309.

Caruso, G., Palai, G., Gucci, R., & D'Onofrio, C. The effect of regulated deficit irrigation on growth, yield, and berry quality of grapevines (cv. Sangiovese) grafted on rootstocks with different resistance to water deficit. Irrig Sci 2022b, 1-15. doi.org/10.1007/s00271-022-00773-3.

COI (International Olive Council). Guide for the Determination of the Characteristics of Oil Olives, COI/OH/Doc. No 1 November 2011. Available online: http://www.internationaloliveoil.org (accessed on 15 September 2021).

Fernandes, R.D.M.; Cuevas, M.V.; Diaz-Espejo, A.; Hernandez-Santana, V. Effects of water stress on fruit growth and water relations between fruits and leaves in a hedgerow olive orchard. Agric. Water Manag. 2018, 210, 32–40. doi.org/10.1016/j.agwat.2018.07.028.

Fernández, J. E. Plant-based sensing to monitor water stress: Applicability to commercial orchards. Agric. Water Manag. 2014., 142, 99-109. doi.org/10.1016/j.agwat.2014.04.017.

Fernández, J. E. Plant-based methods for irrigation scheduling of woody crops. Horticulturae 2017, 3, 35–72. doi: 10.3390/horticulturae3020035.

Fishman, S.; Génard, M. A biophysical model of fruit growth: Simulation of seasonal and diurnal dynamics of mass. Plant Cell Environ. 1998, 21, 739–752. Doi.org /10.1046/j.1365-3040.1998.00322.x.

Fraga, H., Pinto, J. G., Viola, F., & Santos, J. A. Climate change projections for olive yields in the Mediterranean Basin. Int. J. Climatol. 2020., 40(2), 769-781. doi.org/10.1002/joc.6237.

Giorgi, V., Neri, D., Maria Lodolini, E., & Massetani, F. Olive (Olea europaea L.) root growth in soil sectors with olive husks and hay residues. Int. J. Fruit Sci 2008, 7(4), 19-32. doi.org/10.1080/15538360802003209.

Goldhamer, D. A. Regulated deficit irrigation for California canning olives. Acta Hortic 1999, 474, 369–372. doi: 10.17660/ActaHortic.1999.474.76.

Gómez-del-Campo, M. Summer deficit irrigation in a hedgerow olive orchard cv. Arbequina: relationship between soil and tree water status, and growth and yield components. Spanish J. Agric. Res 2013, 11, 547–557. doi: 10.1021/ jf402107t.

Grilo, F. S., Scalisi, A., Pernice, F., Morandi, B., & Lo Bianco, R. Recurrent deficit irrigation and fruit harvest affect tree water relations and fruitlet growth in 'Valencia'orange. Eur. J. Hortic. Sci 2019, 84, 177-187. doi.org/10.17660/eJHS.2019/84.3.8.

Gucci, R.; Lodolini, E.M.; Rapoport, H.F. Water deficit-induced changes in mesocarp cellular processes and the relationship between mesocarp and endocarp during olive fruit development. Tree Physiol 2009, 29, 1575–1585. doi.org/10.1093/treephys/tpp086.

Hernandez-Santana, V., Perez-Arcoiza, A., Gomez-Jimenez, M. C., & Diaz-Espejo, A. Disentangling the link between leaf photosynthesis and turgor in fruit growth. Plant Sci. J. 2021, 107(6), 1788-1801. doi.org/10.1111/tpj.15418.

Jones, H.G. Irrigation scheduling: advantages and pitfalls of plant-based methods. J. Exp. Bot 2004, 407, 2427–243. doi.org/10.1093/jxb/erh213.

Khosravi, A.; Zucchini, M.; Giorgi, V.; Mancini, A.; Neri, D. Continuous Monitoring of Olive Fruit Growth by Automatic Extensimeter in Response to Vapor Pressure Deficit from Pit Hardening to Harvest. Horticulturae 2021, 7, 349. doi.org/10.3390/ horticulturae7100349.

Kottek, M.; Grieser, J.; Beck, C.; Rudolf, B.; Rubel, F. World map of the Köppen-Geiger climate classification updated. Meteorol. Z. 2006, 15, 259–263. Doi.org/ 10.1127/0941-2948/2006/0130.

Lo Bianco, R., and Scalisi, A. Water relations and carbohydrate partitioning of four greenhouse-grown olive genotypes under long-term drought. Trees 2017, 31, 717–727. doi: 10.1007/s00468-016-1502-6.

Lodolini, E. M., Morini, F., Polverigiani, S., & Neri, D. Olive fruit and root growth on different irrigation regimes in central Italy. Acta Hortic. 2011a, 924, 63-68. doi. 10.17660/ActaHortic.2011.924.6.

Lodolini, E. M., Falleroni, P., Polverigiani, S., & Neri, D. Fertigation of young olive trees in Marche region, central Italy: preliminary study results. Acta Hortic 2011b, 888, 289-294. doi: 10.17660/ActaHortic.2011.888.33.

Lodolini, E. M., Ali, S., Mutawea, M., Qutub, M., Arabasi, T., Pierini, F., & Neri, D. Complementary irrigation for sustainable production in olive groves in Palestine. Agric. Water Manag. 2014, 134, 104-109. doi.org/10.1016/j.agwat.2013.12.006.

Lodolini, E. M., Polverigiani, S., Ali, S., Mutawea, M., Qutub, M., Pierini, F., & Neri, D. Effect of complementary irrigation on yield components and alternate bearing of a traditional olive orchard in semi-arid conditions. Spanish J. Agric. Res 2016, 14(2), e1203-e1203. doi.org/10.5424/sjar/2016142-8834.

Lakso, A. N., Corelli Grappadelli, L., Barnard, J., & Goffinet, M. C. An expolinear model of the growth pattern of the apple fruit. J. Hortic 1995, 70(3), 389-394.doi.org/10.1080/14620316.1995.11515308.

Mancini, A., Zucchini, M., Polverigiani, S., Marcheggiani, E., Casavecchia, S., & Neri, D. Cherry fruit growth: monitoring and 'tweeting'. Acta Hortic 2021, 1314, 399-408. doi: 10.17660/ActaHortic.2021.1314.50.

Marino, G., Caruso, T., Ferguson, L., & Marra, F. P. Gas exchanges and stem water potential define stress thresholds for efficient irrigation management in olive (Olea europea L.). Water 2018, 10(3), 342. doi.org/10.3390/w10030342.

Marino, G.; Scalisi, A.; Guzmán-Delgado, P.; Caruso, T.; Marra, F.P.; Lo Bianco, R. Detecting Mild Water Stress in Olive with Multiple Plant-Based Continuous Sensors. Plants 2021, 10, 131. doi.org/10.3390/plants 10010131.

Mayergoyz, I.D. Mathematical Models of Hysteresis and Their Applications, 2nd ed.; Electromagnetism; Academic Press: Cambridge, MA, USA, 2003; ISBN 978-0-12-480873-7.

Measham, P. F., Wilson, S. J., Gracie, A. J., & Bound, S. A. Tree water relations: flow and fruit. Agric. Water Manag. 2014, 137, 59-67. doi.org/10.1016/j.agwat.2014.02.005.

Polverigiani, S., Lodolini, E. M., & Neri, D. Olive root growth observed by field rhizotron. Acta Hortic. 2012, 949, 271-278. doi: 10.17660/ActaHortic.2012.949.39.

Monteith, J.; Unsworth, M. Principles of Environmental Physics: Plants, Animals, and the Atmosphere, 4th ed.; Academic Press: Cambridge, MA, USA, 2013.

Morandi, B.; Manfrini, L.; Zibordi, M.; Noferini, M.; Fiori, G.; Grappadelli, L.C. A Low-cost Device for Accurate and Continuous Measurements of Fruit Diameter. HortScience 2007a, 42, 1380–1382. doi.org/10.21273/HORTSCI.42.6.1380.

Morandi, B., Manfrini, L., Losciale, P., Zibordi, M., and Corelli Grappadelli, L. Changes in vascular and transpiration flows affect the seasonal and daily growth of kiwifruit (Actinidia deliciosa) berry. Ann. Bot. 2010, 105, 913–923. doi: 10.1093/aob/ mcq070.

Morandi, B., Rieger, M., & Grappadelli, L. C. Vascular flows and transpiration affect peach (Prunus persica Batsch.) fruit daily growth. J. Exp. Bot 2007b, 58(14), 3941-3947. doi.org/10.1093/jxb/erm248.

Morandi, B.; Losciale, P.; Manfrini, L.; Zibordi, M.; Anconelli, S.; Galli, F.; Pierpaoli, E.; Grappadelli, L.C. Increasing water stress negatively affects pear fruit growth by reducing first its xylem and then its phloem inflow. J. Plant Physiol 2014, 171, 1500–1509. doi.org/10.1016/j.jplph.2014.07.005.

O'Brien, J.J.; Oberbauer, S.F.; Clark, D.B. Whole tree xylem sap flow responses to multiple environmental variables in a wet tropical forest. Plant Cell Environ. 2004, 27, 551–567. Doi.org/10.1111/j.1365-3040.2003.01160.x.

O'Kane, J.P. Hysteresis in hydrology. Acta Geophys. Pol. 2005, 53, 373–383.

Perez-Martin, A.; Flexas, J.; Ribas-Carbó, M.; Bota, J.; Tomàs, M.; Infante, J.M.; Diaz-Espejo, A. Interactive effects of soil water deficit and air vapour pressure deficit on mesophyll conductance to CO2 in Vitis vinifera and Olea europaea. J. Exp. Bot. 2009, 60, 2391–2405. doi.org/10.1093/jxb/erp145.

Phillips, J.D. Sources of nonlinearity and complexity in geomorphic systems. Prog. Phys. Geogr. 2003, 27, 1–23. doi.org/10.1191/0309133303pp340ra.

Rodrigues, N., Casal, S., Peres, A. M., Baptista, P., Bento, A., Martín, H., ... & Pereira, J. A. Effect of olive trees density on the quality and composition of olive oil from cv. Arbequina. Sci. Hortic. 2018., 238, 222-233. doi.org/10.1016/j.scienta.2018.04.059.

Rodríguez Sousa, A. A., Barandica, J. M., & Rescia, A. J. Estimation of soil loss tolerance in olive groves as an indicator of sustainability: the case of the Estepa Region (Andalusia, Spain). Agronomy 2019, 9(12), 785. doi.org/10.3390/agronomy9120785.

Romero-Trigueros, C., Vivaldi, G. A., Nicolás, E. N., Paduano, A., Salcedo, F. P., & Camposeo, S. Ripening indices, olive yield and oil quality in response to irrigation with saline reclaimed water and deficit strategies. Front. Plant Sci. 2019, 10, 1243. doi.org/10.3389/fpls.2019.01243.

Romero-Trigueros, C., Parra, M., Bayona Gambín, J. M., Nortes Tortosa, P., Alarcon Cabañero, J. J., and Nicolás Nicolás, E. Effect of deficit irrigation and reclaimed water on yield and quality of grapefruits at harvest and postharvest. LWT – Food Sci. Technol 2017, 85, 405–411. doi: 10.1016/j. lwt.2017.05.001.

Scalisi A, O'Connell MG, Stefanelli D and Lo Bianco R. Fruit and Leaf Sensing for Continuous Detection of Nectarine Water Status. Front. Plant Sci. 2019, 10, 805. doi: 10.3389/fpls.2019.00805.

Scalisi A, Marino G, Marra FP, Caruso T and Lo Bianco R. A Cultivar-Sensitive Approach for the Continuous Monitoring of Olive (Olea europaea L.) Tree Water Status by Fruit and Leaf Sensing. Front. Plant Sci. 2020, 11, 340. doi: 10.3389/fpls.2020.00340.

Scalisi, A., Bresilla, K., and Simões Grilo, F. Continuous determination of fruit tree water-status by plant-based sensors. Italus Hortus 2017, 24, 39–50. doi: 10.26353/j.itahort/2017.2.3950.

Seifi, E., Guerin, J., Kaiser, B., & Sedgley, M. Flowering and fruit set in olive: A review. Iran. J. Plant Physiol 2015, 5(2), 1263-1272.

Tuzet, A., Perrier, A., & Leuning, R. A coupled model of stomatal conductance, photosynthesis and transpiration. Plant Cell Environ. 2003, 26(7), 1097-1116. Doi.org/10.1046/j.1365-3040.2003.01035.x.

Zeppel, M.J.B.; Murray, B.R.; Barton, C.; Eamus, D. Seasonal responses of xylem sap velocity to VPD and solar radiation during drought in a stand of native trees in temperate Australia. Funct. Plant Biol. 2004, 31, 461–470. doi.org/10.1071/FP03220.

Zhang, Q.; Manzoni, S.; Katul, G.; Porporato, A.; Yang, D. The hysteretic evapotranspiration—Vapor pressure deficit relation. J. Geophys. Res. Biogeosciences 2014, 119, 125–140. doi:10.1002/2013JG002484.

Zhang, R., Xu, X., Liu, M., Zhang, Y., Xu, C., Yi, R., ... & Soulsby, C. Hysteresis in sap flow and its controlling mechanisms for a deciduous broad-leaved tree species in a humid karst region. Sci. China Earth Sci. 2019, 62(11), 1744-1755. Doi.org/10.1007/s11430-018-9294-5.

Zucchini, M.; Khosravi, A.; Giorgi, V.; Mancini, A.; Neri, D. Is There Daily Growth Hysteresis versus Vapor Pressure Deficit in Cherry Fruit? Horticulturae 2021, 7, 131. doi.org/10.3390/horticulturae7060131.

Zuecco, G., Penna, D., Borga, M. A. R. C. O., & van Meerveld, H. J. A versatile index to characterize hysteresis between hydrological variables at the runoff event timescale. Hydrol 2016, 30(9), 1449-1466. doi.org/10.1002/hyp.10681

Chapter 5.

Introduction of fruit water stress index by means of temperature annotated 3D point cloud

Nikos Tsoulias[1], Arash Khosravi [1,3], Christian Regen[1], Werner Herppich[1], Manuela Zude-Sasse1,*

[1]Leibniz Institute for Agricultural Engineering and Bioeconomy (ATB), Potsdam, Germany
[2]Department of Agricultural, Food and Environmental Science, Marche Polytechnic University, 60131 Ancona, Italy.
[3]Technical University of Berlin, Agromechatronics, Straße des 17. Juni 144, 10623 Berlin, Germany

* Correspondence: Manuela Zude-Sasse[1]

Under submission on Plant physiology journal

Nomenclature

$FWSI_{I,Est}$		Fruit water stress index calculated by equ. 2 (Irmak et al., 2000) using T_{Est} (°C)
$FWSI_{I,Ref}$		Fruit water stress index calculated by equ. 2 (Irmak et al., 2000) using T_{Ref} (°C)
$FWSI_{I,Val}$		Fruit water stress index calculated by equ. 2 (Irmak et al., 2000) using T_{Val} (°C)
$FWSI_{J,Est}$		Fruit water stress index calculated by equ. 4 (Jones, 1992) using T_{Est} (°C)
$FWSI_{J,Ref}$		Fruit water stress index calculated by equ. 4 (Jones, 1992) using T_{Ref} (°C)
$FWSI_{J,Val}$		Fruit water stress index calculated by equ. 4 (Jones, 1992) using T_{Val} (°C)
$FWSI_{N,Est}$		Fruit water stress index calculated by normalisation (equ. 5) using T_{Est} (°C)
$FWSI_{N,Ref}$		Fruit water stress index calculated by normalisation (equ. 5) using T_{Ref} (°C)
$FWSI_{N,Val}$		Fruit water stress index calculated by normalisation (equ. 5) using T_{Val} (°C)
T_{Est} (°C)		Calibrated fruit temperature derived from LiDAR
T_{Raw} (°C)		Fruit temperature obtained by LiDAR
T_{Ref} (°C)		Manually measured fruit temperature
T_{Val} (°C)		Fruit temperature derived from LiDAR using cross-validation data split

5.1 Introduction

Water status detection has been addressed as one of the pivotal topics in the precision orchard management (Agam et al., 2013; Helman et al., 2018), which is closely related to orchard performance by affecting several aspects such as fruit growth (quality and size) (Measham et al., 2014; Fernandes et al., 2018; Bahat et al., 2021) and water use by site-specific Irrigation (Cohen et al., 2017). Therefore, suitable monitoring tools and methods for precise water status detection are essential (Agam et al., 2013b). There are several different ways for categorizing current continuous monitoring systems according to technological point of view, application area and sensor type etc. (Zude-Sasse et al., 2016). Regarding sensor types, water status monitoring can be performed by different proximal or remote sensors. Proximal sensors can be used individually (Khosravi et al., 2022), however several research suggested combination of sensors to achieve precise and cultivar-specific data (Marino et al., 2021). As an example, combination of fruit gauge and leaf patch clamp pressure probe for continuous monitoring of olive (Olea europaea L.) (Scalisi et al., 2020; Marino et al., 2021) and nectarine (Prunus persica L.) (Scalisi et al.,2019); monitoring of apple (Malus domestica.) by integration of fruit gauge and Scholander pressure chamber (Boini et al., 2019); continuous monitoring of orange (Citrus sinensis) by combination of fruit gauge and sap flow sensor (Grilo et al., 2019). Although continuous monitoring by combination of proximal sensors increase accuracy, this method has been restricted by several cons such as difficulty of replicate of continuous measurements on large numbers of trees (commercial orchards), specific knowledge of installation and maintenance of sensors as well as choosing proper indices for water status detection in orchard condition

(Fernandez. 2014; Marino et al., 2021). Consequently, proximal measurements are less common for water stress detection.

Considering remote sensing method for water stress detection by thermal sensors, the standardized crop water stress index (CWSI) has been employed widely. One of the main reasons of popularity of CWSI is related to applicability for large-scale monitoring via airborne systems which make it suitable for real scenario application in the commercial orchards (Sánchez-Piñero et al., 2022). Water status detection by remote sensing have been investigated in several research including the use of aerial thermal imagery to estimate CWSI in date-palm (Phoenix dactylifera L.) trees (Cohen et al., 2012). Photogrammetry using the visible-spectrum and infrared thermography was applied to measure CWSI of pistachio (Pistacia vera L.) trees using convolutional neural networks (Pantelidakis et al., 2022). UAV-based thermal and multispectral images were employed to measure CWSI and normalized difference vegetation index (NDVI) in mild and moderate water stress levels in almond (Prunus dulcis Mill. (D.A. Web)) trees (Gutiérrez-Gordillo et al., 2021).

The CWSI has been calculated based on the empirical (Idso et al., 1981) or theoretical (Jackson et al., 1981) approaches. Recently, the equations have been improved by many researches (Osroosh et al., 2015; Sánchez-Piñero et al., 2022), however all of them measured canopy and air temperature in the actual, well-watered as well as extreme water stress situation. The typical application is the analysis of CWSI of canopies following the causal chain that water stress reduces stomatal conductance and transpiration rate at the leaf level.

It has been shown recently that fruit can be visualized in 3D point clouds of the entire canopy using photogrammetry by means of binocular stereo vision, structure-from-motion, and multi-view stereo vision (Rosell and Sanz, 2012). However, photogrammetry still has limitations due to varying lighting conditions according to angle and intensity of global radiation as well as shading effects into the canopy. Sensors with own light source, particularly, light detection and ranging (LiDAR) overcomes such limits to some extent. In navigation questions, object detection and path following control for autonomous mowing by unmanned ground vehicle was achieved with LiDAR (Kurita et al., 2022). Terrestrial LiDAR sensors have been employed in several research carried out in orchards for canopy volume estimation (Rud et al., 2016), estimation of leaf area (Penzel and Tsoulias, 2022), and fruit detection (Tsoulias et al., 2020; Kang et al., 2022). Having the fruit visualization by LiDAR at hand, the annotation with temperature data would enable to analyze 4D point clouds of canopies and fruit. To our knowledge, no study has yet computed CWSI or, more specific, the fruit water stress index (FWSI) by application of the LiDAR.

Objectives of the present study were (i) to extract the fruit surface temperature from terrestrial remote sensing based on LiDAR and thermal imaging; (ii) to compare estimated and manually measured FWSI; and (iii) to gain first results of the new method when applied in apple trees.

5.2 Material and Methods

5.2.1 Experimental layout

The experiment was conducted in the experimental station of Leibniz Institute for Agricultural Engineering and Bioeconomy (ATB), located in Potsdam-Marquardt, Germany (Latitude: 52.466274◦ N, Longitude: 12.57291◦ E), planted with Malus × domestica Borkh. 'Gala-Brookfield' on M9 rootstock with 0.95 m distance between trees, trained as slender spindle with an average tree height of 2.8 m. Trees were statically supported by horizontally parallel wires. Measurements took place throughout the season at 67, 81, 132 and , 152, 153, 166 days after full bloom (DAFB67, DAFB81, DAFB132,DAFB152 DAFB153 and DAFB166), respectively. Daily measurements were carried out during DAFB152 and DAFB153 , with six intervals at 7:00, 8:00, 10:00 am and at 12:00, 13:00 and 18:00 pm.
Weather data (Uniklima vario, Toss, Germany) were obtained in the orchard in x min interval, recording air temperature (°C), relative air humidity (%), global normal irradiance (GNI; W m-2), and precipitation (mm). The water vapour partial pressure deficit (VPD, kPa) was calculated as:
$VPD = (1-(RH/100)) \times SVP$ and $SVP(Pascals) = 610.7 \times 10(7.5\ T/(237.3+T))$ (1)

5.2.2 Remote sensing

A phenotype sensing system was set up on a circular conveyor platform in the experimental apple orchard after calibration. The platform used an electrical engine operating at 50 Hz and a stainless-steel chain with mechanical suspensions to support the plant sensors (DRN71, SEW Eurodrive, Germany). A mobile 2D LiDAR sensor with a wavelength of 905 nm (LMS-511, Sick AG, Waldkirch, Germany) was mounted vertically on the metal frame at 0.7 m above the ground level. The LiDAR sensor had a configuration with a 0.1667° angular resolution, 25 Hz scanning frequency, and a scanning angle of 180. A thermal camera (A655sc, FLIR Systems Inc., MA, USA) was also installed, positioned 0.2 m above the laser scanner. The camera had a spatial resolution of 640 × 480 pixels at 50 Hz and a spectral range from 7.5 to 14 μm, with an operational temperature range from −40°C to 150°C and a thermal resolution < 0.05°C. A lens (T198065, FLIR Systems Inc., MA, USA) with a focal length of 6.5 mm (diagonal 80o) was attached to the camera. The system underwent intrinsic and extrinsic calibration using a lightbulb pattern (Tsoulias et al., 2022). The data was geo-referenced using a real-time kinematic global navigation satellite system (AgGPS 542, Trimble, Sunnyvale, CA, USA), while orientation information was acquired using an inertial measurement unit (MTi-G-710, XSENS, Enschede, Netherlands), both of which were arranged on the sensor frame. The orientation information had a root mean square error (RMSE) of 0.25° for roll, pitch, and yaw.

5.2.3 Reference temperature

During the growing period, the temperature on the surface of forty apples (n = 200) was manually measured (T_{Ref}) from both sides of three trees (n = 3) with an infrared thermometer (Microscanner D501, Exergen, Watertown, USA), and compared with the corresponding averaged temperature obtained by LiDAR T_{Raw} over the growth stages. To determine the local maximum (T_{max}) and minimum (T_{min}) temperatures among the apples, two individual fruits were covered with Vaseline and soap mixed with water, respectively.
Similarly, during the daily temperature measurements of T_{Ref}, only apples from the west side of five trees (n=5) were sampled (n=55). For each individual tree, one apple was covered with Vaseline to acquire T_{max}, while plastic boxes filled with water were used to measure T_{min}.

5.2.4 Stem water potential

Stem water potential was measured in the orchard with a Scholander bomb (Plant Water Status Console 3000, Soilmoisture Equipment Corp., USA) on three shaded leaves sealed in plastic bags for 30 min. Subsequently, leaves were transported in plastic bags to the laboratory, and frozen at −30 °C. After thawing, centrifuged tissue sap was analyzed with water vapor osmometer (Vapro 5520, Wescor Inc., USA). The osmotic potential of tissue sap was calculated according to the van't Hoff's equation (vonWillert et al., 1995). The measurement was carried out during full bloom, cell division, and harvest. An average out of four measurements was taken for each individual tree sampled (n = 20).

5.2.5 Fruit quality

After each measurement with the phenotyping sensor system, apple samples (n = 10) were collected for reference analyses. Fruit diameter (D) [mm] was manually measured in the laboratory by means of a digital calliper gauge considering the mean diameter of two measurements taken equatorially with 90o difference. The fresh mass (FM) [kg] was measured by weighting each fruit sample. Soluble solids content (SSC) [%] was measured, from juice obtained during the firmness test, collected with pipette and analysed by a digital refractometer (Pal-1, Atago, Tokyo, Japan). Fruit flesh firmness [N] was measured by Texture Analyzer (TA-XT Plus, Stable Micro Systems, Godalming, Surrey, UK) using a 11.13 mm diameter, convex plunger at 4 mm s-1 speed on a peeled area in the equatorial region. Load value was measured at 8 mm depth of penetration and corrected according to the plunger size.
The chlorophyll content of apples' skin and hypodermis tissue (2 mm thickness) was measured destructively at each measuring date during fruit development. The chlorophyll_A, _B, and pheophytin_A contents were determined using spectrophotometry after the extraction with acetone/diethyl ether. Specifically, apples were probed with a cork

borer to obtain equal numbers of 1 mm thick discs. The fruit tissue and pinch of calcium carbonate, was ground (Ultra Turrax, Germany) in acetone containing 0.1% butylated hydroxytoluene on ice. Resulting pigment extracts were filtered using a glass frit (pore size 3) attached to a vacuum pump. Phase separation in separating funnel was achieved by adding distilled water, transferring non-polar pigments like chlorophyll a and b, pheophytin a, and most of the carotenoids to a non-polar diethyl ether phase. The absorbance spectrum of the non-polar phase was recorded (Lambda 950, Perkin Elmer). The standard spectra of the three chlorophylls were considered in the iterative multiple linear regression analysis method used for this purpose (Pflanz and Zude, 2008).
The maximum daily shrinkage of stem was measured using x dendrometers (DD-L, Ecomatic GmbH, Dachau, Germany), installed 70 cm above ground, 50 cm above the grafting zone. Data were recorded with a CR10X data logger with an AM416 multiplexer (Campbell Scientific, Logan, USA).

5.2.6 LiDAR data processing

The 3D point cloud dataset was generated and processed using the Computer Vision Toolbox™ of MATLAB (2018b, Mathworks, Natick, MA, USA). To calibrate the apparent reflectance intensity (RToF) of the LiDAR and obtain the RToF [%] at 905 nm for each point in the 3D point cloud, board targets coated with white barium sulphate (BaSO4, CAS Number: 7727–43-7, Merck, Germany) for maximum values and blackened urethane (S black, Avian Technologies, New London, NH, USA) for minimum values were utilized.
The 3D point cloud data underwent rigid translations and rotations, and the alignment of pairing tree sides was achieved using the iterative closest point algorithm, as described by Tsoulias et al. (2019). To obtain points per tree (PPT) from each plant, trees were segmented based on their stem position and planting distance. The bivariate point density histogram facilitated the detection of the peak of laser hits for each individual tree, assuming that stem points are located at the center of the canopy. Based on the slender spindle tree training system, the area closer to the stem position is expected to have a higher frequency. The estimated stem position coordinates were used as the center for segmentation cylinders, which were used to obtain the points belonging to each individual tree. The points within the cylinder boundaries were segmented and considered as the tree points.

5.2.7 Temperature segmentation in apples

The position and shape of apples were determined by utilizing the geometric feature of linearity (L), curvature, (C) and R_{ToF}, considering each point of the 3D tree point cloud (Tsoulias et al., 2020). Local neighbors were decomposed and eigenvalues were generated, with values closer to 100 indicating a higher likelihood for the shape of point appearance to be curved. The mean of all nearest neighbors was estimated using the total number of neighbourhood points within each tree's cloud, which was then used to produce eigenvalues (λ_1, λ_2, λ_3) after the covariance matrix was decomposed. To distinguish the 3D points of woody parts (W) from leaves, the probability density function was performed to define the thresholds of L, C, and LiDAR's backscattered intensity (R_{ToF}). The most frequent value

within the distribution of L_W, C_W, and $R_{ToF,W}$ was used as the threshold ($R_{th,W}$, $C_{th,W}$, and $L_{th,W}$). Points that met the criteria of $L_W \leq L_{th,W}$, $C_{th,W} \leq C_W$, and $R_{th,W} \leq R_{ToF,W}$ were segmented and subtracted from the total number of PPT. To define threshold values of apple points in terms of C and reflected intensity (C_A and $R_{ToF,A}$), following which the points satisfying the criteria of $C_{th,A} \leq C_A$, and $R_{th,A} \leq R_{ToF,A}$ were segmented and labelled as apple. Subsequently, a density-based scan algorithm was applied to find the point sets, with the mean manually measured diameter of fruit found in the neighborhood search radius and the value 10, based on manual measurements, as the minimum number of neighbors. This allowed to define the temperature values on the surface of canopy and apples by means of LiDAR (T_F).

5.2.8 *FWSI* estimation

The extracted temperature points from the surface of apples, by means of LiDAR point cloud, was exploited to estimate the fruit waster stress index by 3 alternative methods (equations 2, 4 and 5). FWSII was calculated by Irmark method (Irmark et al., 2000) (equation 2):

$$FWSI_I = \frac{T_F - T_{min}}{(T_a+5) - T_{min}} \quad (2)$$

where T_F the extracted temperature for each point on apple surface, T_{min} represents the minimum fruit temperature of the segmented point clouds, measured at each individual measuring day, respectively. T_a is average of air temperature (measured from equation 3) plus 5(°C).

$$Ta = \frac{\sum_{n-5}^{n-2} T}{4} \quad (3)$$

where T is air temperature and n is exact hour of measuring fruit temperature at each individual measuring day. The $FWSI_J$ was calculating according to Jones equation (Jones, 1992):

$$FWSI_J = \frac{T_F - T_W}{T_D - T_W} \quad (4)$$

where T_W is temperature of fully transpiring fruit and T_D is temperature of non-transpiring fruit of the segmented point clouds, measured at each individual measuring day, respectively. $FWSI_N$ called normalized fruit water stress index and was calculated as:

$$FWSI_N = \frac{T_F - T_{Min}}{T_{max} - T_{Min}} \quad (5)$$

T_{Min} and T_{Max} represent the minimum and maximum fruit temperature of the segmented point clouds, measured at each individual measuring day, respectively.

For the demonstration of performance of different FWSI approaches, the parameter of ΔT(°C) has been employed. It was calculated as:

$$\Delta T = T_F - T_{Air} \quad (6)$$

where T_F represents actual fruit temperature (T_{Est}) and T_{Air} is actual air temperature.

5.2.9 Data evaluation

Descriptive statistics were applied to all datasets capturing minimum, maximum, mean, standard deviation. A regression analysis was performed to quantify linear and logarithmic relationships between the manual measurements and LiDAR-derived data over the growing stages, and root mean square error (RMSE), mean bias error (MBE), coefficient of determination (R2) were calculated. Descriptive statistics and graph design were performed using Sigmaplot 14.5 (Systat Software, Inc., San Jose, CA, USA).

5.3. Results and discussion

5.3.1 Fruit surface temperature estimation

Slender spindle form the major training system of apple trees in world-wide production, providing a 3D structure in which the fruit are more or less evenly distributed according to the success of the thinning measure. Apple temperature monitoring is considered as an important step when implementing precision horticulture techniques in orchards. In the present study, a LiDAR laser scanner and a thermal camera were used to monitor the temperature variation in terms of FWSI. The extrinsic calibration applied to acquire the thermal 3D point cloud of trees (Figure 1), revealing an 1.82 RMSE pixel-1. The LiDAR estimated temperature (T_{Raw}) varied in the 3D point cloud of the trees. Tree organs, found above 2 m, revealed reduced T_{Raw} not exceeding 20 °C. Moreover, the T_{Raw} on stem points showed a mean value of 20.6 °C with 0.65 °C standard deviation. The segmented leaf area (Fig. S5.1)

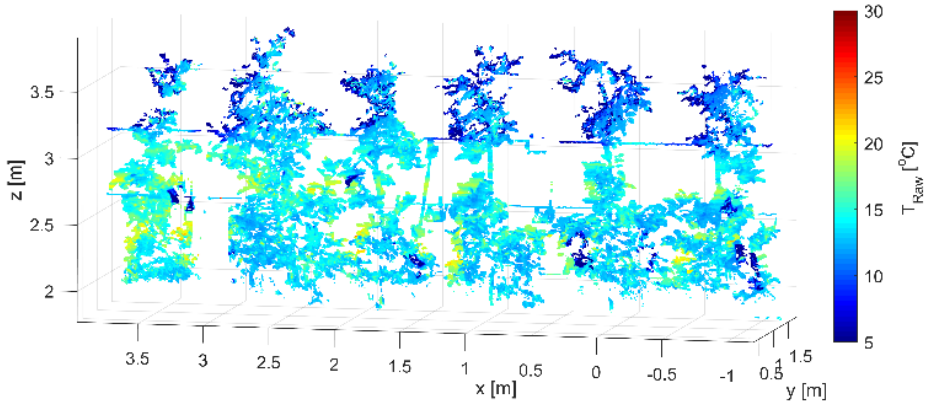

Figure. 5.1: Spatial temperature distribution in the canopy analysed by means of LiDAR and thermal sensors remotely.

The fruit segmentation routine was described earlier (Tsoulias et al., 2020), allowing to exclude leaf area and wood structure from the point cloud. The fruit temperature estimated by means of LiDAR laser scanner (T_{Raw}) ranged from 12 to 48 °C with a mean value of 25.2 °C , while the manually measured temperature on apple surface (T_{Ref})depicted a range from 12 to 40 °C with a mean value of 24.3 °C considering all measuring days. A linear regression model described the relation between the latter two parameters (Table 5.1).

Table 5.1: Descriptive statistics of estimated fruit temperature by means of LiDAR and thermal sensors (T_{Raw}) compared to manually measured data (T_{Ref}) capturing coefficient of determination in the calibration (T_{Est}) and cross validation (T_{val}) , root mean square error, and bias. In the calibration 80 % of data (N=241), whereas remaining 20 % of data (N=61) were used in cross validation.

	Min	*Max*	*Mean*	*Bias (°C)*	*R^2*	*RMSE (%)*
T_{Est}	*8.94*	*43.18*	*22.87*	*-0.99*	*0.93*	*1.59*
T_{val}	*10.37*	*41.1*	*24.14*	*-1.23*	*1.00*	*1.91*

To evaluate the robustness and transferability of the relationship between the T_{Raw} and the T_{Ref} data, calibration and cross-validation were performed, considering 80 and 20 % of the data, respectively. The measuring uncertainty of calibration was 1.59 % with an R^2 of 0.93, while an enhanced coefficient of determination appeared after cross validation. Moreover, the mean bias error increased from 0.99 to 1.23 °C, considering cross validation. In addition, a 1:1 linear relationship was observed among field data and cross validation predicted values (Fig. 5.2c). Whereas, the RMSE values from these cross-validation models were slightly higher than to those obtained by using both training and calibration samples from the same study site.

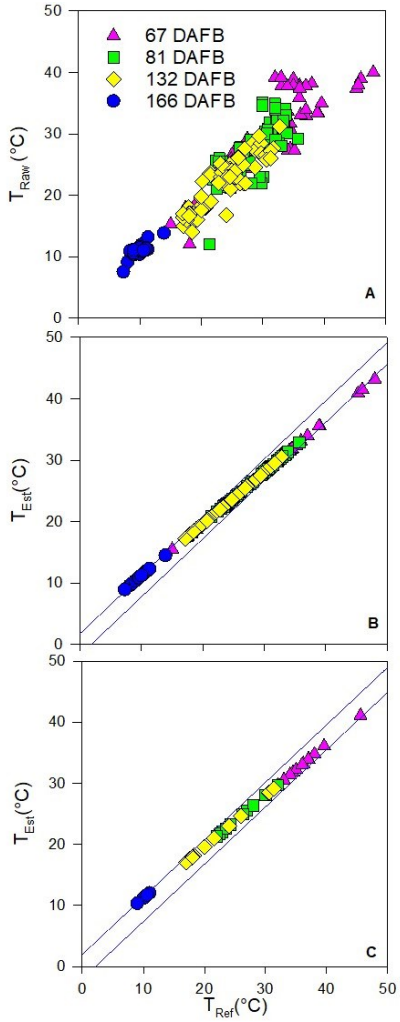

Figure 5.2: Scatter plots of: (a) raw LiDAR-derived temperature (T_{Raw}) (N=302), (b)calibrated data (N=241) (T_{Est}) according the linear regression and (c) cross-validation (T_{val}) (N=61), including all growth stages.

.

5.3.2 Comparison of fruit water stress index approaches

After fruit localization, the fruit water stress index (FWSI) was estimated for all alternative methods, considering the calibrated and cross validated values (Table 5.2). The Jones FWSI index presented an increased variation, ranging from -2.81 to 6.06 and from -1.69 to 5.39 in $FWSI_{I,Est}$ and $FWSI_{I,Val,}$ respectively. Whereas, $FWSI_N$ and $FWSI_I$ presented similar average values for the calibrated and crossed validated cases.

Table 5.2: Descriptive statistics capturing coefficient of determination (R^2), root mean square error (RMSE, %), and bias (%) of fruit water stress index (FWSI) approaches considering the remotely measured fruit temperature compared to manual fruit temperature readings, for $FWSI_{Est}$ N=241 and for $FWSI_{Val}$ N=61.

	Min	Max	Mean	Bias (%)	RMSE (%)	R^2
$FWSI_{I,Est}$	-0.01	1.58	0.48	-0.08	0.11	0.99
$FWSI_{I,Val}$	0.00	1.98	0.50	-0.16	0.24	0.99
$FWSI_{N,Est}$	-0.01	1.00	0.44	0.01	0.02	0.99
$FWSI_{N,Val}$	0.00	1.00	0.46	-0.02	0.05	0.98
$FWSI_{J,Est}$	-2.81	6.06	0.53	-0.89	2.27	0.66
$FWSI_{J,Val}$	-1.69	5.39	0.91	-1.02	2.00	0.80

On the other hand, similar good results were found in $FWSI_I$ and $FWSI_N$ (Figure 5.3 A,D; C,F). More specifically, a higher uncertainty of 0.11 % and 0.24 % RMSE with an underestimation of -0.08 % and -0.16 % was observed in $FWSI_{I,Est}$ and $FWSI_{I,Val}$, respectively. Generally, enhanced measuring uncertainty was noticed in the $FWSI_{J,Est,}$ presenting an 0.66 R^2 with an 2.27 % RMSE, while a moderate correlation was revealed in $FWSI_{J,Val}$ (Figure5.3 B,E).

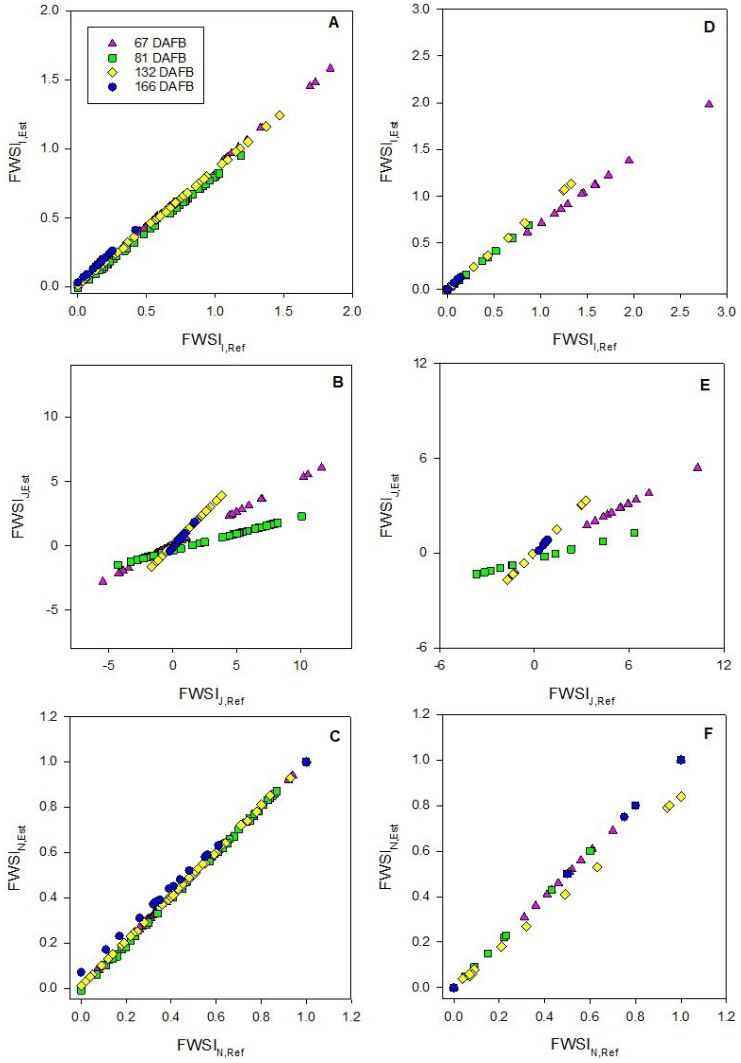

Figure. 5.3: Scatter plots of correlation of FWSI obtained from T_{Ref} and T_{Est} A and B and C is calculated by validated data (N=241). D and E and F is calculated by cross validated data (N=61).

.

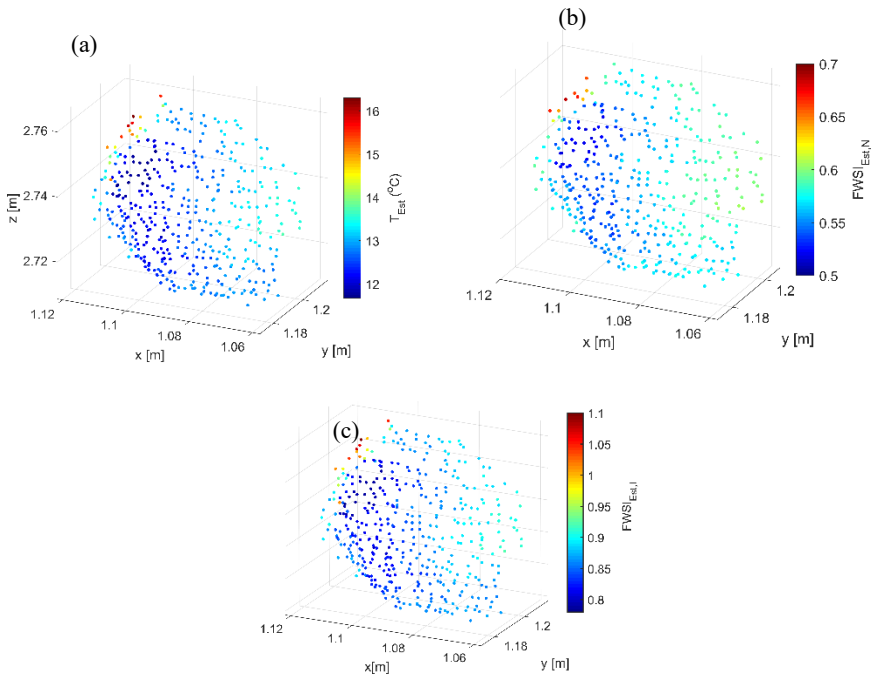

Fig. 5.4: (a) Segmented fruit temperature, (b) $FWSI_{N,Est}$ and (c) $FWSI_{I,Est}$ measured by means of LiDAR and thermal sensors remotely. During midday at DAFB153 .

*) The values of $FWSI_{N,Est}$ were highly variated between 2 and 3 m. Whereas lower values found at the top of the tree.
*) A less pronounced variation / or a more homogenous result was observed in $FWSI_{I,Est}$. The values mainly deviated between 0.8 and 1

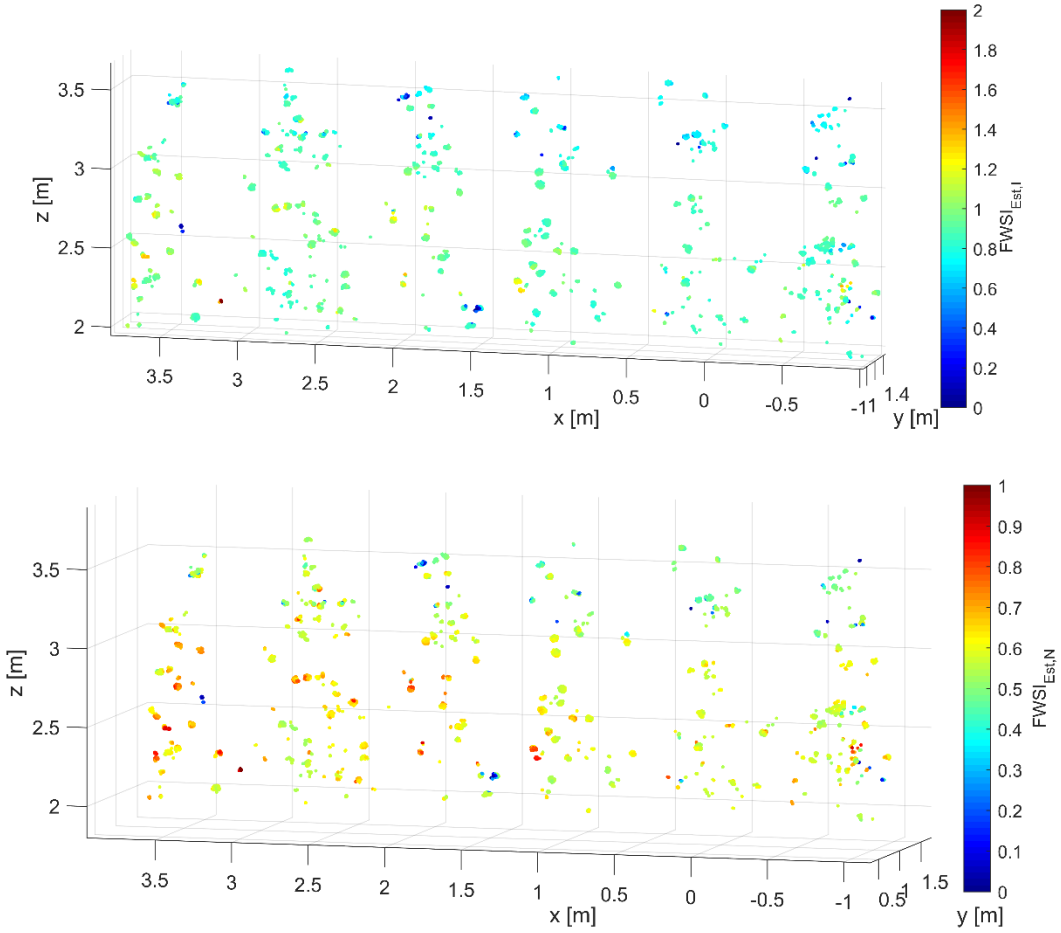

Fig. 5.5: Segmented apple waster stress index during midday at $DAFB_{153}$ of (Top) $FWSI_{N,Est}$ and (Down) $FWSI_{I,Est}$ measured by means of LiDAR and thermal sensors remotely.

5.3.3 Seasonal course of FWSI

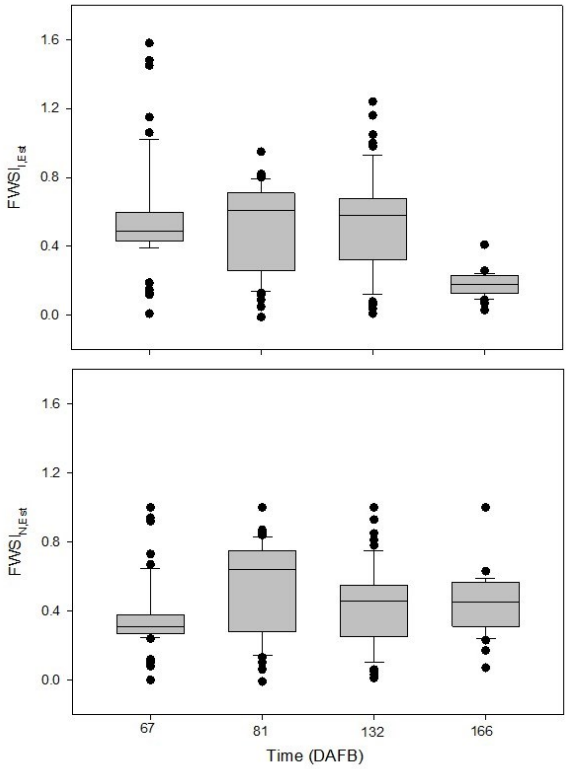

Figure 5.6: Seasonal curse of FWSI calculated as normalized index considering the max and min fruit temperature measured and according to Irmak et al. 2000. (N=302).

- The $FWSI_{I,Est}$ showed higher mean value than $FWSI_{N,Est}$ during DAFB 67
- Similar values between 81 and 132 DAFB.
- Steep decrease of mean values and of variability for both cases.

5.3.4 Diel course of FWSI

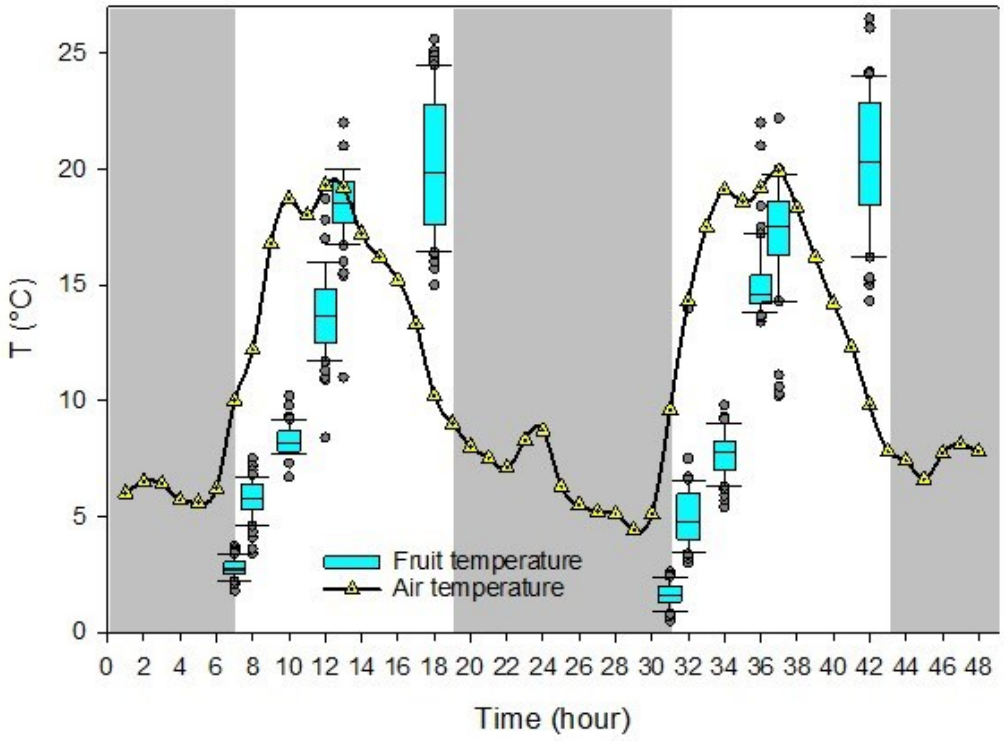

Figure 5.7: Diurnal courses of air and fruit temperature measured on 21th and 22th September (DAFB 152 and 153, respectively). Fruit were measured each measuring time (N=600).

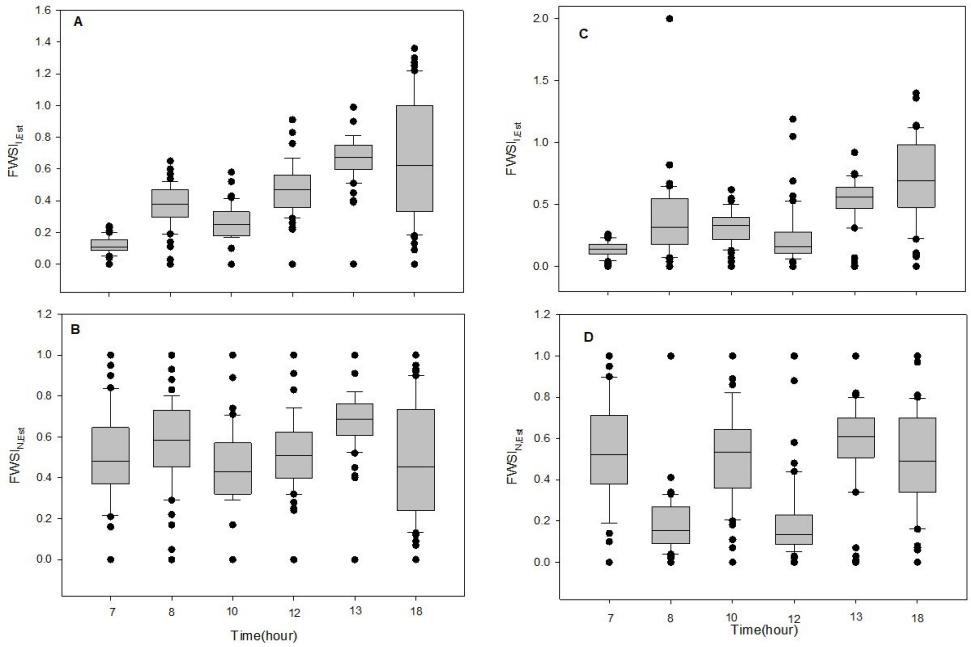

Fig. 5.8: Diurnal courses of FWSI. (A and C) calculated by Irmak equation; (B and D) calculated by Normalized equation.. N=600.(A and B) Are related to 21th September(DAFB152); (C and D) are related to 22th September(DAFB153).

5.4 Conclusion

Computing FWSI based on 3D fruit temperature (obtained from integration LiDAR and thermal camera) is an innovative methodology which can be used in precision orchard management. The developed methodology calculated FWSI with 3 methods and with good relation to FWSI calculated by reference data. However, $FWSI_{N,Est}$ and $FWSI_{I,Est}$ was high related to the $FWSI_{I,Ref}$ and $FWSI_{N,Ref}$ (Table5.2). The method is under development and we are going to publish data till end of the June (Approximately).

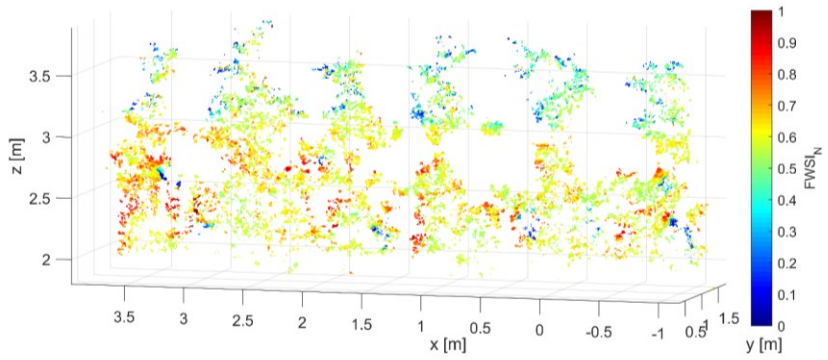

Figure S5.1: Spatial distribution temperature of normalized fruit water stress index ($FWSI_N$) of entire canopy analysed by means of LiDAR and thermal sensors.

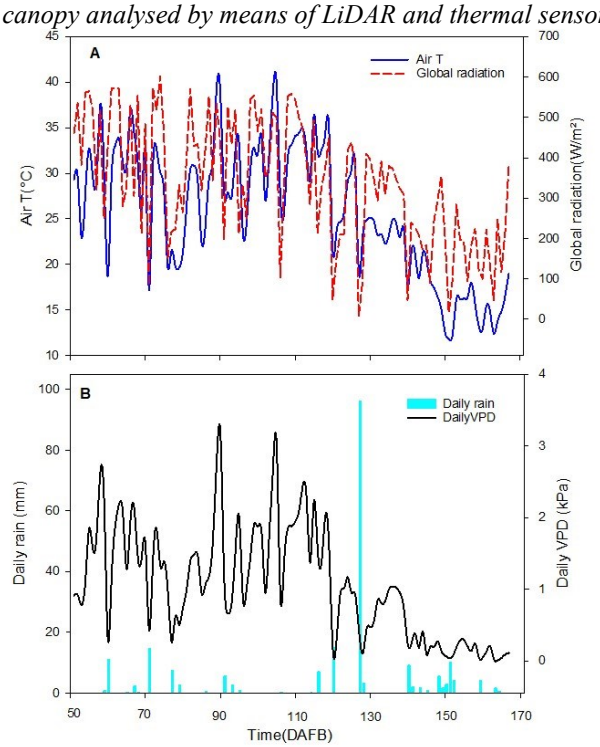

Figure S5.2: Air temperature and global radiation at 15:00 (A), wind speed at 15:00 (B), from 50 to 170 days after full bloom (DAFB). On the 166 DAFB, all data were collected at 13:00.

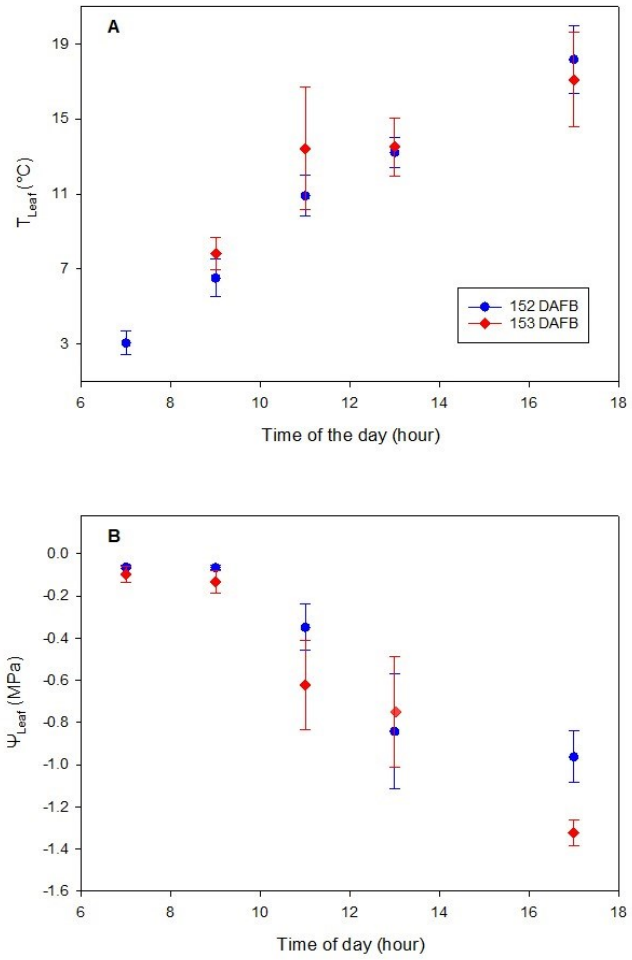

Figure S5.3: Leaf temperature in 152 and 153 DAFB (A); Leaf water potential in 152 and 153 DAFB (B). data are related to means (n=15 ± SD).

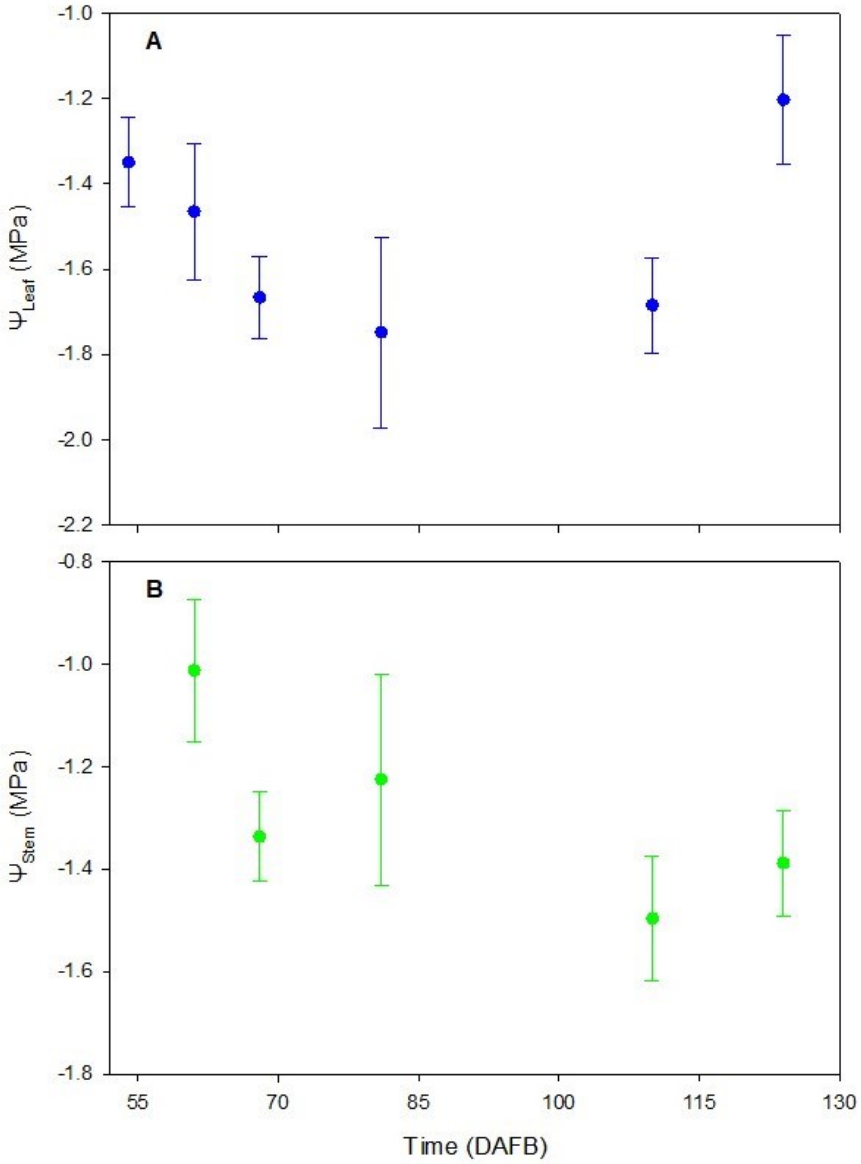

Figure S5.4: Leaf water potential (A); stem water potential (B). means (n=6± SD).

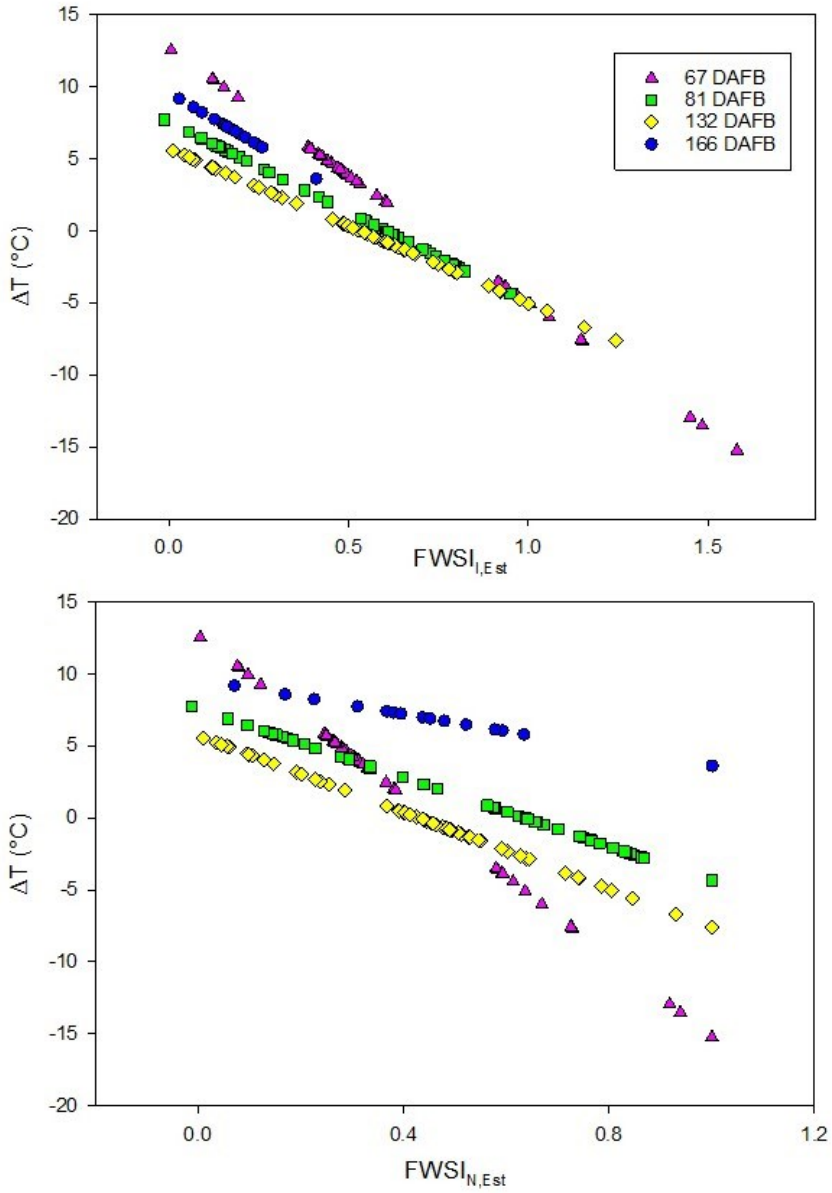

Figure S5.5: Scater plot of ΔT and FWSI.

References:

Agam, N., Cohen, Y., Alchanatis, V., & Ben-Gal, A. (2013a). How sensitive is the CWSI to changes in solar radiation?. International journal of remote sensing, 34(17), 6109-6120.

Agam, N., Cohen, Y., Berni, J. A. J., Alchanatis, V., Kool, D., Dag, A., ... & Ben-Gal, A. (2013b). An insight to the performance of crop water stress index for olive trees. Agricultural Water Management, 118, 79-86.).

Bahat, I., Netzer, Y., Grünzweig, J. M., Alchanatis, V., Peeters, A., Goldshtein, E., ... & Cohen, Y. (2021). In-season interactions between vine vigor, water status and wine quality in terrain-based management-zones in a 'Cabernet Sauvignon'vineyard. Remote Sensing, 13(9), 1636.

Boini, A., Manfrini, L., Bortolotti, G., Corelli-Grappadelli, L., & Morandi, B. (2019). Monitoring fruit daily growth indicates the onset of mild drought stress in apple. Scientia Horticulturae, 256, 108520.

Cohen, Y., Alchanatis, V., Prigojin, A., Levi, A., & Soroker, V. (2012). Use of aerial thermal imaging to estimate water status of palm trees. Precision Agriculture, 13(1), 123-140.

Cohen, Y., Alchanatis, V., Saranga, Y., Rosenberg, O., Sela, E., & Bosak, A. J. P. A. (2017). Mapping water status based on aerial thermal imagery: comparison of methodologies for upscaling from a single leaf to commercial fields. Precision Agriculture, 18(5), 801-822.

Fernandes, R. D. M., Cuevas, M. V., Diaz-Espejo, A., & Hernandez-Santana, V. (2018). Effects of water stress on fruit growth and water relations between fruits and leaves in a hedgerow olive orchard. Agricultural water management, 210, 32-40.

Fernández, J. E. (2014). Plant-based sensing to monitor water stress: Applicability to commercial orchards. Agricultural water management, 142, 99-109.

Grilo, F. S., Scalisi, A., Pernice, F., Morandi, B., & Lo Bianco, R. (2019). Recurrent deficit irrigation and fruit harvest affect tree water relations and fruitlet growth in 'Valencia'orange. Eur. J. Hortic. Sci, 84(3), 177-187.

Gutiérrez-Gordillo, S., de la Gala González-Santiago, J., Trigo-Córdoba, E., Rubio-Casal, A. E., García-Tejero, I. F., & Egea, G. (2021). Monitoring of Emerging Water Stress Situations by Thermal and Vegetation Indices in Different Almond Cultivars. Agronomy, 11(7), 1419.

Helman, D., Bahat, I., Netzer, Y., Ben-Gal, A., Alchanatis, V., Peeters, A., & Cohen, Y. (2018). Using time series of high-resolution planet satellite images to monitor grapevine stem water potential in commercial vineyards. Remote Sensing, 10(10), 1615.

Idso, S.B., Jackson, R.D., Pinter, P.J., Reginato, R.J., Hatfield, J.L., 1981. Normalizing the stress-degree-day parameter for environmental variability. Agric. Meteorol. 24, 45–55.

Jackson, R.D., Idso, S.B., Reginato, R.J.E., Pinter, P.J., 1981. Canopy temperature as a crop water stress indicator. Water Resour. Res. 17, 1133–1138.

Kang, H., Wang, X., & Chen, C. (2022). Accurate fruit localisation using high resolution LiDAR-camera fusion and instance segmentation. Computers and Electronics in Agriculture, 203, 107450.

Khosravi, A., Zucchini, M., Mancini, A., & Neri, D. (2022). Continuous Third Phase Fruit Monitoring in Olive with Regulated Deficit Irrigation to Set a Quantitative Index of Water Stress. Horticulturae, 8(12), 1221.

Kurita, H., Oku, M., Nakamura, T., Yoshida, T., & Fukao, T. (2022). Localization Method Using Camera and LiDAR and its Application to Autonomous Mowing in Orchards. Journal of Robotics and Mechatronics, 34(4), 877-886.

Marino, G., Scalisi, A., Guzmán-Delgado, P., Caruso, T., Marra, F. P., & Lo Bianco, R. (2021). Detecting mild water stress in olive with multiple plant-based continuous sensors. Plants, 10(1), 131.

Measham, P. F., Wilson, S. J., Gracie, A. J., & Bound, S. A. (2014). Tree water relations: flow and fruit. Agricultural Water Management, 137, 59-67.

Osroosh, Y., Peters, R. T., Campbell, C. S., & Zhang, Q. (2015). Automatic irrigation scheduling of apple trees using theoretical crop water stress index with an innovative dynamic threshold. Computers and Electronics in Agriculture, 118, 193-203.

Pantelidakis, M., Panagopoulos, A. A., Mykoniatis, K., Ashkan, S., Eravi, R. C., Pamula, V., ... & Chalkiadakis, G. (2022). Identifying sunlit leaves using Convolutional Neural Networks: An expert system for measuring the crop water stress index of pistachio trees. Expert Systems with Applications, 209, 118326.

Penzel, M., & Tsoulias, N. (2022). Annual shoot growth on apple trees with variable canopy leaf area and crop load in response to LiDAR scanned leaf area to fruit ratio. International Agrophysics, 36(3), 173-180.

Pflanz, M., & Zude, M. (2008). Spectrophotometric analyses of chlorophyll and single carotenoids during fruit development of tomato (Solanum lycopersicum L.) by means of iterative multiple linear regression analysis. Applied Optics, 47(32), 5961-5970.

Rosell, J. R., & Sanz, R. (2012). A review of methods and applications of the geometric characterization of tree crops in agricultural activities. Computers and electronics in agriculture, 81, 124-141.

Rud, R., Käthner, J., Giesser, J., Pasche, R., Giebel, A., Selbeck, J., ... & Alchanatis, V. (2016, October). Monitoring spatial variability in an apple orchard under different water regimes. In International Symposium on Sensing Plant Water Status-Methods and Applications in Horticultural Science 1197 (pp. 139-146).

Sánchez-Piñero, M., M. J. Martín-Palomo, L. Andreu, A. Moriana, and M. Corell. "Evaluation of a simplified methodology to estimate the CWSI in olive orchards." Agricultural Water Management 269 (2022): 107729.

Scalisi, A., O'Connell, M. G., Stefanelli, D., & Lo Bianco, R. (2019). Fruit and leaf sensing for continuous detection of nectarine water status. Frontiers in Plant Science, 10, 805.

Scalisi, A.; Marino, G.; Marra, F.P.; Caruso, T.; Lo Bianco, R. A Cultivar-Sensitive Approach for the Continuous Monitoring of Olive (Olea europaea L.) Tree Water Status by Fruit and Leaf Sensing. Front. Plant Sci. 2020, 11, 340.

Tsoulias, N., Jörissen, S., & Nüchter, A. (2022). An approach for monitoring temperature on fruit surface by means of thermal point cloud. MethodsX, 9, 101712.

Von Willert, D.J., Matyssek, R., Herppich, W.B., 1995. Experimentelle Pflanzenökolo gie, Grundlagen und Anwendungen. Georg Thieme Verlag, Stuttgart, Germany.

Zude, M., Herppich, W. B., Dou, H., & Miller, W. M. (2002). Non-destructive Prediction Of Grapefruit Sensitivity To Chilling Injury. In 2002 ASAE Annual Meeting (p. 1). American Society of Agricultural and Biological Engineers.

Zude-Sasse, M., Fountas, S., Gemtos, T. A., & Abu-Khalaf, N. (2016). Applications of precision agriculture in horticultural crops.

Chapter 6.

Development of territory through the production of extra virgin olive oil

6.1 Introduction

The olive tree (*Olea europaea*) represents a principal element of Mediterranean landscape, where it has been cultivated for its fruits and wood since the prehistoric period (Carrión et al., 2010; Kaniewski et al., 2012; Brunori et al., 2018). Indeed in the Mediterranean Basin, olive groves (plantations of Olea europaea L.) constitute a very traditional land use presenting highly recognized ecological, cultural, social and economic values (Loumou and Giourga, 2003; Torres-Miralles et al., 2017). The timing of the domestication of the olive is controversial and genetic analyses of modern olive trees provide varied results, suggesting that domestication did not occur as a single event, but rather as a long and gradual process that might have developed in different places at different times in the wider region of the Mediterranean (Besnard et al., 2001; Breton et al., 2009; Belaj et al., 2012; Diez et al., 2015; Caracuta, 2020). In Italy olive cultivation has been a pillar of culture and economy since antiquity and olive growing continues to thrive even today in many regions (Rodrigo-Comino et al., 2021). Comprehensive studies of the presence of olive on the Italian peninsula show records of it there since the Early Holocene (Caracuta, 2020; Rodrigo-Comino et al., 2021). The earliest evidence (ca. 6700–5700 BC) comes from Sicily, where Olea pollen is recorded in the pollen sequences from Lago di Pergusa and Gorgo Basso (Sadori and Narcisi, 2001; Tinner et al., 2009; Caracuta, 2020) and olive charcoal has been found in the Mesolithic layers of Grotta dell'Uzzo (ca. 6600–6100 BC) (Costantini, 1989). The transition from management of wild olives to cultivation on a large scale happened much later, during the Iron Age–Archaic period, coinciding with the time when the Greeks extended their influence over a large part of southern Italy through their colonies (Caracuta, 2020). For centuries, olive growing has played a major role in the central regions of Italy, with hectares of olive groves surrounding hill towns and hamlets as part of a strong deep-rooted farming tradition (Palazzo et al., 2017). However, driving forces, such as demographic dynamics, urban development, market-oriented behaviors and climate change, are challenging landscape characters (Palazzo et al., 2017; Rodrigo-Comino et al., 2021). In some cases, these issues were hypothesized to force farmers to adopt, in a sufficiently long time window, practical solutions to maintain as high of olive oil production as possible (e.g., rethinking the spatial localization of olive trees). Besides, in the case of olive oil, high quality product is emphasized, where the nutritional value, the link with the territory, the environmental and social responsibility are an added value and a marketing tool to both attract and protect consumers (Lombardo et al., 2021).The olive oil quality is certified under the brands of Protected Designation of Origin (PDO) and Protected Geographical

Indication (PGI) which meet the criteria and indices established by European Union (de Salvo et al ., 2013). These typical products (DOP and IGP) are associated to numerous eco-social benefits including benefit increase for the agricultural firms located in the rural areas, establishment and enhancement of a qualified occupation, conservation of the traditional activities, gastronomic tourism development which can help improving the economical sustainability of the referring territories (de Salvo et al., 2013). Recent research explained the phenomenon of olive oil tourism and mentioned that olive oil is a particular food product with potential attraction for a category of curious tourists willing to become familiar with the culture and the identity of a territory through its food products. Furthermore, it is also clear that high-quality olive cultivation is nowadays asked to provide multifunctional outcomes including ecosystem services (e.g. hydrological functions, biodiversity, etc.) and even support for ecotourism (e.g. monumental trees, cultural heritage, etc.) (Manna et al., 2020). Consequently, enhancement of olive cultivation techniques and sustainable production of EVOO will lead to development of local products, territory and agritourism. Olive cultivation systems were defined by obsolete production structures having high costs and low profits, also due to poor mechanization (Lombardo et al., 2021). In addition to this, olive fruit growth is the result of genetic, metabolic, hormonal and environmental interactions that determine the size, shape and oil composition (Gucci et al., 2009). It is influenced and regulated by endogenous factors such as genetic differences and fruit load, and exogenous factors such as water availability and ambient temperature (Corelli-Grappadelli and Lakso, 2002; Hammami et al., 2011). Such degree of complexity in olive fruit growth demands a more accurate management in cultivating this crop (Khosravi et al., 2021a). In this sense implementation of innovative techniques for optimization of orchard performance is advantageous. One the most recent management approach that has been implemented in orchards is precision farming (PF). The PF concept is based upon observing, measuring and responding to inter and intra-field variability in crops or in various aspects of animal husbandry (Zarco-Tejada et al., 2014). PF aims to utilize technology to record and manage the variation of crops and soils within a field, thus reducing surplus inputs (e.g. fertilizer), increasing yields and aiding environmental sustainability (Morgado et al., 2020). In order to improve the efficiency of the data collection procedure, and to improve the precision with which agricultural operations are managed, it is helpful to use an automated system that collects data, especially to record long-term and up-to-the-minute fluctuations (Jiang et al., 2008). Thus, continuous monitoring and collecting data is a fundamental component in precision agriculture. One of its main research foci in pomology consist in monitoring of fruit transversal diameter by an application of sensors, to represent fruit growth (Khosravi et al., 2021). Observation of circadian cycles applied to fruit growth contributes to gathering information regarding this phenological stage and to yield more data for developing precision farming technologies (Marino et al., 2021; Zucchini et al., 2021; Khosravi et al., 2021a).

Therefore taking into account the significance of high quality olive products for development of territory and the necessity of application of the continuous fruit growth monitoring in optimization of orchard performance (quality and quantity), the present chapter contributes to describe the importance of maturation detection and precision water status detection via continuous olive fruit monitoring (which explained on the chapter 3 and 4) for territorial development.

6.2 Results and Discussion

6.2.1 Maturation and Olive Oil Quality (*Related to the Article of Continuous Monitoring of Olive Fruit Growth by Automatic Extensimeter in Response to Vapor Pressure Deficit from Pit Hardening to Harvest (Published in Horticulturae 2021, 7, 349; see chapter 3*)

Maturation of olive fruit is integration of physiological and biochemical changes influenced by environmental and cultural conditions (kong et al., 2019). Additionally, during ripening, chemical composition, enzymatic activity, and physical properties of the fruit will be changed and lead to changing of EVOO composition and quality (Lukić et al., 2017). The pungency and bitterness in EVOO are resulted from Phenolic compounds, so the adequate amount of them is important to guarantee the best palatability of the EVOO (Cecchi et al., 2013). With fruit maturation, the amount of polyunsaturated fatty acids, increases, and the amount of total phenol decreases, photosynthetic activity decreases, and the concentrations of both chlorophylls and carotenoids progressively decrease (Khosravi et al., 2021b; Amanpour et al., 2019). Therefore, accurate detecting of maturation status is vital. The common ripening index are detachment index (DI) (Camposeo and Godini, 2010), pigment index (PI) (Camposeo and Vivaldi, 2013; Bellincontro et al., 2012), colorimetric index (CI) (Camposeo and Vivaldi, 2013). The DI method is based on detachment force (measured by dynamometer) and fruit fresh weight. It can reach up to 95% of accuracy (Camposeo and Godini, 2010), however it is a time consuming and destructive approach. The PI method works by monitoring the color changing of mesocarp and epicarp of fruit (Camposeo and Vivaldi, 2013; Bellincontro et al., 2012). Because of its great laboriousness and variability, the PI is used in combination with the flesh firmness, which is destructive (Garcia et al., 1996). The CI is a quick and nondestructive method and easy to use and based on monitoring of the olive fruit color (Camposeo and Vivaldi, 2013). Recent research tried to make a relation between DI and CI to obtain the best harvesting time but it is not suitable for all varieties. A good ripening index must be well correlated with ripening, simple and easily detectable, objective, economic and preferably not destructive (Crisosto, 1994). Proximal and remote sensing methods are suitable for ripening assessment where they are able to detect maturation status with high accuracy, in real-time and in a non-destructive way. Besides, with recent developments in soft computing (i.e. enhancement of algorithms and deep learning techniques), ripening assessment by proximal and remote sensing methods have become less laborious.

In 2019, from August 6th to October 24th (DOY (Day Of the Year) 118 to DOY 297), continuous monitoring of olive fruit growth by combination of extensimeter (synonym of fruit gauge) and RGB camera have been performed by us (Khosravi et al., 2021a). Data was recorded by CR1000X data logger (Campbell scientific, Inc., Logan, UT, USA) every hour. Our experiment was designed to hourly monitor olive (*Olea europaea* L. cv. 'Frantoio') fruit transversal diameter from approximately initial pit hardening (II Phase), extension (III Phase) until harvest time (IV Phase) in the attempt to determine whether fruit growth dynamically responds to environmental variables such as diurnal vapor pressure deficit (VPD) change in different stages of fruit development (Khosravi et al., 2021a). A common

challenge with tree-based sensors is to adjust their output to physiologically meaningful parameters in a consistent manner (Marino et al., 2021; Fernández , 2017; Jones , 2006). The phenomenon of hysteresis has been employed to analyze proximal sensor (extensimeter) outputs. The root of the word hysteresis is Greek and means to “lag behind”. Hysteresis is non-linear loop-like behavior that does not show affine similarity with respect to time (Phillips , 2003; O’Kane , 2005). In other words, when the time argument of an input function is stretched or compressed, the corresponding output function is not stretched in the same way (O’Kane , 2005 ; Zhang et al., 2014). We studied the hysteresis curve of transversal diameter versus VPD. The latter has been shown to be especially important in woody plants, where it is the main variable affecting their diurnal evolution of transpiration (Perez-Martin et al., 2009). For description of the hysteresis curve, the terms of clockwise and anticlockwise loops (or curves) were used. To obtain the whole-day picture of the hysteresis curve, the best starting point for drawing each circadian graph was sunrise, due to the physiological effect of solar energy and its role in the photosynthesis and fruit growth. Consequently, our day started from sunrise and continued for 24 hours (Khosravi et al., 2021a). For characterization of hysteresis form, three concepts of partial, incomplete, and complete were used. When the hysteresis curve appeared in some part of the day and was not representative of the whole day, it was called partial. When the ending point of the hysteresis loop reached the same level of the starting point of the loop, it was defined as complete. Lastly, when the ending point of the hysteresis loop did not reach the same level of the starting point of the loop, so the loop was not completely closed, it was called incomplete hysteresis curve (Khosravi et al., 2022). According to the daily growth pattern of the fruit, The experiment was divided in two periods (see chapter3). The first period (DOY 218–276) included II phase and the whole III phase of fruit growth and the second period of the experiment (DOY 277–297) which corresponded to the IV phase of fruit growth. In the first period of experiment (DOY 218–276) and from DOY 218 to 259, the percentage of complete clockwise hysteresis was 92.86 which declined to 35.3 in the period of DOY 260–276. This showed that with increasing fruit ripening, the percentage of complete clockwise hysteresis declined. Furthermore, in the same period data showed that the percentage of partial clockwise hysteresis and incomplete clockwise hysteresis increased from 2.38 to 29.4. The percentage for both kinds of hysteresis was the same. Therefore, with enhancing ripening percentage the partial clockwise hysteresis and incomplete clockwise hysteresis showed a reverse trend in comparison with complete clockwise hysteresis. In the second period of the experiment (DOY 277–297) the percentage for complete clockwise hysteresis was 2.4, for incomplete hysteresis 64.3 and for partial hysteresis was 33.3. Moreover, the images of RGB camera were analyzed to add more information about fruit growth phases. The camera acquisition system based on a custom 5 Mpix RGB camera (Raspberry Pi Foundation, Cambridge, UK) was set on the orchard near to the tree to take pictures hourly. The images from the camera were labeled by olive maturation experts using Labelbox platform (Labelbox Inc., San Francisco, CA, USA); for each olive, the experts assigned a ripening stage according to 0–4 of Jaen index (International Olive Council, 2011). The results of image analysis (see chapter 3) showed that the percentage of ripening in the second period of experiment is 50%, so the fruit was at IV phase (maturation phase). Limitations to fruit growth and different fruit growth patterns at the ripening stage could be linked to changing in daily growth trends. In fact,

with increasing fruit maturation the complete hysteresis loop started to show abnormality which appeared with incomplete or partial daily hysteresis loop, or with no daily hysteresis loop. When the percentage of black fruits is near 50%, the presence of a complete clockwise hysteresis loop diminished sensibly. Detecting the moment of disappearance of the complete clockwise hysteresis curve could be useful to evaluate more precisely the IV phase (fruit maturation) of the double sigmoid growth curve of olives (Khosravi et al., 2021a).

6.2.2 Precision Irrigation and Olive Oil Quality (*Related to the Article of Continuous Third Phase Fruit Monitoring in Olive with Regulated Deficit Irrigation to Set a Quantitative Index of Water Stress (Published in Horticulturae 2022, 8, 1221. See chapter 4; see chapter 4*)

In recent decades, olive fruit and olive oil consumption has increased on a global scale (Amanpour et al., 2019). Consequently, major increases in olive production through agricultural intensification are generally deemed necessary to meet the demands of a fast-increasing global population (Crist et al., 2017; Morgado et al., 2020). The new intensive high-yielding irrigated orchards (400–700 trees ha^{-1}), or high intensive irrigated hedgerow systems (1,000–2,500 trees ha^{-1}) have been developed, which facilitate the use of the mechanical harvesters and the achievement of very high yields (Tous et al., 2014; Connor et al., 2014; Silveira et al., 2018; Morgado et al., 2020). The changes in the orchard structure (intensification) is associated with higher water input (Tous et al., 2014; Sánchez-Martínez and Cabrera, 2015; Infante-Amate et al., 2016; Russo et al., 2016; Morgado et al., 2020). Therefore, precision irrigation treatment plays a key role in olive grove management.

On the other hand, several researches explained that tuned irrigation has a significant effect on the olive oil quality and olive fruit properties (Romero-Trigueros et al., 2019; Caruso et al., 2017; Rosecrance et al., 2015). Romero-Trigueros et al. (2019), explained reduction in the acidity and peroxides and an increase in the polyphenols of the oil by water stress. Caruso et al. (2017) explained the negative correlation between volume of water applied and the concentrations of phenols, ortho-diphenols and secoiridoids. Rosecrance et al. (2015) suggested that moderate water stress can increase olive oil yield and quality and accelerate fruit maturity. Therefore, precision irrigation management is beneficial in olive orchards (Khosravi et al., 2022). The most common technique for optimizing water efficiency is Regulated Deficit Irrigation (RDI) (Ahumada-Orellana et al., 2017), in which water deficits are imposed during phenological periods when the tree is most insensitive to water stress (Ahumada-Orellana et al., 2017; Lodolini et al., 2011) , and complementary irrigation (Lodolini et al., 2014 and 2016). Furthermore, the results of Goldhamer,(1999) and Gómez-del Campo, (2013) showed that RDI strategies resulted in a saving of about 20% of the total amount of water applied without reducing the yield, fruit and oil content. Moreover, numerous studies show that deficit irrigation avoids or minimizes the negative impact of irrigation on erosion, in particular by reducing surface runoff and contributing less to the infiltration of pollutants (herbicides and pesticides) into groundwater (Rodríguez Sousa yet al., 2019). To achieve precise irrigation results, some recent research suggested

continuous assessment of plant water status indices (Marino et al., 2021; Khosravi et al., 2022). The indices could obtained from the soil or plant continuous monitoring, However
In the soil plant atmosphere continuum (SPAC), plants play an interface role between soil and the environment, and its physiological response is a combination of results (Scalisi et al., 2020; Khosravi et al., 2022). However, the olive species (*Olea europaea*) has a very wide genetic pool, which can respond to drought using different leaf and fruit physiological and morphological mechanisms (Scalisi et al., 2020; Khosravi et al., 2022). Therefore development of non- cultivar specific indices of water status detection is essential.

In 2021, from August 12th to 3rd October (DOY (Day Of the Year) 224 to DOY 276), The fruit transversal diameter (FD) (synonym to equatorial diameter) of four olive cultivars ('Ascolana dura', 'Piantone di Falerone', 'Arbequina', and 'Lea') were studied during the third phase (cell extension) of fruit growth (Khosravi et al., 2022). We used two kinds of extensimeters; one model was Winet (Winet s.r.l. Cesena, Italy) and another model was DEX20 (Dynamax Inc., Houston, TX, USA). The Winet extensimeters were connected to the wireless data-logger system (Winet s.r.l. Cesena, Italy) and the DEX20 extensimeter were connected to CR1000X data logger (Campbell scientific, Inc., Logan, UT, USA).
The daily diameter fluctuation (ΔD, mm), the daily growth (ΔG, mm), the cumulative fruit growth (CFG, mm), and the fruit relative growth rate (RGR, mm mm^{-1} h^{-1}) were studied during the third phase of fruit growth. The phenomenon of hysteresis has been employed to analyze proximal sensor (extensimeter) outputs. The daily hysteretic pattern of FD versus the environmental variable of vapor pressure deficit (VPD) was evaluated using the data of a local weather station. For description of rotational pattern of hysteresis loop the terms of clockwise and anticlockwise loops (or curves) were used and for explanation of characteristics of hysteresis loop, three concepts of partial, incomplete, and complete were used (Khosravi et al., 2022). Two deficit irrigation levels were performed and the higher dose (DI-20) was supplied to big fruit varieties while the lower dose (DI-10) was supplied to medium-small fruit varieties. DI-20 had 20% of the amount of ET_c and was supplied to Ascolana dura and Piantone di Falerone trees, while DI-10 had 10% of the amount of ET_c and was supplied to Lea and Arbequina trees (see chapter 4).
In the four olive cultivars (Ascolana dura, Piantone di Falerone, Arbequina and Lea), fruit growth parameters including CFG and RGR showed different responses to irrigation treatment which resulted by cultivar specific drought response mechanisms and suggest cultivar-specific water stress detection strategy. On the other hand, the daily hysteretic pattern of FD versus VPD was detected in all the studied cultivars, and a quantitative index (height of hysteresis curves) used for explanation of hysteresis magnitude's changed according to the deficit irrigation treatments. The quantitative differences of hysteresis curves for two deficit irrigated cultivars of Ascolana dura and Piantone di Falerone were demonstrated and discussed that the height of the hysteresis curve was significantly affected by irrigation. The results showed a significant reduction of height of hysteresis curves by irrigation treatments which were not cultivar-specific. The quantitative index for hysteresis curve magnitude's change in the four olive cultivars of Ascolana dura, Piantone di Falerone, Arbequina and Lea can efficiently estimate the plant water response to irrigation treatment in olive orchards (Khosravi et al., 2022).

6.3 Conclusion

The development and promotion of EVOO as a typical product (consisting of DOP and IGP certification), becomes a territorial development strategy, especially in those areas which are most vulnerable, as the rural ones (de salvo et al., 2013). Taking territorial development advantage of EVVO depends on precision management of the olive orchard to maintain production constant and high (quality and quality). In our studies, continuous fruit growth monitoring has been applied to enhance orchard performance by accurate ripening detection and setting a quantitative index of water status detection (Khosravi et al., 2021a and 2022). Both ripening and water status detection are fundamental aspects for production of high quality EVOO, whereas nutritional and organoleptic quality EVOO are affected by them (Sáinz et al., 2019). During fruit maturation, the levels of the Phenolic compounds, amount of polyunsaturated fatty acids, and changing concentrations of both chlorophylls and carotenoids change, therefore producing EVOO with specific organoleptic quality is related to proper identification of ripening status. Additionally, water availability in the soil is another important aspect that can affect organoleptic quality of EVOO by changing the level of acidity, peroxides as well as polyphenols. Therefore Tuned irrigation by precise detection of water status of fruit is beneficial too.

These results will be useful for creating more robust and precise models for olive fruit ripening detection and setting up more robust and precise indicators to detect water stress in olive orchards and improve olive orchard performance through the resilient production of extra virgin olive oil.

References

Ahumada-Orellana, L. E., Ortega-Farías, S., Searles, P. S., & Retamales, J. B. (2017). Yield and water productivity responses to irrigation cut-off strategies after fruit set using stem water potential thresholds in a super-high density olive orchard. Frontiers in Plant Science, 8, 1280.

Amanpour, A., Kelebek, H., & Selli, S. (2019). LC-DAD-ESI-MS/MS–based phenolic profiling and antioxidant activity in Turkish cv. Nizip Yaglik olive oils from different maturity olives. Journal of Mass Spectrometry, 54(3), 227-238.

Bellincontro, A., Taticchi, A., Servili, M., Esposto, S., Farinelli, D., Mencarelli, F., 2012. Feasible application of a portable NIR-AOTF tool for on-field prediction of phenolic compounds during the ripening of olives for oil production. J. Agric. Food Chem. 60, 2665–2673, http://dx.doi.org/10.1021/jf203925a.

Besnard G, Baradat P, Breton C, Khadari B, Bervillé A (2001) Olive domestication from structure of oleasters and cultivars using nuclear RAPDs and mitochondrial RFLPs. Genet Sel Evol 33(Suppl 1):251–268.

Belaj A, del Dominguez-García MC, Atienza SG et al (2012) Developing a core collection of olive (Olea europaea L) based on molecular markers (DArTs, SSRs, SNPs) and agronomic traits. Tree Genet Genomes 8:365–378. https://doi.org/10.1007/s1129 5-011-0447-6.

Breton C, Terral J-F, Pinatel C et al (2009) The origins of the domestication of the olive tree. C R Biol 332:1,059–1,064. https://doi. org/10.1016/j.crvi.2009.08.001.

Brunori, E., Salvati, L., Antogiovanni, A., & Biasi, R. (2018). Worrying about 'vertical landscapes': Terraced olive groves and ecosystem services in marginal land in central Italy. Sustainability, 10(4), 1164.

Camposeo, S., Godini, A., 2010. Preliminary observations about the performance of 13 varieties according to the super high-density oliveculture training system in Apulia (southern Italy). Adv. Hortic. Sci. 24 (1), 16–20.

Camposeo, S., Vivaldi, G. A., & Gattullo, C. E. (2013). Ripening indices and harvesting times of different olive cultivars for continuous harvest. Scientia Horticulturae, 151, 1-10.

Caracuta, V. (2020). Olive growing in Puglia (southeastern Italy): a review of the evidence from the Mesolithic to the Middle Ages. Vegetation History and Archaeobotany, 1-26.

Caruso, G., Gucci, R., Sifola, M. I., Selvaggini, R., Urbani, S., Esposto, S., ... & Servili, M. (2017). Irrigation and fruit canopy position modify oil quality of olive trees (cv. Frantoio). Journal of the Science of Food and Agriculture, 97(11), 3530-3539.

Cecchi, L., Migliorini, M., Cherubini, C., Giusti, M., Zanoni, B., Innocenti, M., & Mulinacci, N. (2013). Phenolic profiles, oil amount and sugar content during olive ripening of three typical Tuscan cultivars to detect the best harvesting time for oil production. Food research international, 54(2), 1876-1884.

COI (International Olive Council). Guide for the Determination of the Characteristics of Oil Olives, COI/OH/Doc. No 1 November 2011. Available online: http://www.internationaloliveoil.org (accessed on 15 September 2021.

Connor, D.J., Gómez-del-Campo, M., Rousseaux, M.C., Searles, P.S., 2014. Structure, management and productivity of hedgerow olive orchards. A review. Sci. Hortic. 169, 71–93. https://doi.org/10.1016/j.scienta.2014.02.010.

Corelli-Grappadelli, L., & Lakso, A. N. (2002, August). Fruit development in deciduous tree crops as affected by physiological factors and environmental conditions (keynote). In XXVI

International Horticultural Congress: Key Processes in the Growth and Cropping of Deciduous Fruit and Nut Trees 636 (pp. 425-441).
Carrión Y, Ntinou M, Badal E (2010) Olea europaea L in the North Mediterranean Basin during the Pleniglacial and the Early Middle Holocene. Quat Sci Rev 29:952–968. https://doi.org/10.1016/j.quascirev.2009.12.015.
Costantini L (1989) Grotta dell'Uzzo, Sicily: new evidence for the transition from Mesolithic to Neolithic subsistence in southern Europe. In: Harris D, Hillman GC (eds) Foraging and farming: the evolution of plant exploitation. Unwin Hyman, London, pp 197–206.
Crisosto, C.H., 1994. Stone fruit maturity indices: a descriptive review. Postharvest News Inf. 5 (6), 65–68.
Crist, E., Mora, C., Engelman, R., 2017. The interaction of human population, food production, and biodiversity protection. Science 356 (6335), 260–264. https://science.sciencemag.org/content/356/6335/260.
de Salvo, P., Hernández Mogollón, J. M., Di Clemente, E., & Calzati, V. (2013). Territory, tourism and local products. The extra virgin oil's enhancement and promotion: a benchmarking Italy-Spain. Tourism and hospitality management, 19(1.), 23-34.
Diez CM, Trujillo I, Martinez-Urdiroz N et al (2015) Olive domestication and diversifcation in the Mediterranean Basin. N Phytol 206:436–447. https://doi.org/10.1111/nph.13181.
Fernández, J. E. (2017). Plant-based methods for irrigation scheduling of woody crops. Horticulturae, 3(2), 35.
García, J.M., Seller, S., Pérez-Camino, M.C., 1996. Influence of fruit ripening on olive oil quality. J. Agric. Food Chem. 44, 3516–3520, http://dx.doi.org/10.1021/jf950585u.
Goldhamer, D. A. (1997, September). Regulated deficit irrigation for California canning olives. In III International Symposium on Olive Growing 474 (pp. 369-372).
Gómez-del-Campo, M. (2013). Summer deficit irrigation in a hedgerow olive orchard cv. Arbequina: relationship between soil and tree water status, and growth and yield components. Spanish Journal of Agricultural Research, 11(2), 547-557.
Gucci, R., Lodolini, E. M., & Rapoport, H. F. (2009). Water deficit-induced changes in mesocarp cellular processes and the relationship between mesocarp and endocarp during olive fruit development. Tree physiology, 29(12), 1575-1585.
Hammami, S. B., Manrique, T., & Rapoport, H. F. (2011). Cultivar-based fruit size in olive depends on different tissue and cellular processes throughout growth. Scientia horticulturae, 130(2), 445-451.
Infante-Amate, J., Villa, I., Aguilera, E., Torremocha, E., Guzmán, G., Cid, A., González, M., 2016. The making of olive landscapes in the south of Spain. A history of continuous expansion and intensification. In: In: Agnoletti, M., Emanueli, F. (Eds.), Biocultural diversity in Europe. Environmental History, vol. 5 Springer, Cham. https://link.springer.com/chapter/10.1007/978-3-319-26315-1_8.
Jones, H. G. (2007). Monitoring plant and soil water status: established and novel methods revisited and their relevance to studies of drought tolerance. Journal of experimental botany, 58(2), 119-130.
Jiang, J. A., Tseng, C. L., Lu, F. M., Yang, E. C., Wu, Z. S., Chen, C. P., ... & Liao, C. S. (2008). A GSM-based remote wireless automatic monitoring system for field information: A case study for ecological monitoring of the oriental fruit fly, Bactrocera dorsalis (Hendel). Computers and electronics in agriculture, 62(2), 243-259.

Kaniewski D, van Campo E, Boiy T et al (2012) Primary domestication and early uses of the emblematic olive tree: Palaeobotanical, historical and molecular evidence from the Middle East. Biol Rev 87:885–899. https://doi.org/10.1111/j.1469-185X.2012.00229.x.

Khosravi, A., Zucchini, M., Giorgi, V., Mancini, A., & Neri, D. (2021a). Continuous monitoring of olive fruit growth by automatic extensimeter in response to vapor pressure deficit from pit hardening to harvest. Horticulturae, 7(10), 349.

Khosravi, H., Saedi, S. I., & Rezaei, M. (2021b). Real-time recognition of on-branch olive ripening stages by a deep convolutional neural network. Scientia Horticulturae, 287, 110252.

Khosravi, A., Zucchini, M., Mancini, A., & Neri, D. (2022). Continuous Third Phase Fruit Monitoring in Olive with Regulated Deficit Irrigation to Set a Quantitative Index of Water Stress. Horticulturae, 8(12), 1221.

Kong, W., Han, R., Liu, N., Bai, W., Ma, J., Bai, X., ... & Zhang, J. (2019). Dynamic assessment of the fruit quality of olives cultivated in Longnan (China) during ripening. Scientia Horticulturae, 253, 8-16.

Lodolini, E. M., Morini, F., Polverigiani, S., & Neri, D. (2010, August). Olive fruit and root growth on different irrigation regimes in central Italy. In XXVIII International Horticultural Congress on Science and Horticulture for People (IHC2010): Olive Trends Symposium-From the 924 (pp. 63-68).

Lodolini, E. M., Ali, S., Mutawea, M., Qutub, M., Arabasi, T., Pierini, F., & Neri, D. (2014). Complementary irrigation for sustainable production in olive groves in Palestine. Agricultural Water Management, 134, 104-109.

Lodolini, E. M., Polverigiani, S., Ali, S., Mutawea, M., Qutub, M., Pierini, F., & Neri, D. (2016). Effect of complementary irrigation on yield components and alternate bearing of a traditional olive orchard in semi-arid conditions. Spanish Journal of Agricultural Research, 14(2), e1203-e1203.

Lombardo, L., Farolfi, C., & Capri, E. (2021). Sustainability certification, a new path of value creation in the olive oil sector: The Italian case study. Foods, 10(3), 501.

Loumou, A., Giourga, C., 2003. Olive groves: the life and identity of the Mediterranean. Agric. Human Values 20, 87–95.

Lukić, I., Žanetić, M., Špika, M. J., Lukić, M., Koprivnjak, O., & Bubola, K. B. (2017). Complex interactive effects of ripening degree, malaxation duration and temperature on Oblica cv. virgin olive oil phenols, volatiles and sensory quality. Food chemistry, 232, 610-620.

Manna, P., Bonfante, A., Colandrea, M., Di Vaio, C., Langella, G., Marotta, L., ... & Basile, A. (2020). A geospatial decision support system to assist olive growing at the landscape scale. Computers and electronics in agriculture, 168, 105143.

Marino, G., Scalisi, A., Guzmán-Delgado, P., Caruso, T., Marra, F. P., & Lo Bianco, R. (2021). Detecting mild water stress in olive with multiple plant-based continuous sensors. Plants, 10(1), 131.

Morgado, R., Santana, J., Porto, M., Sánchez-Oliver, J. S., Reino, L., Herrera, J. M., ... & Moreira, F. (2020). A Mediterranean silent spring? The effects of olive farming intensification on breeding bird communities. Agriculture, Ecosystems & Environment, 288, 106694.

O'Kane, J. P. (2005). Hysteresis in hydrology. Acta Geophysica Polonica, 53(4), 373-383.

Palazzo, A. L., & Aristone, O. (2017). Peri-urban matters. Changing olive growing patterns in central Italy. Sustainability, 9(4), 638.

Perez-Martin, A., Flexas, J., Ribas-Carbó, M., Bota, J., Tomàs, M., Infante, J. M., & Diaz-Espejo, A. (2009). Interactive effects of soil water deficit and air vapour pressure deficit on mesophyll

conductance to CO2 in Vitis vinifera and Olea europaea. Journal of Experimental Botany, 60(8), 2391-2405.
Phillips, J. D. (2003). Sources of nonlinearity and complexity in geomorphic systems. Progress in physical geography, 27(1), 1-23.
Rodrigo-Comino, J., Salvia, R., Quaranta, G., Cudlín, P., Salvati, L., & Gimenez-Morera, A. (2021). Climate Aridity and the Geographical Shift of Olive Trees in a Mediterranean Northern Region. Climate, 9(4), 64.
Rodríguez Sousa, A. A., Barandica, J. M., & Rescia, A. J. (2019). Estimation of soil loss tolerance in olive groves as an indicator of sustainability: the case of the Estepa Region (Andalusia, Spain). Agronomy, 9(12), 785.
Romero-Trigueros, C., Vivaldi, G. A., Nicolás, E. N., Paduano, A., Salcedo, F. P., & Camposeo, S. (2019). Ripening indices, olive yield and oil quality in response to irrigation with saline reclaimed water and deficit strategies. Frontiers in Plant Science, 10, 1243.
Rosecrance, R. C., Krueger, W. H., Milliron, L., Bloese, J., Garcia, C., and Mori, B. (2015). Moderate regulated deficit irrigation can increase olive oil yields and decrease tree growth in super high density 'Arbequina' olive orchards. Sci. Hortic. 190, 75–82. doi: 10.1016/j.scienta.2015.03.045.
Russo, C., Cappelletti, G.M., Nicoletti, G.M., Di Noia, A.E., Michalopoulos, G., 2016 Comparison of European olive production systems. Sustainability 8, 825. https://doi. org/10.3390/su8080825.
Sadori L, Narcisi B (2001) The Postglacial record of environmental history from Lago di Pergusa, Sicily. Holocene 11:655–671.
Sáinz, J. A., Garrido, I., Hernández, M., Montaño, A., Llerena, J. L., & Espinosa, F. (2019). Influence of cultivar, irrigation, ripening stage, and annual variability on the oxidant/antioxidant systems of olives as determined by MDS-PTA. Plos one, 14(4), e0215540.
Sánchez Martínez, J. D., & Paniza Cabrera, A. (2015). The olive monoculture in the south of Spain. European Journal of Geograph, 6(3), 16-29.
Scalisi, A., Marino, G., Marra, F. P., Caruso, T., & Lo Bianco, R. (2020). A Cultivar-Sensitive Approach for the Continuous Monitoring of Olive (Olea europaea L.) Tree Water Status by Fruit and Leaf Sensing. Frontiers in Plant Science, 11, 340.
Silveira, A., Ferrão, J., Munoz-Rojas Morenes, J., Pinto-Correia, T., Guimarães, M. H., & Schmidt, L. (2018). The sustainability of agricultural intensification in the early 21st century: insights from the olive oil production in Alentejo (Southern Portugal). Changing societies: legacies and challenges. Vol. 3. The diverse worlds of sustainability, 247-275.
Tinner W, van Leeuwen JFN, Colombaroli D et al (2009) Holocene environmental and climatic changes at Gorgo Basso, a coastal lake in southern Sicily, Italy. Quat Sci Rev 28:1,498–1,510.
Torres-Miralles, M., Grammatikopoulou, I., & Rescia, A. J. (2017). Employing contingent and inferred valuation methods to evaluate the conservation of olive groves and associated ecosystem services in Andalusia (Spain). Ecosystem Services, 26, 258-269.
Tous, J., Romero, A., Hermoso, J.F., Msallem, M. & Larb, A. (2014). Olive orchard design and mechanization: present and future. Acta Horticulturae, 1057, 231-246. https://doi.org/10.17660/ActaHortic.2014.1057.27.
Zarco-Tejada, P.J.; Hubbard, N.; Loudjani, P. Precision Agriculture: An Opportunity for EU Farmers—Potential Support with the CAP 2014–2020; Joint Research Centre (JRC) of the

European Commission; Monitoring Agriculture ResourseS (MARS) Unit H04: Brussels, Belgium, 2014.
Zhang, Q., Manzoni, S., Katul, G., Porporato, A., & Yang, D. (2014). The hysteretic evapotranspiration—Vapor pressure deficit relation. Journal of Geophysical Research: Biogeosciences, 119(2), 125-140.
Zucchini, M., Khosravi, A., Giorgi, V., Mancini, A., & Neri, D. (2021). Is There Daily Growth Hysteresis versus Vapor Pressure Deficit in Cherry Fruit?. Horticulturae, 7(6), 131.

Chapter 7.

Concluding Remarks

The Project was developed under Innovative PhD programs with industrial characterization which was financed by Marche Region. Two experiments were carried out in olive orchards in the Marche region (central Italy), and one innovative methodology was developed in Potsdam (Germany) to calculate water stress index of apple fruit. The aims of the two experiments in the olive orchard were optimization of the olive grove's performance (both quality and quantity), and enhancement of olive fruit growth monitoring systems for development of local olive production. The goal for the innovative methodology for apple fruit monitoring was the integration of different remote sensing techniques to calculate fruit water stress index (FWSI).

In the first research, the idea was observing fruit growth patterns (ranging from seasonal period up to hour intervals) in the intensive olive orchard (*Olea europaea* L., cv. 'Frantoio') at the experimental research station and botanical garden of Polytechnic University of Marche at Gallignano of Ancona (AN), in the attempt to determine whether fruit growth dynamically responds to environmental variables such as diurnal vapor pressure deficit (VPD) change in different stages of fruit development. The seasonal and circadian models of fruit growth were extracted. Besides, the shift between the end of the third phase (cell expansion) and the beginning of the fourth phase (fruit maturation) of fruit growth has been detected. Identification of the fruit maturation (fourth phase) by non-destructive method is recommended tools for enhancement of orchard performance (quality and quantity).

In the second research, the idea was setting a water status index through assessment of fruit growth parameters under different deficit irrigation regimes in a high-density olive orchard in four olive (*Olea europaea* L.) cultivars of 'Ascolana dura', 'Piantone di Falerone', 'Arbequina' and 'Lea' at the experimental farm of the Polytechnic University of Marche, at Agugliano of Ancona (AN). The assessment of fruit growth parameters showed cultivar-specific response to water stress. However, monitoring hysteresis curve of fruit diameter versus VPD showed a significant reduction of hysteresis curve magnitude by irrigation treatments which were not cultivar-specific. The quantitative index for hysteresis curve magnitude's change in the four olive cultivars of 'Ascolana dura', 'Piantone di Falerone', 'Arbequina' and 'Lea' can efficiently estimate the plant water response to irrigation treatment in olive orchards.

In the third research, the idea was the development of an innovative methodology for FWSI calculation, based on 3D fruit temperature (by integration of LiDAR and thermal camera), where data come from the apple orchard (*Malus* x *domestica* , cv. 'Gala'/M9) at the experimental field of ATB (Field Lab for digital agriculture) Potsdam, Germany. The 3D estimated temperature showed close relation with manually measured temperature. In addition, three alternative approaches have been employed for calculation of FWSI. Statistical analysis demonstrated that FWSI calculated via 3D estimated temperature are strongly related to FWSI calculated via manually measured temperature. However, the accuracy of all three calculation approaches were not the same.

All the studies in this thesis revealed innovative utilizations and output analysis of fruit monitoring (by proximal or/and remote sensing techniques) with an aim to enhance orchard performance by precision orchard management. Moreover, accurate ripening detection and water status assessment in the olive orchards will provide beneficial data for appropriate management of orchards to achieve high quality olive products (olive oil and table olive which are associated with numerous eco-social benefits, which can help territorial development (Figure 7.1).

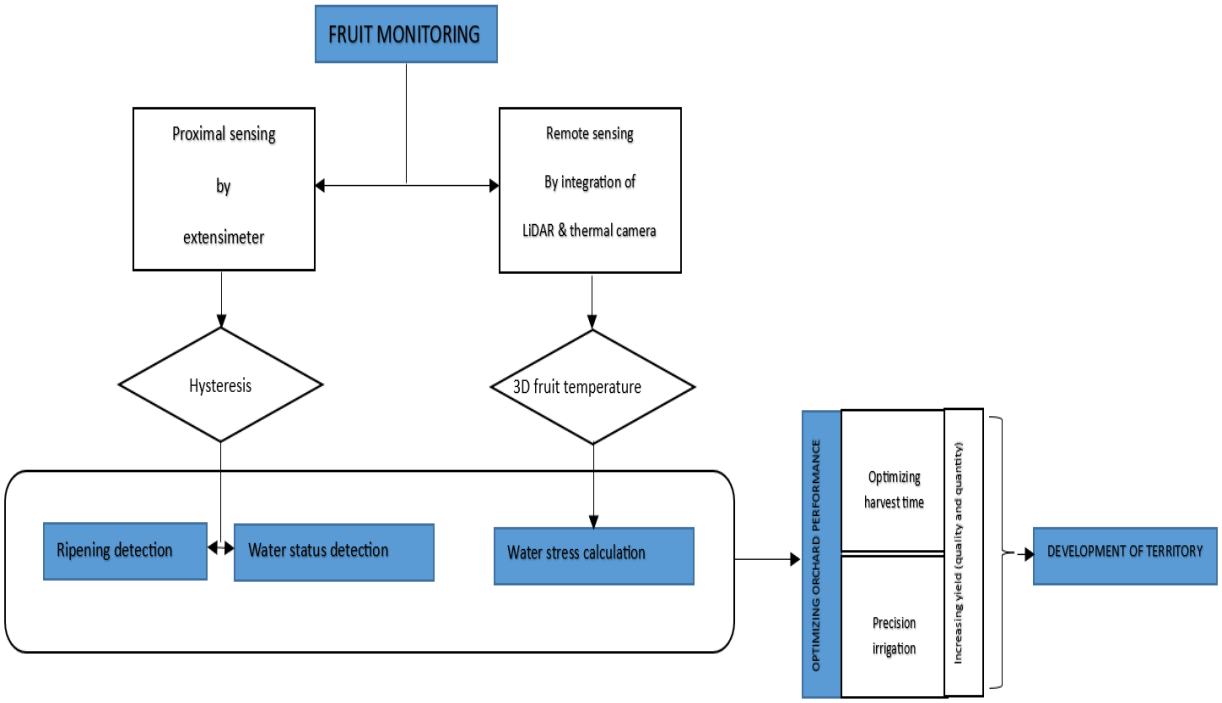

Figure 7.1. Flow chart of concluding of remarks

To promote our project findings to the international level, we published two peer reviewed articles in the international Journal and 2 other articles are under submission. In addition, several webinars, seminars and field demonstrations were organized involving universities, olive producers and private and public organizations with our university research body. Part of the work will be presented at the IX International olive symposium in September 2023 at Davis, CA (United States of America).